INSTITUTO POTOSINO DE INVESTIGACIÓN CIENTÍFICA Y TECNOLÓGICA, A.C.

POSGRADO EN NANOCIENCIAS Y MATERIALES

Synthesis, characterization and evaluation of membrane based on polyurethane for Contact Direct Membrane Distillation

Tesis que presenta

MC. Yareni Aguilar Costumbre

Para obtener el grado de

Doctora en Nanociencias y Materiales

Director(a) de la Tesis:

Dra. Juliette Alexandra Lambert (Co-directora)

Dr. Vladimir A. Barrios Escobar (Director)

San Luis Potosí, S.L.P., 26 junio de año 2023

Constancia de aprobación de la tesis

La tesis **Synthesis, characterization and evaluation of membrane base on polyurethane for Contact Direct Membrane Distillation** presentada para obtener el Grado de Doctor(a) en Nanociencias y Materiales fue elaborada por **Yareni Aguilar Costumbre** y aprobada el **día 26 de junio de 2023** por los suscritos, designados por el Colegio de Profesores de la División de Materiales Avanzados del Instituto Potosino de Investigación Científica y Tecnológica, A.C.

_____

Dra. Juliette Alexandra Lambert
Codirectora de la tesis

_____

Dr. Vladimir A. Escobar Barrios
Director de la tesis

_____

Ing. Milena Špírková, CSc.
Miembro del Comité Tutoral

_____

Dr. Sergio Díaz Castañón
Miembro del Comité Tutoral

_____

Dr. Gustavo Adolfo Fimbres Weihs
Miembro del Comité Tutoral

Créditos Institucionales

Esta tesis fue elaborada en el Laboratorio de Polímeros de la División de Materiales Avanzados del Instituto Potosino de Investigación Científica y Tecnológica, A.C., bajo la dirección del Dr. Vladimir Escobar Barrios, así como Laboratorio de Magnetismo de la División de Materiales Avanzados, bajo la dirección del Dr. Armando Encinas Oropesa.

La autora recibió el apoyo para la asistencia a 36th EMS Summer School en Edimburgo, 2019 por parte de la División de Materiales Avanzados.

La autora recibió beca 23rd Postgraduate Course in Polymer Science bajo el auspicio de la UNESCO e IUPAC, 2018 para la realizar el proyecto Polyurethanes with integrated inorganic/organic blocks and controllable hydrolytic stability en el grupo de trabajo Nanostructured Polymers and Composites en Institute of Macromolecular Chemistry, Praga, RC bajo la dirección de Ing. Milena Špírková, CSc. e Ing. Martina Čubová Urbanová, Ph.D.

Durante la realización del trabajo el autor recibió una beca académica del Consejo Nacional de Ciencia y Tecnología (296686) y del Instituto Potosino de Investigación Científica y Tecnológica, A. C.

Página en Blanco que se va a utilizar para colocar la copia del acta de examen.

Dedicatorias

Dedicar la tesis a las personas e instituciones deseadas.

Acknowledgements

I acknowledge the access to the facilities of the national laboratories LINAN and LANBAMA at the IPICYT, Dra. Gladis Labrada, M.C. Ana Iris and MC. Beatriz, Dra. Gladis Judith Labrada Delgado, M.C. Ana Iris Peña Maldonado and MC. Beatriz Adriana Rivera Escoto, especially to the technicians whom support the analysis by SEM and XRD.

Also, I acknowledge the access to the facilities of the Process Polymer Laboratory at the CIATEQ, especially to Dra. Mayra del Angel.

My special acknowledgements to the Institute of Macromolecular Chemistry for hosting me during the UNESCO-IUPAC Postgraduate Polymer Course, specially the group, Dra. Milena Spirkova, Dra. Martina Urbanova, Dra. Beata Strachota, Iveta Vlasáková, Dr Jiri Hodan, and Dra. Jelena Pavlicevic University of Novi Sad, Serbia.

Table of Content

List of Tables

List of Figures

Abbreviations

MD	Membrane Distillation
DCMD	Direct Contact Membrane Distillation
TPU	Thermoplastic Polyurethane
PUD	Waterborne dispersionPolyurethane
PVDF	Poly(vinylidene fluoride)
PTFE	Polytetrafluoroethylene
PEO	Poly (ethylene oxide)
TEOS	Tetraethyl orthosilicate
LEP	liquid entry pressure
FTIR	Fourier-transform Infrared Spectroscopy
DSC	Differential Scanning Calorimetry
AFM	Atomic Force Microscopy
SEM	Scanning Electron Microscopy
TEM	Transmission Electronic Microscopy
DMTA	Dynamic Mechanical Thermal Analysis
SS	Soft segment
HS	Rigid segment
WVP	Water vapor permeability

Resumen

Síntesis, caracterización y evaluación de membranas base poliuretano para Destilación Directa por Contacto en Membranas.

El poliuretano (PU) es un material con baja conductividad térmica con un potencial aislante térmico interesante, además de ser hidrofóbico por lo tanto su potencial uso como membrana para un sistema destilación por membrana en purificación se ha evaluado. Es importante señalar que han sido muy escasos los trabajos publicados con este material para dicha aplicación.

En este contexto, este trabajo tiene como objetivo el desarrollo de una membrana base poliuretano, ya sea como dispersión (PUD) o como termoplástico (TPU), obtenida mediante diferentes métodos de fabricación (electrohilado, inversión de fases y estiramiento) para su potencial uso en el sistema arriba indicado.

En primer lugar, se sintetizaron dispersiones acuosas de poliuretano (PUD) a base de diol de policarbonato, ácido 2,2-bis(hidroximetil)propiónico, 1,6-diisocianotehexano y trietilamina, mediante la inversión de fase. Se obtuvieron películas de PUD con diferentes contenidos de nanopartículas de SiO_2, notándose que la presencia de dichas nanopartículas modificaron el comportamiento mecánico de las membranas. Por ejemplo, la membrana con un 30 % en peso de sílice coloidal presentó el valor más alto de tenacidad y el segundo valor más alto de tensión de tracción. Asimismo, los estudios morfológicos de la película muestran que la superficie es diferente entre las películas de PU puro y las películas que contienen nanopartículas de sílice. El análisis FTIR indica una interacción significativa entre el polímero y el relleno. En cuanto a las propiedades térmicas (DSC, junto con DMTA), no hay diferencias entre el polímero puro y los compuestos poliméricos (que contienen el relleno). Además, las propiedades de transporte de gas revelaron específicamente que la permeabilidad al vapor de agua aumentó en presencia de sílice.

Por otro lado, las membranas de TPU obtenidas por extrusión son permeables al vapor de agua e impermeables al agua, además de elásticas y mecánicamente resistentes. La modificación de porosidad el material mediante la perforación aumentó la permeabilidad al vapor de agua sin ir detrimento de las propiedades mecánicas.

Por último, se obtuvieron películas de poliuretano termoplástico (TPU) mediante la técnica de electrohilado con modificación por solución piraña (PS). Dichas películas de TPU se caracterizaron mediante ángulo de contacto, porosidad, morfología y espesor con el fin de identificar la correlación entre los parámetros de síntesis y las propiedades. Los resultados indican que tiene un ángulo de contacto de 140°, una porosidad de 80% y al ser modificado a 30% SP el ángulo de contacto disminuye a 133° y su porosidad a 70%.

Palabras clave: Electrohilado, dispersión de poliuretano en agua, estirado

Abstract

Synthesis, characterization and evaluation of membrane base on polyurethane for Contact Direct Membrane Distillation.

Polyurethane (PU) is a low thermal conductivity material with an interesting insulating and hydrophobic potential as membrane for water purification using a direct contact membrane distillation system. It is worth to mention that even its interesting potential, membranes based on PU, few works have been published on this material for such application.

This work aims to study a polyurethane-based membrane obtained by different fabrication methods (electrospinning, phase inversion and stretching) for their potential in the above mentioned system.

First, waterborne polyurethane dispersions (PUD) based on polycarbonate diol, 2,2-bis(hydroxymethyl)propionic acid, 1,6-diisocyanotehexane and triethylamine, were synthetized by phase inversion method. Membranes with different SiO_2 nanoparticles content were fabricated, and such nanoparticules modified the mechanical behavior of the membranes. For instance, the membrane with 30 wt % colloidal silica had the highest value of toughness and second highest value of tensile stress. In addition, the morphology studies of film show that the surface is different between the pure PU films and the films containing silica nanoparticles. The FTIR analysis indicates significant interaction between polymer and filler. Regarding thermal properties (DSC and DMTA), there is not differences between the pure polymer and the polymeric composites (containing the filler). In addition, gas transport properties revealed that the water vapor permeability increased in presence of silica.

In addition, TPU membrane obtained by extrusion are water vapor permeable but waterproof, besides elastic and mechanically strength. The modification by drilling increased the mechanical properties as well as the permeation of water vapor.

Finally, the Thermoplastic polyurethane (TPU) films were obtained by electrospinning technique with different thickness. TPU based polyether, N,N-Dimethylformamide (DMF), tetrahydrofuran (THF) were used to obtain polymer solution at 18% wt and relation of solvent 70/30 respectively. TPU films have been characterized by tensile test, contact angle, porosity, morphology and thickness in order to identify correlation between synthesis parameter with properties.

Key words: Electrospinning, polyurethane water dispersion, stretching

Chapter 1. Introduction

1.1 Motivation

The development and well-being of societies depends fundamentally on the right management and supply of water, as it is indispensable not only for human consumption, but also for industry and agriculture. Population growth and its requirements are constantly increasing; but it is not proportional to the freshwater available in natural occurrence. Thus, in 2020, more than 2 billion people lived without safe water management services in the world, i.e. 34% of the total population[1] . For this reason, the relationship between the supply of water with storage, reuse and sanitation infrastructure and the challenges and opportunities associated with water technologies have been considered globally.

Several technologies have been explored to reverse this situation. For instance, Jones, 2019 reports that 15,906 plants are in operation with a desalination capacity of 34.81 billion m^3/year, which represents 81% of the total number of plants built and 93% of their total capacity. It is worth mentioning that most of the used technologies are reverse osmosis (69%) and multi-stage flash distillation (18%). However, new technologies such as direct osmosis, membrane distillation and hybrid systems are being developed.

Desalination is a common practice, however, the choice of technology depends on economic and environmental reasons, as well as on the volumes to be treated and the final water quality required. This is why desalination represents an increasingly important alternative for future water management plans, as it is obtained from a climate-independent with consistently high quality [2]

Membrane distillation is a hybrid system of a membrane system and pure distillation. It relies on the pressure difference, as the driving force, through the membrane. The membrane is usually hydrophobic and microporous. The generated vapor in the feed solution passes through the membrane and passes to the other side as a condensate[3]. The feed solution is at medium temperatures (around 90 ºC) with high salt concentrations ($>70{,}000$ ppm) and the condensate stream will depend on the configuration of the system, among them are DCMD (Direct Contact Membrane Distillation, where the water stream temperature is lower than temperature in the feed), VMD (vacuum stream), AGMD (air gap) and SGM (sweep gas).

Membrane distillation has a pilot scale scope; however, it has several advantages in terms of energy consumption, membrane potential and water quality, which have been the motivation for several researchers to contribute in both theoretical and experimental studies to use this technology on a large scale.

1.2 Outline of thesis

1.2.1 Challenges and objectives

Membrane distillation (MD) has been considered a potential alternative for conventional methodologies for water desalination, as a complementary thermal-membrane hybrid technology with minimal pre-treatment and reduced fouling. Suitable for use with renewable energy for wastewater systems[4].

Thus, a comprehensive minireview of MD technology and membrane needs recently being worked on it is provided.

The Polymer Laboratory, IPICYT has dabbled in membrane development since 2016 in water as well as energy purification systems[5–7].Recent activities have focused on the modification of polymers for application as a membrane. This is why this work aims adds knowledge to the commercial challenge of MD that has not yet been achieved, contributing to membranes science advancement. Furthermore, it is a contribution in the design of the direct contact module, which presents great opportunity areas, then continuous improvements can still be achieved.

The choice of the obtaining method of membranes and the selection of the materials considering the physicochemical, thermal, morphological and mechanical characteristics is essential to achieve a good and consistent performance in the DCMD module.

Also, in reported publications, some results focused on direct laboratory scale use and some others on pilot scale, in both cases the fundamental research has been linked to experimental and modelling. However, the selection of membrane materials has not yet been fully defined.

The scope of this thesis is to contribute to bridging the gap between fundamental membrane research and applied experimental application in a laboratory level module.

The objective is to develop polyurethane based materials to obtain a membrane by different methodologies (extrusion, electrospinning, evaporation) for establishing the structure-properties-performance correlation, giving the basic understanding of the phenomena involved in the transport of water vapor through the membrane to evaluate the potential application of membranes for direct contact distillation desalination (DCMD).

The control of porosity and hydrophobicity through the different membrane production techniques will contribute to the performance of the membrane by increasing vapor permeability and decreasing pore wetting. The nature of the polyurethane will decrease the interfacial thermal conductivity and heat loss in both streams, which is very important for this application.

The development of future materials requires a great deal of effort for their fabrication, considering methodologies that minimize the cost and the complexity of prototyping. The material must be characterized by specific properties and evaluated in terms of its performance in a DCDM module.

The quantitative information obtained from the evaluation and characterization of the material should be transferable and reliable at larger scale. Considering the individual project conditions provides a comparison and feasibility with respect to the limitations of the system itself.

1.2.2 Thesis structure and scientific approach

The thesis was divided into seven chapters:

- Chapter 1 presents the motivation, challenges and objectives that were raised throughout the project.

- Chapter 2 contains a comprehensive literature review of the advances and considerations that have been raised for the improvement of membrane distillation technology, focusing mainly on the development of membrane materials.

- Chapter 3 presents the development of water-dispersed polyurethanes with the incorporation of inorganic materials, the experimental methodology from their synthesis to their characterization, and obtaining a membrane by phase inversion.

- Chapter 4 describes the technique of obtaining films by extrusion, as well as the post-processing modification to obtain the membranes. The processing conditions, methodology, and the characterization are also presented and discussed.

- Chapter 5 provides the conditions and methodology for the fabrication of membranes by electrospinning, which underwent piranha solution modification and subsequent particle impregnation by the sol-gel technique.

- Chapter 6 explores the performance of the membranes in a DCMD module under specific conditions and compares the performance for each membrane.

- Chapter 7 provides the conclusions and future work for this project.

Chapter 2. Membrane distillation: The state of the art

The largest quantity of water available in natural reserve is seawater, with its main characteristic being its high salinity, i.e. the total amount of dissolved salts in a given volume. The salinity range from 35000 to 45000 ppm, varying according to local conditions, as it affects the environment and topographical conditions. For example, seas that are in areas of high temperatures or that receive a high rate of saline water drainage have a high degree of salinity. Another example is that enclosed seas have higher salinity than open seas or oceans.

The main ions that make up seawater include Na^{-}, Ca^{++}, K^{+}, Mg^{++}, $(SO_4)^{-}$ and Cl^{-}, and other ions but in lower concentration, as it can be seen in Figure 1. The composition of open sea is constant, however, the amount of total dissolved solids may change according to local conditions.

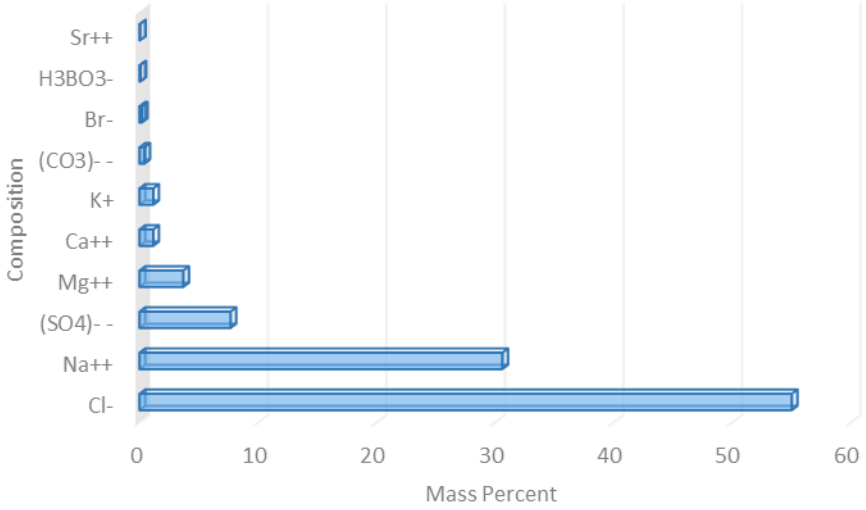

Figure 1. Typical composition of seawater with a total salinity of 36,000 ppm[8]**.**

As can be seen in Figure 1, chlorine and sodium are the ions that are found in greater quantities. According to NOM-127-SSA1-1994 the acceptable value of NaCl for human consumption is from 200 to 250 mg/L. This implies that high salt content limits its use for human consumption then its reduction is the main interest in the development of desalination processes.

Despite being an ancient technique, the first large desalination plants were installed in the Middle East in the 1930s with thermal processes. It was not until 1959 when Reis and Breton first demonstrated the possibility of desalination using cellulose-based polymeric membranes, four years later Loeb and Sourirajan showed that asymmetric cellulose acetate membranes could desalinate seawater [9]

2.1 Desalination processes

Currently, desalination is carried out by two main systems, thermal and membrane systems, the choice of one of them depends on the type of water, quantity of water and amount of energy required. The Table 1 shows the desalination process classification.

Table 1. Classification of desalination processes [10]

Energy	Process	System
Thermal	Evaporation	Solar Distillation Multi-stage flash (MSF) Flash Distillation (MF) Thermal vapor compression (TVC)
Cool	Crystallization	Hydrate formation Freezing
Mechanical	Evaporation Filtration	Mechanical Vapor Compression (MVC) Reverse Osmosis (RO)

In the case of thermal processes, it is based on evaporation, i.e. applying heat the water is evaporated, then condenses producing water without salts, although water with concentrated brine is also produced.

In the case of membrane processes, they are based on the mechanical separation of salts, i.e. a stream with a concentrated flow and a stream without salts is obtained. The particle size retained will depend on the pore size of the membrane. In the case of a dense membrane, it will depend on the selectivity of the membrane.

In a comparison of thermal and membrane processes, the former has a high energy demand due to the change of state required by the water, which has a high heat capacity. As a result, it has been displaced by the membrane process, which is more efficient in the recovery of product water and has a low energy demand.

2.1 Membrane Technology

Here, the membrane is the heart of the process, as it acts as a barrier that separates two phases from each other, generating a restriction in the movement of components through it with a selective character [11]. It is classified like asymmetric or symmetric, synthetic nature in solid or liquid, porous and non-porous structure. In addition, it can be negatively, positively, bipolar charged or neutral. The Figure 2 shows the classification.

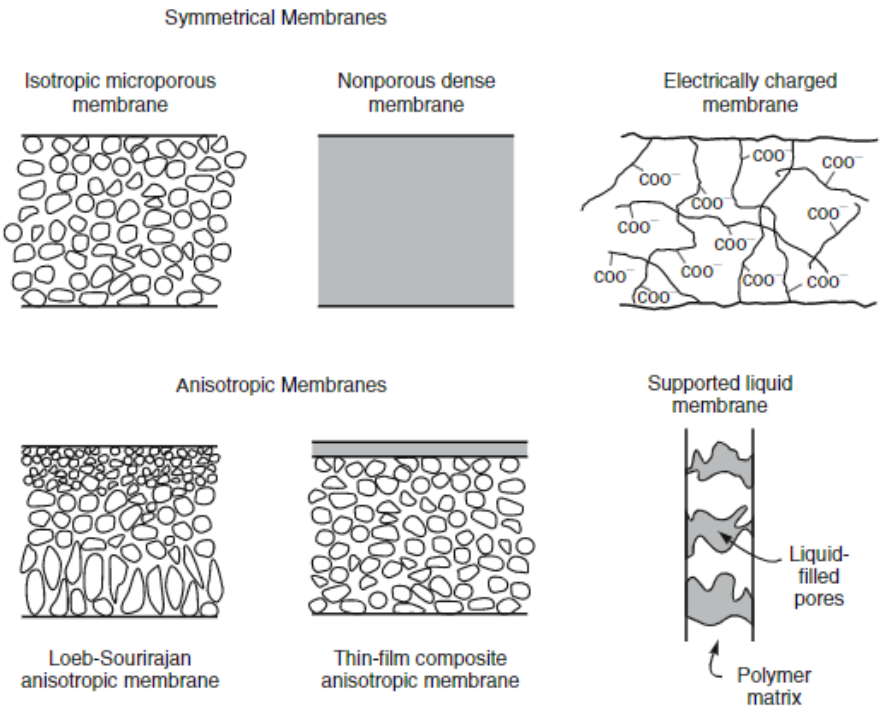

Figure 2. Schematic diagrams of the types of membranes[12]**.**

In the case of isotropic membranes, their composition and structure is uniform, and they can be microporous or dense. Anisotropic membranes are not uniform, they are formed by different layers with different structure and composition, commonly the last layer is selective and supported by another layer that is permeable. It is important to mention that applications depend on the characteristics of the membranes.

However, not only the composition of the membrane plays an important role in the membrane process. For instance, the driving force determines the transport of the feed components into the permeate. Therefore, the classification of the process according to the driving force is presented in Table 2:

Table 2. Classification of membrane processes according to their driving forces [13]

Pressure difference	**Concentration difference**	**Temperature difference**	**Electrical Potential difference**
Microfiltration Ultrafiltration Nanofiltration Reverse Osmosis Piezodialysis	Gas Separation Pervaporation Carrier mediated transport Dialysis Diffusion dialysis	Membrane distillation Thermo-osmosis	Electrodialysis Electro-osmosis Membrane electrolysis

In addition to the energy savings of membrane technology, other advantages include compactness, light weight and high productivity. This is why reverse osmosis has become the most common and commercially viable technology [14]. Despite the

technical and economic advantages, the new environmental regulations represent a challenge to improve these systems, as they have imposed requirements and restricted brine discharges. Thus, technologies such as electrodialysis [15] and membrane distillation [16] have been introduced. The latter still has momentum to reach an industrial scale.

2.2 Membrane distillation

Membrane distillation is a process that involves the transfer of vapor across a porous membrane, with a high temperature stream on one side and a lower temperature stream on the other side. The permeate is obtained from condensation near the membrane, due to the difference in vapor pressures, which act as a driving force[17]. Regarding the wetting of membrane, it is completely wetted by capillary effect. The selectivity of this process is determined by the involved liquid-vapor equilibrium, as the membrane only participates as a barrier between the two phases. The Figure 3 describes the basic concept of membrane distillation.

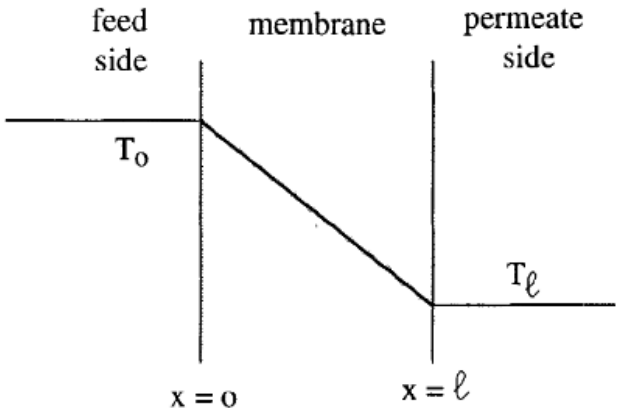

Figure 3. Temperature profile across a homogenous membrane. To is feed stream temperature, Tℓ is permeate temperature, xo and xl is membrane thickness at feed and permeate side, respectively [13].

In the desalination process, fossil fuels are the most usual option as a source of energy. However, alternative energies have increased their presence in the integration of the processes, in particular solar, geothermal and waste heat from other processes.

On the other hand, the membrane distillation process has four possible configurations on the permeate side [18].

1. Direct Contact Membrane Distillation (DCMD)
In this configuration both streams are aqueous solutions, the permeate side is of lower temperature than the feed stream. The flow is tangential to the membrane surface, in this case the transmembrane temperature difference induces the vapor

pressure transfer. That is, the vapor from the hot stream passes through the membrane pores and condenses in the cold liquid stream, which is usually pure water.

2. Vacuum membrane distillation (VMD)
Vacuum is applied to the permeate side by a pump with a pressure lower than the saturation pressure of volatile molecules and the condensate is collected outside the module.

3. Air Gap Membrane Distillation (AGMD)
In this configuration an air gap is located between the membrane and the cold stream. The volatile molecules are condensed until they touch the surface of the cold liquid.

4. Sweep gas membrane distillation (SGMD)
In this configuration a cold inert gas (sweep gas) entrains the permeate through the membrane and condenses it outside the module.

The Figure 4 shows the representation of the modules described above.

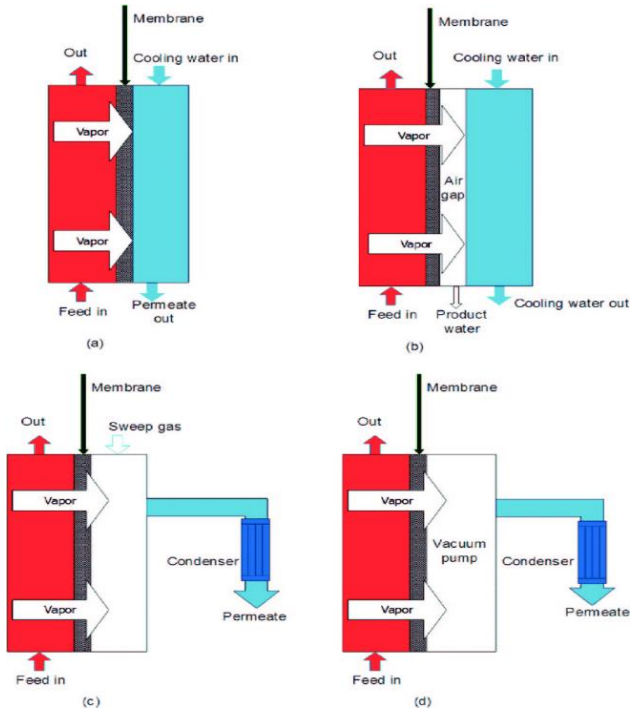

Figure 4. Configurations of membrane distillation. (a) DCMD. (b) AGMD. (c) SGMD. (d) VMD[19]**.**

2.3 Transport mechanism

2.3.2 Mass transfer

The heat and mass transfer mechanisms are complex as both have the same direction, due to the vapor pressure gradient between the feed and permeate stream [20]. Mass transport takes place in stages:

- First the volatile molecules are transported from the bulk feed solution to the membrane surface.
- Then these gas-phase molecules diffuse through the membrane.
- Finally, the gas-phase molecules pass from the membrane surface on the permeate side to the permeate stream [21].

So far, mass transfer has been described by three possible independent mechanisms, Knudsen diffusion, viscous flow or Poiseuille and molecular diffusion:

1. Knudsen diffusion model (R_K): It considers that the density of the gas is very low or the size of the pore is very small, so they disregard the collision between them, what is considered are the collisions between molecules and pore walls [22] as it is described in Equation 1[23]:

$$\boldsymbol{R_K^{-1} = \frac{\varepsilon r}{\tau \delta}\left(\frac{M_w}{RT_m}\right)^{1/2}} \qquad \textbf{Equation 1}$$

Where porosity (ε), mean pore size (r), tortuosity (τ), molecular weight of water vapor (M_i) and membrane thickness (δ) are related.

2. Molecular diffusion model (R_M): It is considered that the pore size is relatively large, and the mass transfer is given by the collision between molecules and the different species of the mixture move among themselves by the influence of concentration gradients, the Equation 2 describes it:

$$\boldsymbol{R_M^{-1} = \frac{\varepsilon}{\tau \delta}\left(\frac{DM_w}{P_{\alpha M} RT_m}\right)} \qquad \textbf{Equation 2}$$

Where long-mean air pressure at both side of the membrane ($P_{\alpha M}$), are related. Also, binary diffusion coefficient (D) is calculated by the next expression:

$$\boldsymbol{D = 1.19X10^{-4}\left(\frac{{T_m}^{1.75}}{P_m}\right)} \qquad \textbf{Equation 3}$$

3. Viscous flow or Poiseuille model (R_p): It is considered when the pore size is bigger than the free path of the molecules transported, is calculated by the next equation:

$$R_M^{-1} = \frac{\varepsilon r^2}{\tau \delta}\left(\frac{p_m M_w}{\mu R T_m}\right) \qquad \textbf{Equation 4}$$

Where P_m is the mean water vapor pressure inside the membrane, it is the result of the next equation:

$$p_m = \frac{p_{f,m}+p_{p,m}}{2} \quad \textbf{Equation 5}$$

Where $p_{f,m}$ is the partial vapor pressure of feed solution and $p_{p,m}$ partial vapor pressure of permeate solution based on the Roult's law:

$$p_{f,m} = (1 - x_f)p_{w,m} \quad \textbf{Equation 6}$$

Where x_f is the molar fraction in liquid phase of feed solution and $p_{w,m}$ is partial vapor pressure of water based on Antonie's equation as next:

$$p_{w,m} = \exp\left(23.1964 - \frac{3816.44}{T-46.13}\right) \quad \textbf{Equation 7}$$

Once the variables used to obtain the mass transfer coefficient (B) have been defined, the following equation is used:

$$B = (R_k + R_M)^{-1} + R_p \quad \textbf{Equation 8}$$

Finally, the parameter that defines the mass transfer is the permeate flux (J) through the membrane correlated with the mass transfer coefficient and the pressure.

$$J = B(p_{f,m} - p_{P,m}) \quad \textbf{Equation 9}$$

2.3.3 Energy transfer

At the same time to the mass transport, heat transport occurs in the system DCMD. The mechanism of heat transfer through the membrane considers in three steps [24] [25]:

1. Convective heat transfer from the bulk feed solution to the boundary layer to the membrane surface:

$$Q = h_f(T_f - T_1) \quad \textbf{Equation 10}$$

Where h_f is the heat transfer coefficient in feed boundary layer, T_f is the temperature of bulk feed stream and T_1 is the temperature at feed membrane surface.

2. Conduction heat transfer the vapor flow through the membrane pores:

$$Q = J\lambda + \frac{k_m}{\delta}(T_1 - T_2)$$ **Equation 11**

Where J is the permeate flux, λ is the heat of vaporization, T_2 is the temperature at permeate membrane surface, k_m is the thermal conductivity of the membrane. The k_m can be calculated with the next equation [26]:

$$k_m = \varepsilon k_g + (1 - \varepsilon)k_s$$ **Equation 12**

Where k_g is the thermal conductivity of the gas phase and k_s is the thermal conductivity of solid phase, in this case of polymer.

3. Convective heat transfer from the membrane surface to the bulk permeate solution:

$$Q = h_p(T_2 - T_p)$$ **Equation 13**

Where h_p is the heat transfer coefficient in permeate boundary layer, T_2 is the temperature at permeate membrane surface.

When carrying out the energy balance, a stationary state is considered, so the surface temperatures of the membrane (T_1 and T_2) can be estimated by the following equations:

$$T_1 = T_f - (T_f - T_p)\frac{\frac{1}{h_f}}{\frac{1}{(h_c+h_v)}+\frac{1}{h_f}+\frac{1}{h_p}}$$ **Equation 14**

$$T_2 = T_p + (T_f - T_p)\frac{\frac{1}{h_p}}{\frac{1}{(h_c+h_v)}+\frac{1}{h_f}+\frac{1}{h_p}}$$ **Equation 15**

Where h_c is the condition coefficient and h_v is the vapor heat transfer coefficient, both define as the next equations:

$$h_c = \frac{k_m}{\delta} \qquad h_v = \frac{J\lambda}{T_1 - T_2}$$ **Equation 16 and Equation 17**

Also, h_p and h_f coefficients are correlated with empirical dimensionless Nusselt number, Reynolds and Prandtl number.

2.3.1 Polarization

MD is a thermal separation process, then the effect of polarization is present both in temperature and concentration. Temperature polarization refers to the loss of driving force caused by thermal gradients in the membrane bounding fluids [27].

The causes of temperature polarization are due to the difference in temperature between the layer adjacent to the membrane which is different from the temperature of the feed and permeate stream. Its value will depend on the conditions of heat exchange in the module [28].

On the other hand, concentration polarization is related to membrane fouling or scaling and influences the performance of the system. That is, a rapid accumulation of solute particle concentration is generated near the membrane surface, while the permeate flux decreases [29].

2.4 Membrane for MD

Initially, the commercially available microporous MF membranes were based on polymeric materials such as PP, PVDF and PTFE, being in tubular, capillary or flat sheet configurations [30]. Such conventional membranes are hydrophobic and they still present areas of opportunity due to the trade-off between water vapor flux and conductivity decrease.

2.4.1 Membrane characteristics for MD

Table 3 summarizes some typical characteristics of the membranes used for the MD process.

Table 3. Essential characteristics of MD membranes[31].

Characteristics	**Preferable value**
Pore size	<0.3 Mm
Hydrophobicity	>90 °
Thickness	<200Mm
Porosity	>50%
Liquid entry pressure	>1 bar
Surface Energy of the material and pore	Low

There are two characteristics of the membrane which are closely related to intrinsic properties of the material or modification of the material, these are hydrophobicity and thermal conductivity.

Hydrophobicity is the ability of a surface to repel water, thus preventing wetting towards the membrane pores. Therefore, the contact angle should be greater than 90° and the pore size in the range of 0.05-1 mm for maximum water flux. It is also important to consider the relationship with porosity and mechanical properties [32].

Thermal conductivity in a polymer depends on crystallinity, crystal shape and temperature difference. This conductivity should be as low as possible, otherwise it increases heat transfer through the membrane. Thermal conductivity values of some polymers used for membranes, as well as for water vapor and air, are mentioned in the Table 4.

Table 4. Thermal conductivity of different materials[33], [34]

Material	Thermal conductivity (W/mK)
Water vapor	0.03
Air	0.022
PDVF	0.21
PTFE	0.29
PP	0.2
PU	0.18

The pore size is usually less than 0.3 microns because there is a direct relationship between permeate flux and pore size. That is, a small pore size prevents liquid from entering, on the contrary, a high pore size is required for a high permeate flux [35]. On the other hand, depending on the pore size the mechanism of further transfer is considered, as the pore size is not uniform the pore size distribution is considered and it is possible that several mechanisms occur simultaneously.

The liquid enter pressure (LEP) corresponds to the pressure applied in the inlet and the liquid passes through the hydrophobic membrane [36]. It is desired that the inlet liquid does not enter the membrane pores. This characteristic depends on the maximum pore size and hydrophobicity of the membrane and is directly related to the inlet concentration. In the case of organic solvents LEP is reduced.

The thickness has an inversely proportional relationship with the permeate flux, i.e. the thicker the membrane, the lower the permeate flux, due to increased thermal resistance and heat loss [37]. Optimal thicknesses to avoid this effect are less than 200 mm.

Porosity is defined as the pore volume divided by the membrane volume, which represents the void volume fraction [38]. In a MD system it varies from 30 to 85%. Tortuosity represents the deviation of the pore structure from the shape of a cylinder. This characteristic is related to the permeate flow rate, which decreases as the tortuosity increases.

These characteristics depend on the method by which the membrane is obtained, which are explained below.

2.5 Membrane fabrication techniques in MD

2.5.1 Stretching

This method consists of four consecutive stages. The first one is to generate a film through a melt extrusion, secondly the film is annealed at high temperatures to improve the crystalline structure, thirdly stretching usually at room temperature to separate the films and create pores before stretching at elevated temperature to enlarge the pores. Finally, the heat setting stage which prevents shrinkage and maintains dimensional stability[39][40].

2.5.2 Phase inversion

This process is a thermodynamically controlled transformation of a polymer solution into a solid membrane that may or may not be porous. A common step in the methodology implies that the polymer solution is poured into a mold or support, but the solidification process can be by various techniques:

- Non-solvent induction (NIPS); it is very commonly used to obtain asymmetric membranes. Initially the polymer solution is poured to shape the membrane to a certain thickness, then it is put in contact with a non-solvent, which is not miscible with the solution[41].
- Thermal induction (TIPS); the polymer solution may have a solvent or mixture of solvents, it is cooled to allow phase separation [42].
- Evaporative induction (EIPS), the polymer is precipitated by evaporation of the solvent, this can be at room temperature or in an inert atmosphere [43]
- Vapor induction (VIPS), in which the polymer precipitation is by evaporation of the solvent in a vapor environment of a non-solvent [44]

3.5.3 Electrospinning

The technique of electrospinning applied to the membrane distillation process has become increasingly common due to the easiness and robustness of the technique, and fibers, from nanometers to microns in diameter, can be obtained. The principle of this technique is based on the potential difference generated by an electric field between a molten polymer or polymer solution and a grounded metal collector. The polymer material is charged until the surface tension is overcome from the supply to the collector. In the case of the polymer solution, the fibers are formed as the solvent evaporates and are usually collected as nonwoven fabric[45].
The main parameters affecting the average fiber diameter of the non-woven are the properties of the solution (molecular weight, concentration, viscosity, conductivity), environmental conditions (humidity, temperature) and processing conditions (applied voltage, distance from collector to needle) [46].

2.6 Advances in MD

The increase in the MD field research is reflected in the incremental number of MD publications. This can be seen in the figure below, which is generated by the Scopus database.

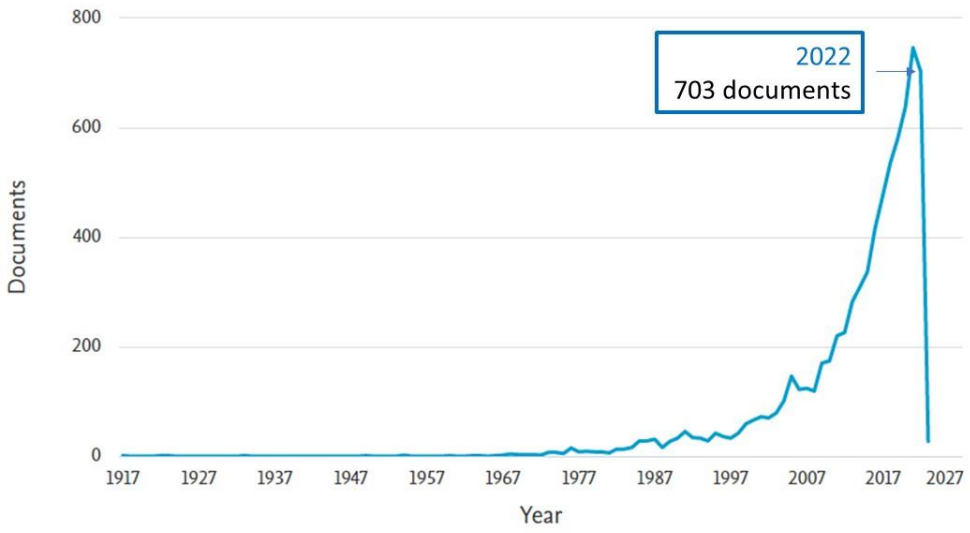

Figure 5. Documents published by year on DM.

The Figure 5 shows that publications have fluctuated along the time. However, in the last 20 years there has been a significant increment in the number of studies on the subject. Specific studies been carried out on the system, such as the modification of membranes for better performance or module configurations. Also, comprehensive studies focused on the thermal and energy efficiency of the system, in some cases even economic studies, have been done. In addition, scaling up studies at pilot plants or heat integration with renewable energy systems have been aborded.

2.7 Potential fields of application

Due to the broad characteristics of MD, this technology has a variety of applications. MD has been used in water treatment for the removal of representative pollutants such as ibuprofen, boron and arsenic [47], removal of inorganic components such as calcium, magnesium, iron and aluminum from the mining industry [48], removal of uncoagulated latex, proteins or carbohydrates and inorganic salts in rubber industry wastes [49].

The use of MD for desalination has attracted increased attention in the desalination field, because the rejection of high salt loaded streams with a high recovery as high as 98.8 % is possible, opposed to RO of 30-50% [50]. This technology is promising to meet zero liquid discharge (ZLD), which is considered one of the main environmental problems in desalination [51].

Chapter 3. Development of water polyurethane (PUD) membrane using the phase inversion process

3.1 Background

3.1.1 Water dispersion polyurethane (PUD)

Water dispersion polyurethane (PUD), is a solvent-free colloidal system, where polyurethane particles are dispersed in water. The main backbone contains urethane groups (-NHCOO-), which is formed by a polyaddition reaction between a hydroxyl (-OH) and an isocyanate (-NCO). The basic chemical components of polyurethanes that are known from solvent-borne polyurethanes are essentially polyols, diisocyanates, catalysts and additives [52].

Isocyanates are compounds that can be cyclic, aliphatic or aromatic, the most common of which are 2,4-TDI (Toluene diisocyanate), NDI (Naphthalene diisocyanate), HDI (Hexamethylene diisocyanate), 4,4'-MDI (Methylene diphenyl diisocyanate), IPDI (Isophorone diisocyanate), H12MDI (cycloaliphatic diisocyanate). The isocyanate group (R-N=C=O) has an accumulated double bond sequence, the reactivity of this group is governed by the carbon atom due to its electrophilic character, with the ability to accept a pair of free electrons and be attacked by groups provided with labile hydrogens [53].

On the other hand, polyols are hydroxyl terminated compounds that may contain in their structure most common ether and ester groups, while some special ones are acrylic base, carbonate, amide and other functional groups. Polyols tend to make up the largest proportion of the components and provide flexibility and softness[54]. It is common for polyols to be used as mixtures of molecules with different molecular weights, although similar in nature, but with different numbers of -OH groups. [55].

Additionally, for the urethane formation reaction, catalysts have organic, inorganic and organometallic nature. The most commonly used organic-based catalysts are especially tertiary amines. The reactivity of this compound can be affected by basicity and steric hindrance. In addition, catalytic selectivity is affected by the ability to form hydrogen bridges as well as the spatial separation between the active sites. In the case of organometallics are dibutyltin oxide (DBTO), butyltin trichloride, stannic chloride and dibutyltin dilaurate (DBTDL)[56,57].
In the case of PUDs, as it is a system in which the particles are dispersed in an aqueous medium, hydrophilic groups are required to make it compatible with water, since polyurethane is incompatible with it. That is why ionic molecules called internal emulsifiers, which are hydrophilic monomers that contain ionic functionality, including carboxylate, quaternary ammonium or sulfonate groups are used [58].

Regarding the individual components, the properties are different. In general, polyurethane is constituted by two segments, a soft segment (SS) and a hard segment (HS), the first is constitutive by polydiol, and the second is composed by isocyanate and chain extender [59–61]

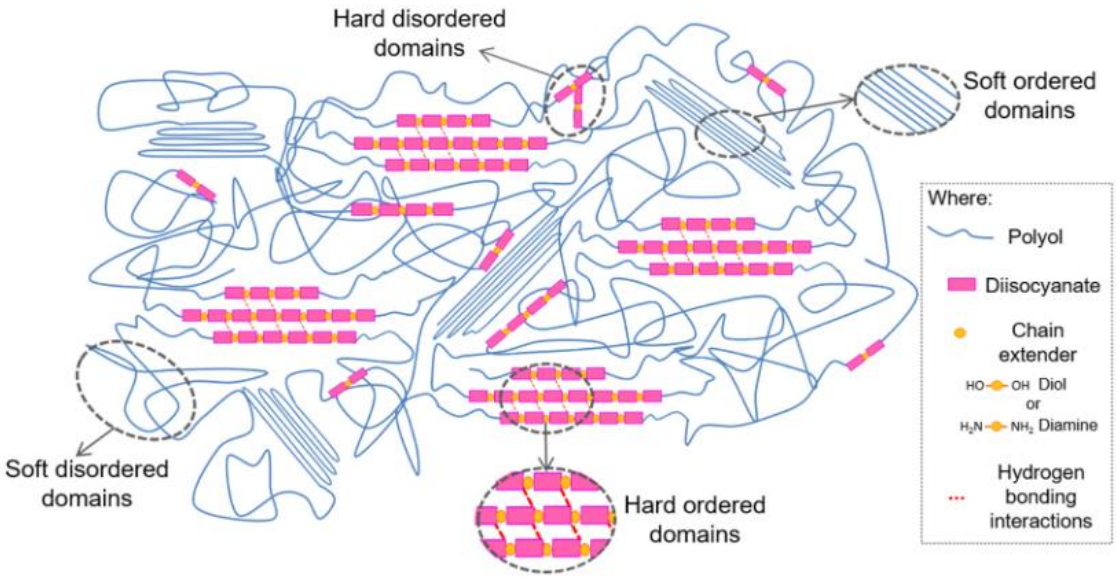

Figure 6. Scheme of segment conformations and hydrogen bonding interactions of polyurethanes or polyurethanes urea (when diamine is used) and the resulting ordered and disordered microdomains [62].

There is a thermodynamic incompatibility between the hard segment (HS) and soft segment (SS) which can cause a microphase separation, for consequence can affect physical properties. HS can have a significant effect on mechanical properties, thermal stability, and solvent resistance for materials, while the presence of SS provide flexibility and elasticity to PU[63].

3.1.2 Polycarbonate (diol component)

Depending on the purpose of the application and its functionality, the type of polyol is chosen. In the case of polycarbonate-based polyols, they have been characterized by generating greater resistance to hydrolysis to polyurethanes, improving resistance to aging, improving behavior at low temperatures, and increasing resistance to fungal growth[64]. Due to its chemical nature, that is to say its polarity and the strong bond of the carbonate unit, they confer an improvement to the mechanical properties of PUD. It is the major characteristic compared to other ether and ester-based polyols.[65].In such a way that the presence of a carbonate group can improve the miscibility between soft segments and soft segments [66].

The polycarbonates used as polyols for the soft segment in the synthesis of polyurethane are generally obtained by transesterification of five-membered cyclic carbonate or by polycondensation of diols with phosgene [67]
Varying the dispersion stage using polycarbonate diol base, that is, the way of adding the water, influences the molecular weight of the polyurethane in dispersion and the formation of the film of this polymer affects the tensile stress[68].

3.1.3 Nanocomposites polyurethane

In recent studies, the use of fillers in PUD has been carried out. Depending on the type of filler, particle size, state and degree of dispersion, materials for different applications can be obtained[69].
In the case of the type of filler, two have been investigated, organic and inorganic. Some of the examples of inorganic species are TiO_2, SiO_2, Ag, ZnO and $CaCO_3$ at nanometric scale. Meanwhile, examples of organic species are cellulose and graphene. It is considered that the best is to have the largest surface area and, in practice, to avoid the particle agglomeration and exfoliation of lamellar structures [70,71].

Silver nanoparticles have been incorporated into the polyurethane matrix to increase antibacterial properties, but it has been difficult to achieve a homogeneous dispersion, since they are easily agglomerated giving incompatibility between the organic and inorganic phases [72].

In previous studies of polycarbonate-based polyurethane with 1% organoclay, it was found that the interaction between it and the hard segments by hydrogen bonds and, an adequate dispersion of the nanoparticles does not promote the phase separation.[73] This effect was also found using organically modified bentonite and montmorillonite at 1% by weight [74].

Silica has been used for polymeric compounds due to its large surface area and stability, for reducing shrinkage during curing, improving adhesion, reducing coefficients of thermal expansion, and increasing corrosion resistance. Furthermore, by adding silica in layers of the polymer matrix, it is enhanced the formation of hydrogen bonds between the hard segments and the filler, which in turn improves the mechanical and thermal properties of the polyurethane nanocomposite [73].

It has been found that polyurethane using polyether-based diol with silica nanoparticles increases its mechanical properties[71]. Polycarbonate-based compounds using colloidal silica showed that at 5% by weight they increased their resistance to water, increasing the percentage of load improved their thermal stability, however at 32% by weight it is the maximum found to improve mechanical properties, after that percentage decreases[75].

Nevertheless, it is not enough previous articles of the effect of nanoparticle morphology on mechanical and thermal properties are still ongoing, so this work seeks to contribute to the interactions between these properties.

3.2 Materials and methods

3.2.1 Materials

Polycarbonate-based macrodiol T5652 was provided by Asahi Kasei Co. Japan. 1,6-hexamethylene diisocyanate (HDI), 2,2/Bis(hydroxymethyl) propionic acid (DMPA), trimethylamine (TEA) were received from Sigma-Aldrich. Dried acetone was provided by Merck, Germany. The catalyst, dibutyltin dilaurate (DBTDL) was dissolved at 10% by weight with mineral oil (Macrol). Ludox® AS 40, is the monodisperse, ammonium counter ion colloidal silica 40% wt suspended in water.

3.2.2 Synthesis of PUD's

Samples with different ratio macrodiol:diisocyanate (Y), containing different structure, linear or branched, were prepared as follows. Polycarbonate macrodiol T5652 was mixed with DMPA in dried acetone and they were mixed until dissolution, then HDI (7.8265 mmol) and DBTDL (0.0209 g) were added, heated at 60 ℃ for 5 hours and mixed with magnetic bars. Then, TEA (1.5051 mmol) and more acetone were added to maintain the viscosity, and it soaked for 12 hours. Then, water was added drop by drop under continue stirring (700 rpm) at room temperature, because is the re-arrangement for the large chains to microspheres, and wait for 3 hours to efficiently mix. Finally, the acetone was removed using a rotavapor under vacuum at 60 ℃. The reaction schema is presented in the Figure 7.

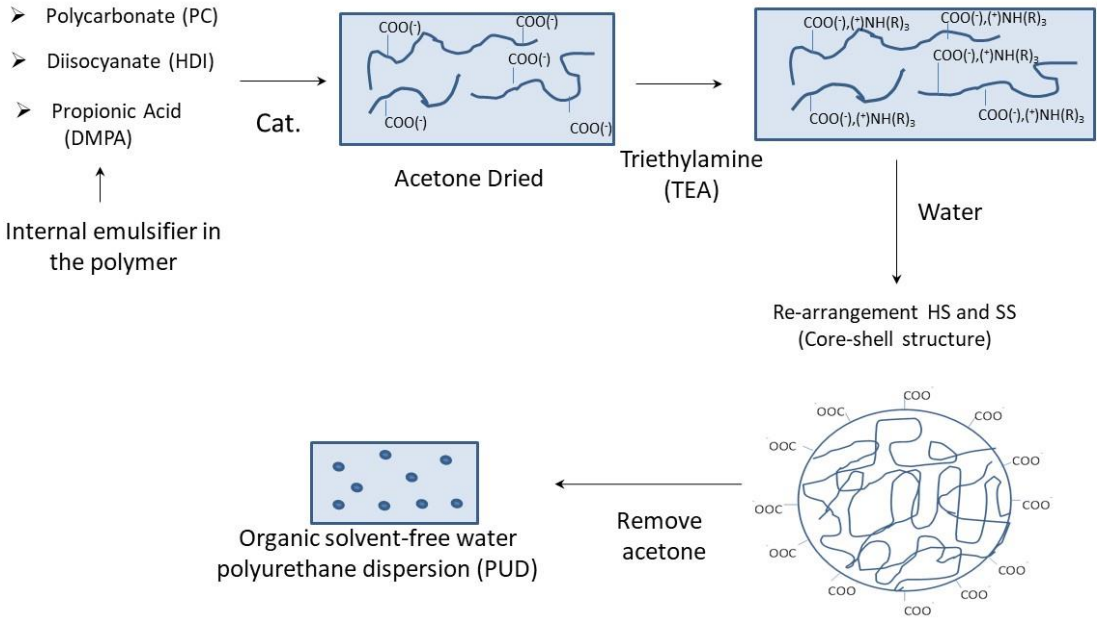

Figure 7. Scheme of PUD reaction.

3.2.3 PUD's Composites

The PUD was mixed with appropriate amount of nanosilica, in order to obtain nanocomposite film containing 5 wt %, 10 wt %, 20 wt %, 30 wt %, 40 wt % of

colloidal silica for 1.5 h by magnetic stirring, after 2 cycles of 15 minutes by ultrasonic bath, then the solution soaked for 30 min. The Figure 8 show the scheme of PUD composite.

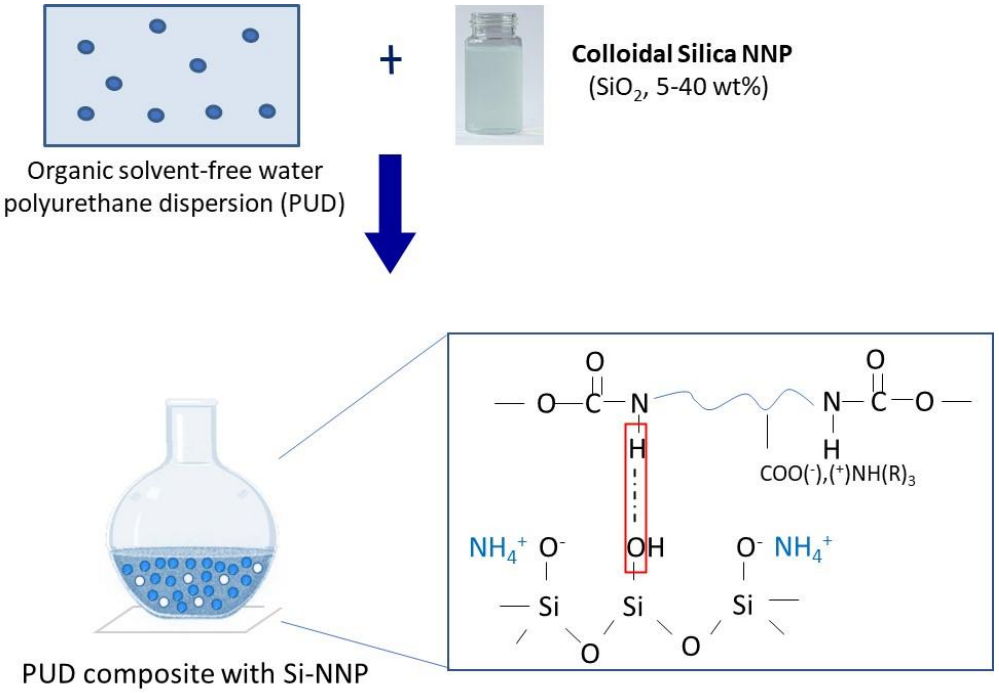

Figure 8. Scheme of PUD composite.

3.2.4 Membrane preparation

All films were prepared by casting the PUD or PUD- filler into Teflon mold followed by slow drying at room temperature for 4 days. After such time the rest of water was removed at 50 ℃ for 20 h and finally dried at 50 ℃ with vacuum for 2 h (Figure 9).

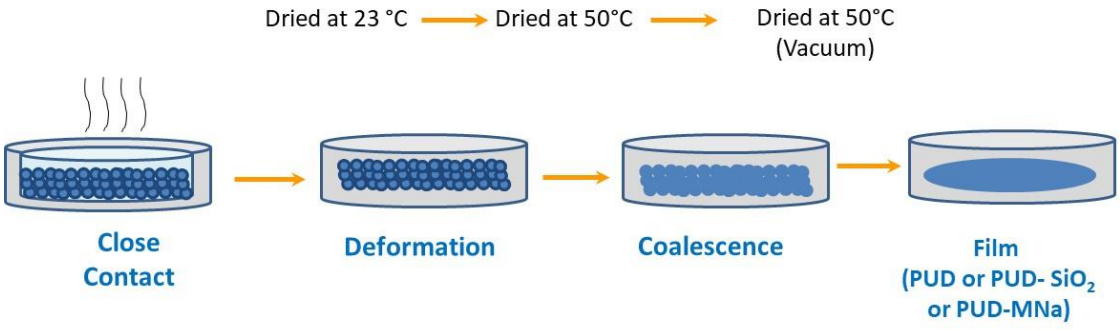

Figure 9. Scheme of film formation.

3.3 Membrane Characterization

3.3.1Tensile test

The stress-elongation tests of each sample were obtained using a universal machine model 5800 (Instron) equipped with a 100 N load cell, according to ISO 527 (speed of 100 mm/min at room temperature).

3.3.2 Fourier-transform Infrared Spectroscopy (FTIR)

The correlation of the content of microdiol for formation of polyurethane was determined by infrared spectroscopy (Fourier transform, FTIR) using Perkin-Elmer Paragon 1000PC FT-IR spectrometer with ATR (attenuated total reflection) additament. All the spectra were measured at wavelength range 4400–450 cm^{-1}, with a resolution of 4 cm^{-1} and 64 scans per sample. Spectrum v2.00 software was used for processing the spectra. In addition, Magic plot was used for deconvolution or the spectra to obtained the degree of phase separation.

3.3.3 Solid state Nuclear magnetic resonance spectroscopy (ss-NMR)

Solid-state NMR spectra was measured at 11.7 T on a Bruker Avance III HD 500 US/WB NMR spectrometer (Karlsruhe, Germany, 2013), and the following techniques were applied: ^{1}H static; ^{1}H, ^{13}C, and ^{29}Si magic angle spinning (MAS) and cross-polarization (CP) MAS NMR experiments.

3.3.4 Differential Scanning Calorimetry (DSC)

Thermal behavior and changes on structure of the hard or soft segments were studied by Differential Scanning Calorimetry using a PerkinElmer DSC-7 with constant nitrogen flow. Around 10 mg of each sample was, 10 ºC/min heating rate from -90 ºC up to 200 ºC.

3.3.5 Atomic Force Microscopy (AFM)

Analysis of the topology of PUD films and dispersity of silica and montmorillonite particles into PUD matrix and analysis of the nanocomposite structure were analyzed by Atomic Force Microscopy model Dimension Icon, Bruker, equipped with the SSS-NCL probe, Super Sharp SiliconTM-SP-Sensor (NanoSensor ™ Switerland; spring constant 35 N/m, resonant frequency around 170 kHz). The measurements were performed under ambient conditions using tapping mode AFM technique.

3.3.6 Scanning Electron Microscopy (SEM)

The morphological analysis of the sample was carried out by Scanning Electron Microscopy model Vega Plus TS 5135 from Tescan, Czech Republic. Before SEM analysis the samples were recovered with 4 nm Pt layer using vacuum sputter coater SC 050 by Balzers.

3.3.7 Transmission Electronic Microscopy (TEM)

The films were cut on as ultrathin sections by ultramicrotome with cryo attachment (Ultracut UCT, Leica) at -110 ºC. The sections were transferred to supporting Cu grids and observed using a transmission electron microscope (JEM 200CX, Jeol) at 100kV. The TEM photographs were digitized with a digital camera (DXM1200, Nikon). The contrast and brightness of the digitized TEM photographs were adjusted using standard software.

3.3.8 Dynamic Mechanical Thermal Analysis (DMTA)

Dynamic mechanical thermal analysis was carried out on ARES LS2, Rheometrics Scientific (now TA instruments) using oscillation frequency of 1 Hz, deformation ranging from 0.01% (glassy state) to 3.5% (maximum deformation allowed), over a temperature range of –100 to 180 C, at a heating rate of 3 ºC/min. Dynamic torsion measurements were performed using rectangular samples, to which a constant tension force of 5 g was applied. The standard specimens dimensions were 25 mmx3mmx2 mm. Storage modulus (G'), loss modulus (G") and loss factor (tan δ, tan δ=G"/G') were measured. In this work, the glass transition temperature was defined as temperature of maximum value of tan δ curve.

3.4 Results and Discussion

3.4.1 Water based polyurethane with different NCO:OH ratio

3.4.1.1 Synthesis, chemical structure and hydrogen bonding

The synthesis of polyurethanes was carried out by acetone process, without any chain extender. However, as water reacts with excess of isocyanate during the phase transition, it is possible to consider water as a special chain extender/crosslinker. Figure 10 shows the steps involving the process to obtain the waterborne polyurethane dispersion (PUD). The ratio leading to the different formulations is $[NCO]:[OH]_{total}$, where $[OH]_{total}=[OH]_{PC}+[OH]_{DMPA}$, in this case varied from 1:05 to 1:50.

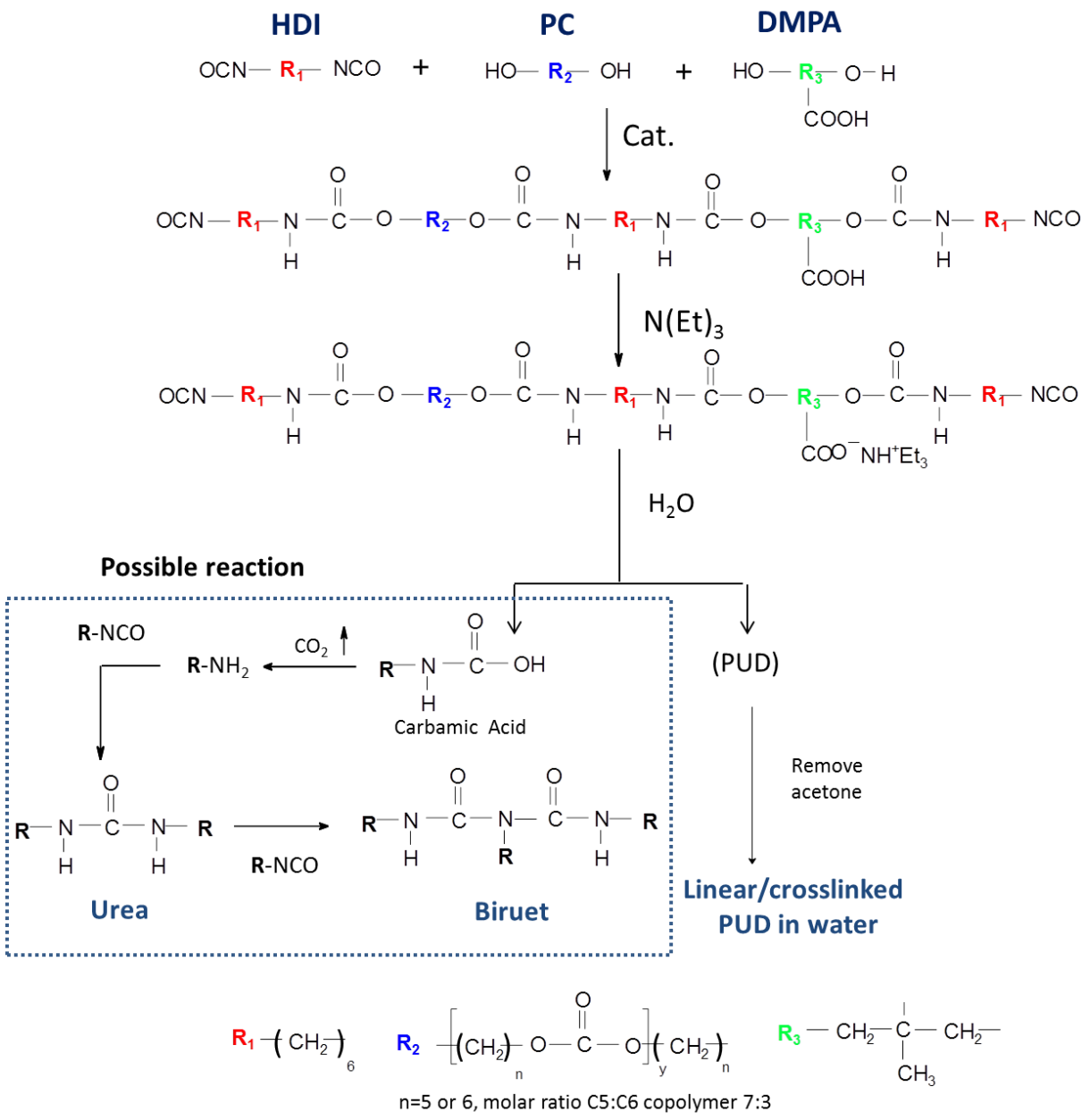

Figure 10. Reaction scheme of waterborne polyurethane dispersion synthesis.

The chemical structure was identified by FT-IR spectroscopy, it was possible to demonstrate the complete conversion of isocyanate groups and the formation in hard segments into PU (Figure 11).

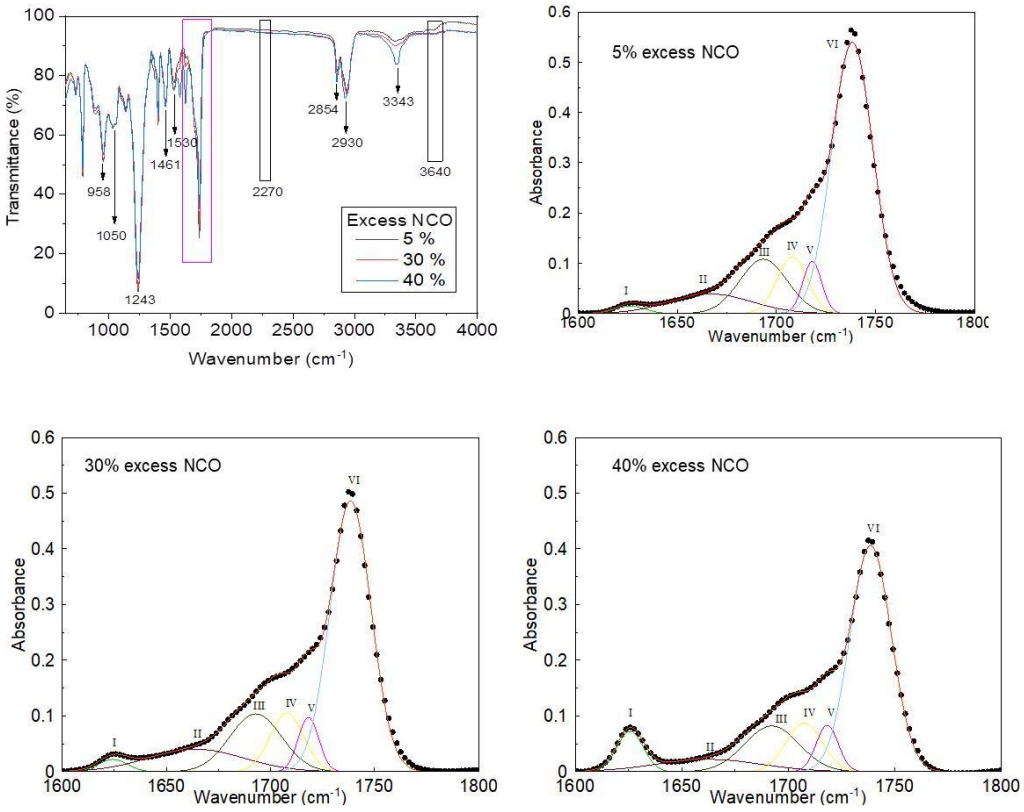

Figure 11. FT-IR of PU with different isocyanate: diol ratio.

In Figure 11, it is possible to observe the vibrations corresponding to PU. The absence of peak 2270 cm^{-1} shows that all isocyanate reacted and it does not appear any residual, also does not appear the peak at 3640 cm^{-1} corresponding to free amidic NH groups not engaged in H-bonds, the vibration at 3343 cm^{-1} of the amidic NH engaged in the hydrogen bond is weak, indicating a low concentration of these groups. Anti-symmetric and symmetric stretching of CH_2 corresponding to soft chain segment are visible in peaks 2854 and 2930, respectively, also the peak 1471 cm^{-1} corresponding to symmetrical bending of CH_2. The peak at 1530 cm^{-1} corresponds to couple symmetry bent vibration of N-H bond and stretch vibration of the amidic C-N. The strong peak at 1243 cm^{-1} corresponds to anti-symmetrical O-C=O in the soft segment and the peaks 1050 and 958 cm^{-1} corresponding to stretch vibration of C-O-C in urethane group and symmetric stretch C-O-C in carbonate group. In addition, it was analyzed the stretching region of carbonyl, between 1600 to 1800 cm^{-1}, that was necessary to deconvoluted, because in this range of carbonyl group different vibrations are overlapped. Table 5 shows the vibration of carbonyl group.

Table 5. Vibrations of carbonyl group.

Number	v (cm^{-1})	Vibration

I	1624-1626	Strongly bonded urea
II	1661-1667	Weakly bonded urea
III	1692-1693	Biuret+H-bonded carbonate
IV	1707-1708	Free carbonate
V	1717-1718	H-bonded urethane
VI	1738-1739	Free urethane

The Figure 12 shows the spectra of FT-IR composites of PU with 5 wt % SiO_2.

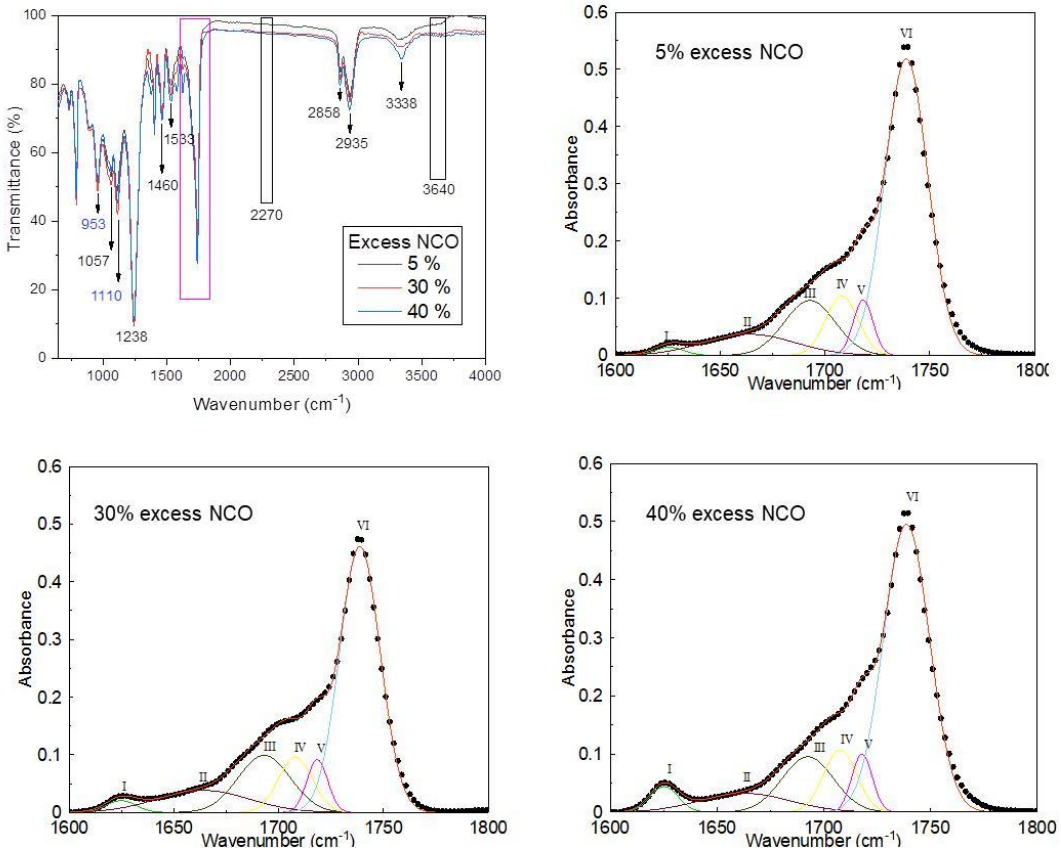

Figure 12. FT-IR of PU with 5% SiO2 different ratio of isocyanate.

The samples of PU with 5 wt % SiO_2 show the specific peaks corresponding to stretching vibration of Si-O at 1030 cm^{-1} and the peak at 880 cm^{-1} shows a slight shift corresponding to Al-Al-OH. It is slight the change in the peaks when increase of NCO excess, because they are overlap with the PU peaks. Finally, the degree of phase separation 'DPS' (hard segment linking with hard segment) and the degree of

phase mixing ‘DPM’ (degree of soft segment with hard segment), were calculated by equation 4 and 5 and are reported in Table 6 [74].

$$DPS = \frac{C_{bonded}}{C_{bonded}+C_{free}} \qquad \textbf{Equation 3}$$

$$DMP = 1 - DPS \qquad \textbf{Equation 4}$$

The carbonyl groups deconvolution allowed to found the peaks that are hided in the curve, once that is obtain all the peaks in the Table 6 is possible to obtain the area behind curve from 1600 to 1800 cm^{-1} with Gaussian-A.

Table 6. Degree of phase separation and degree of mixing in PU.

Sample code	DPS	DPM
5/Pure	0.39	0.61
5/SiO_2	0.38	0.62
30/Pure	0.44	0.56
30/SiO_2	0.44	0.56
40/Pure	0.45	0.55
40/SiO_2	0.39	0.61

As it can be seen from Table 6, the values of pure sample increased as the amount of NCO groups increased, and also the filler concentration increase the degree of phase mixing since the filler reduces the molecular degree freedom to rotate and the rigid segment affected the hydrogen interactions.

3.4.1.2 Structural and segmental dynamics

For structural and segmental dynamics characterization ^{13}C and ^{13}C CP/MAS NMR spectra was used. ^{13}C MAS NMR applying with the relatively short repetition delay (2s) the measurement preferentially detects NMR signals of highly flexible polymer segments and ^{13}C CP/MAS NMR to detect of rigid and semi-flexible components. The ^{13}C and ^{13}C CP/MAS NMR of the prepared samples with the 5 % mol, 30 % mol and 40 % mol NCO excess relative to the hydroxyl groups its present in the Figure 13.

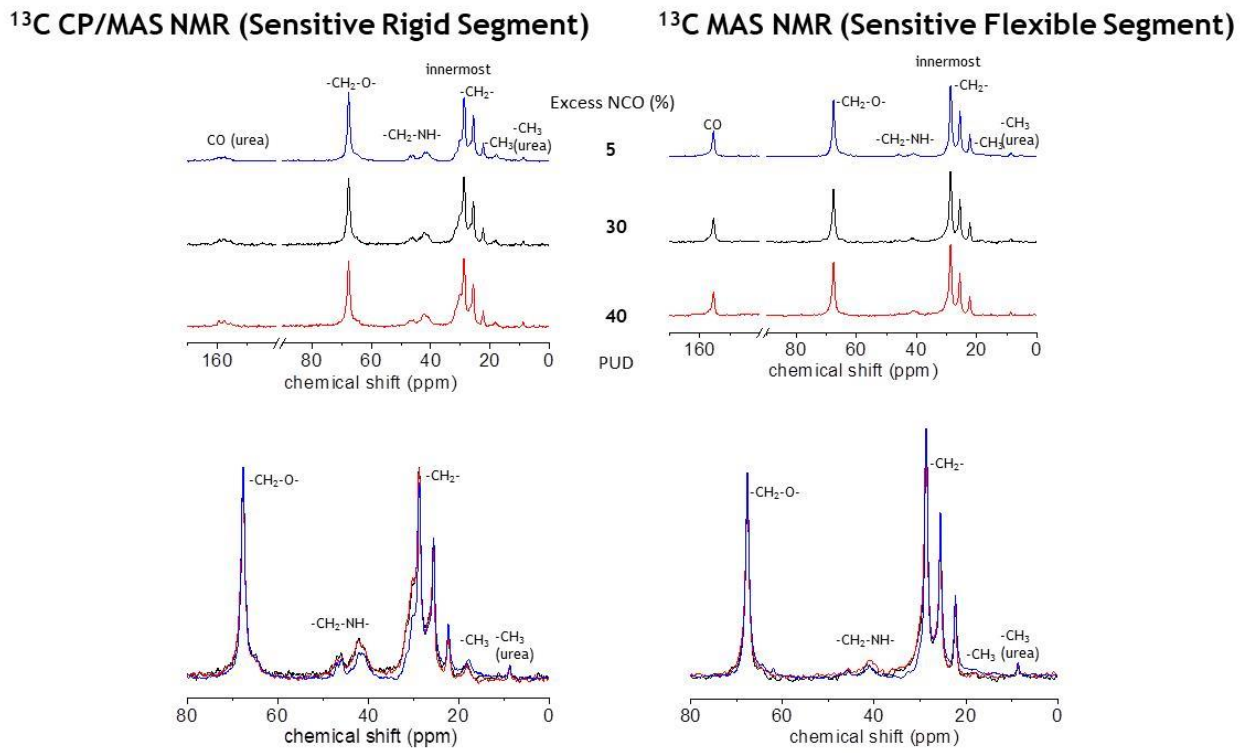

Figure 13. The ^{13}C and ^{13}C CP/MAS NMR spectra of the prepared samples with the excess NCO 5 mol %, 30 mol % and 40 mol %.

The results indicate small differences in sample 5 % mol (blue spectra) in comparison with samples 30 %. mol and 40 % mol. Thus, confirmed that the variations in macroscopic properties such as mechanical properties are not emerge at the molecular or segmental levels.

3.4.1.3 Thermal and mechanical stability

The mechanical properties were evaluated by universal machine to analyze the effect of fillers into the PU matrix. Figure 14 shows the curves for PU pure, and samples with different NCO:diol ratios.

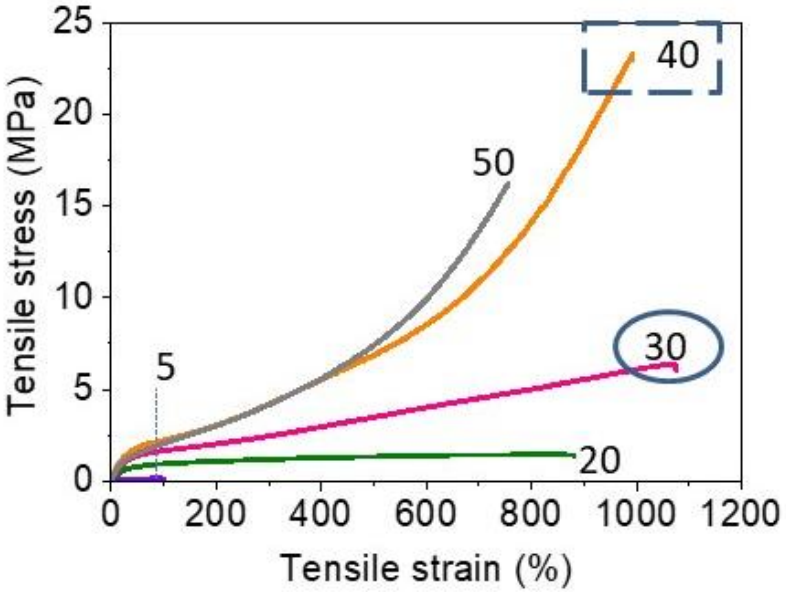

Figure 14. Tensile properties of PU pure films with different fillers and variety ratio of isocyanate. (The number 5, 10, 20, 30, 40 and 50 means molar isocyanate excess percentage).

It is possible to observe that the lowest ratio with 5% NCO excess has the lowest tensile stress because the structure is linear unlike the others. In case of the 30% NCO excess, the highest tensile strain was achieved, and 40% NCO excess leads to the highest tensile stress of all samples tested. As a result of the increase hydrogen bonding formation with urea and biurea, they started to generate entanglements stronger than linear structure.

Meanwhile, Silica has different interaction with PU matrix, because it is possible to observe that the value of the tensile strain decreases slightly in contrast with PU pure (Figure 15) in all the different ratios.

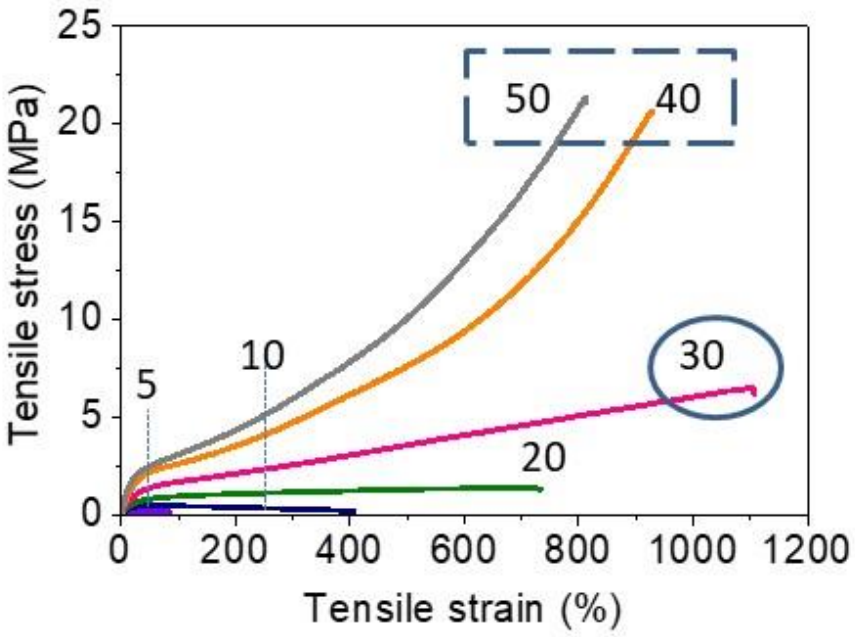

Figure 15. Tensile properties PU nanocomposite films with 0.5 wt % SiO2 at different ratio of isocyanate. (The number 5, 10, 20, 30, 40 and 50 means molar isocyanate excess percentage).

Due to, it is possible that when incorporating the silica nanoparticles, the contraction between the chains is generated and does not allow the free movement of these.

Concerning about thermal characteristics the Differential Scanning Calorimetry (DSC) was used to obtain the thermal transitions for the lineal structure PU (5 wt% of isocyanate excess), 30 and 40 mol % excess of isocyanate groups that they have the highest elongation and tensile stress respectively. The DSC thermogram in the Figure 16 shows the transitions of all the PUs without any filler.

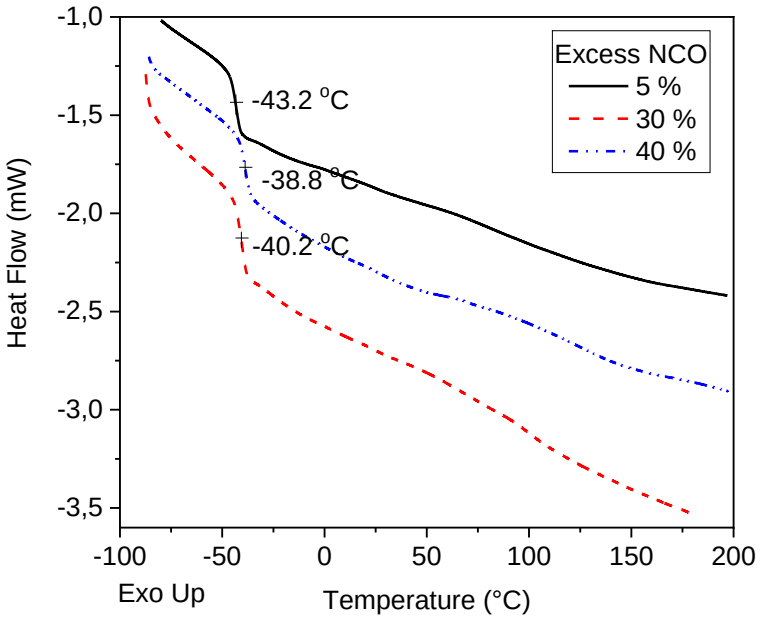

Figure 16. DSC thermogram of PU pure with different ratio of isocyanate.

It is possible to observe the Tg transition associated to soft segment, around - 43 °C, in the temperature interval evaluated. The slight difference of Tg values for the samples is not significative.

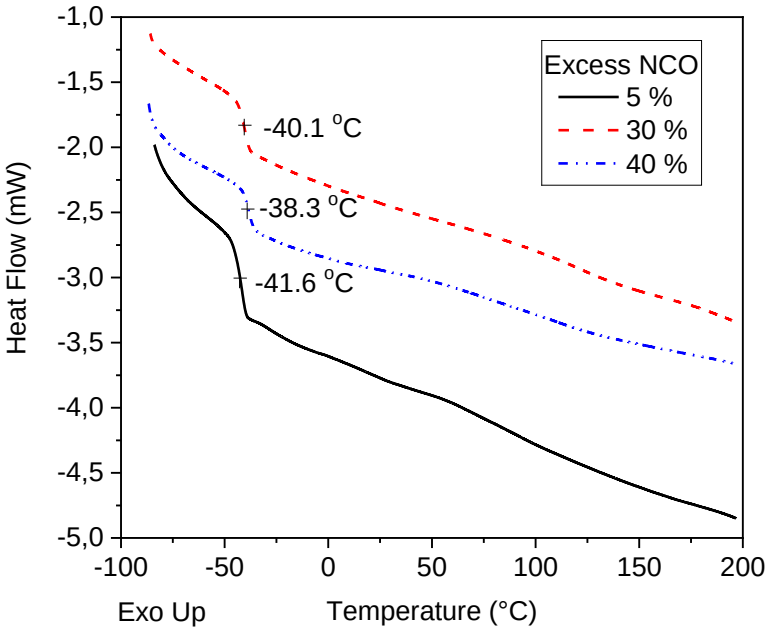

Figure 17. DSC thermogram of PU- 5% SiO_2 with different ratio of isocyanate.

The difference between the composite and pure PU is around 2°C and it is clear that it is not significant. From Figures 16 and 17 follows that Tg of pure PU and nanocomposites are practically not modified by the insertion of fillers.

3.4.1.4 Structure of PU and arrangement of filler in nanocomposites

The PU's are formed by soft and hard segments but they are not detectable by TEM analysis (Figure 18). On the other hand, the supramolecular arrangement of chain into organized formations (spherulites) were detected. The diameter of spherulites is about 1 μm in all three types of PUs, i.e. without or with nanofillers. In comparison with the literature, the spherulites size are smaller, since it is reported to be around 2.5 to 5 μm, but it depends on the content of the hard segment [76].

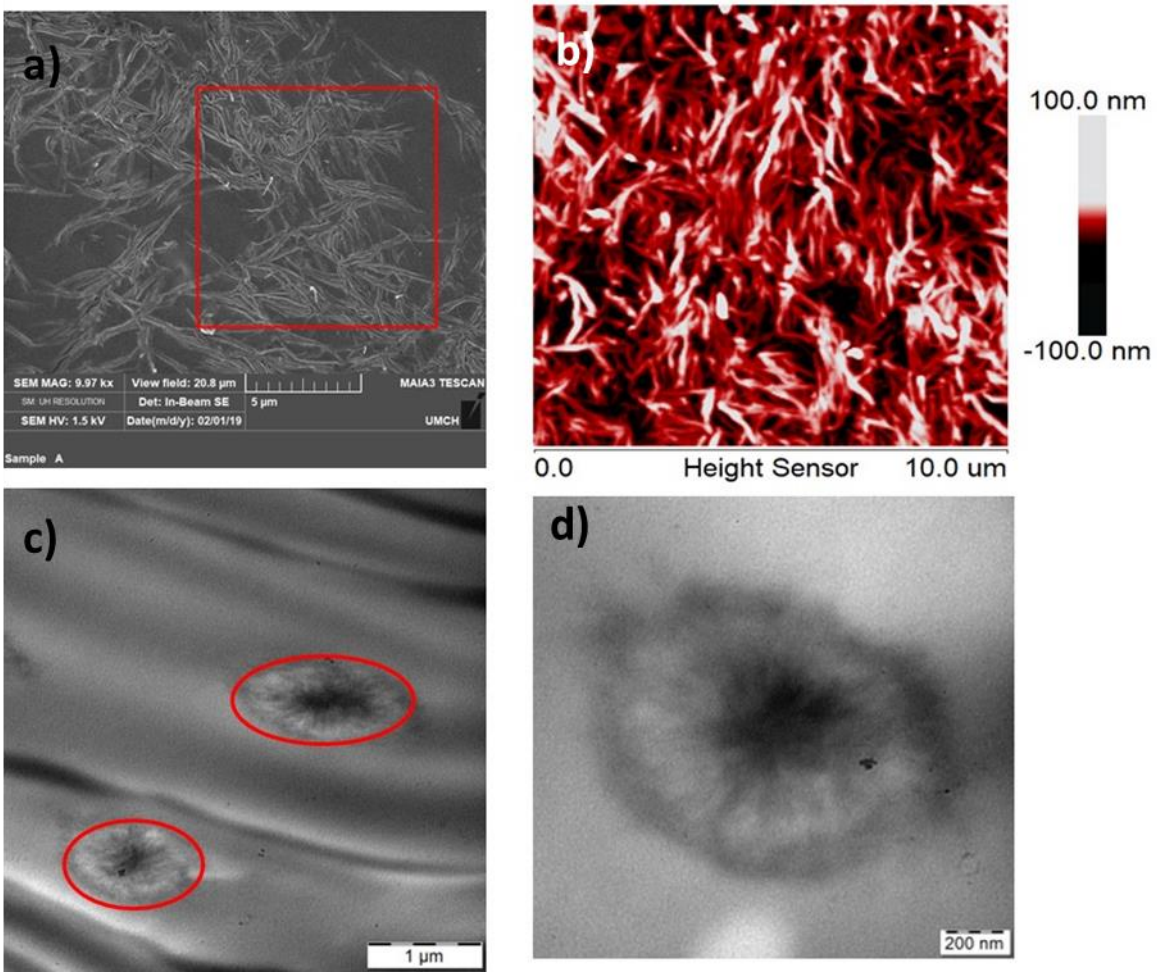

Figure 18. Micrographs by a)SEM, b)AFM, c) and d)TEM of films made from PUD prepared with 40 mol % NCO excess.

The surface morphology was evaluated by SEM and AFM, which successfully have made match, i.e., the results of both were congruent, it means, the fibril-structure of the surface was detected by both microscopy techniques.

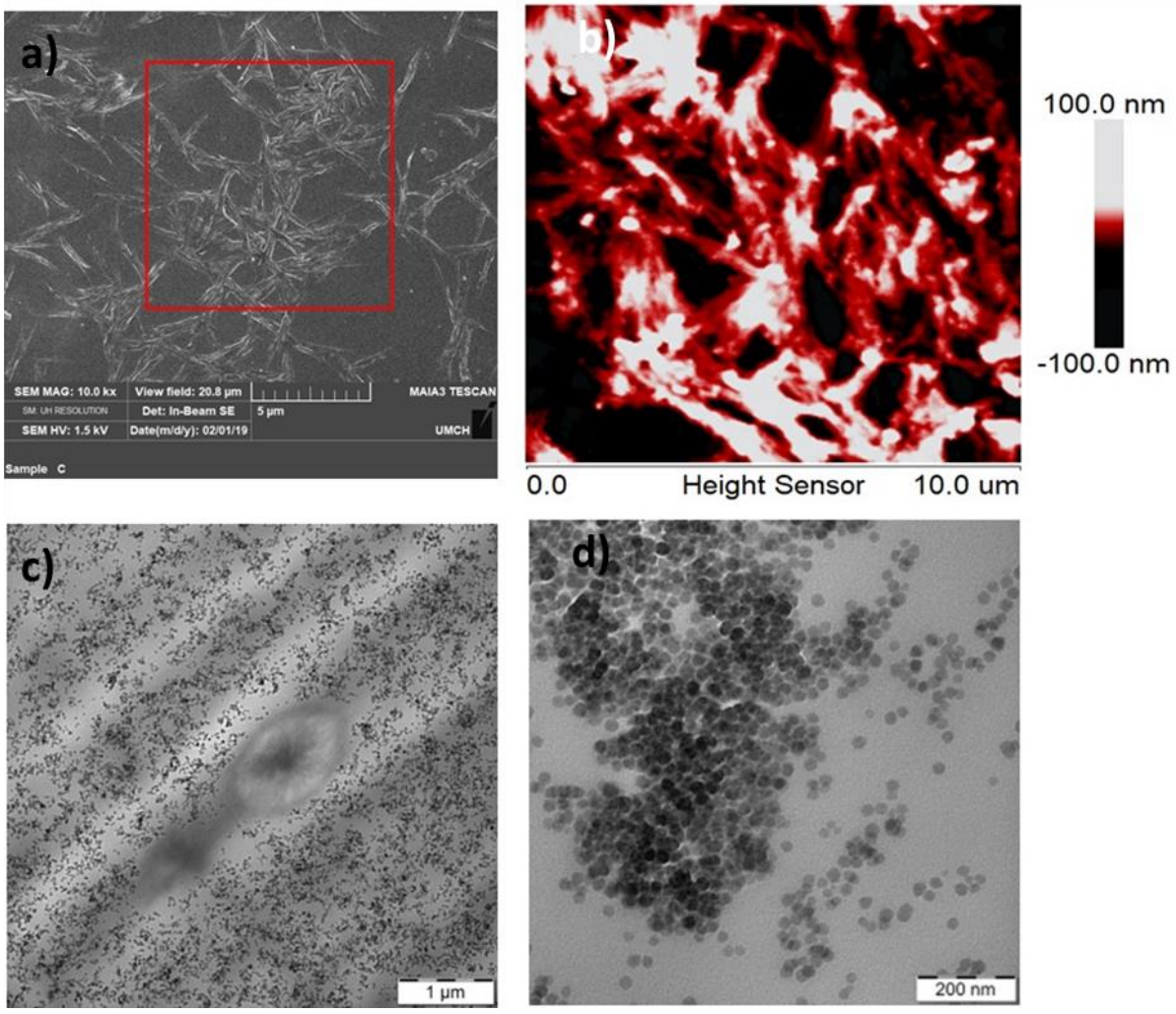

Figure 19. Micrographs by a)SEM, c) and d)TEM and b)AFM correspond to films made from PUD prepared with 40 mol % NCO excess with 5% SiO2.

On the other hand, colloidal silica has properly interaction with PU, resulting is well distributed, due to sphere structure, because the surface charge it is distribute around the all geometry and repulsion for another same particle. However, it is possible to find some particle agglomeration, due to the viscosity of the polymeric solution, to see Figure 19.

3.4.2 Composites with 40% molar ratio NCO:OH with different percentage of SiO_2

The addition of SiO_2 as filler for reinforcing PU was done after synthesis in these experiments. These hybrid materials has been attractive because the increase of mechanical properties as a consequence of the capability of silica particles to form hydrogen bonding with the PU matrix. The effect of the addition of filler on the properties of the film compounds is mentioned in the following analysis.

3.4.2.1 Effect of different content of SiO_2 on Transparency

The final film thickness was controlled by adjusting the volume of the dispersion used per unit area of the of the Teflon mold. Transparency resulted depending on the particular composition. The optical micrographs of the sample of 40 mol % excess of NCO with different content of SiO_2 (5, 10, 20, 30, 40 and 50 wt%) are shown in Figure 20.

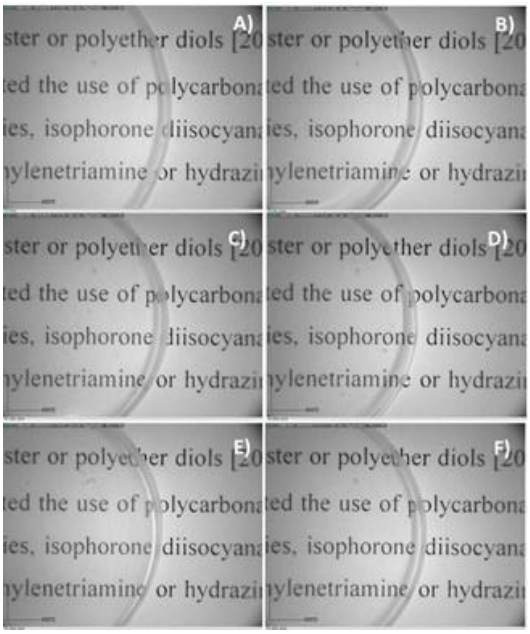

Figure 20. Optical transparency A) PU-pure, B)PU-5 wt % SiO2, C)PU-10 wt % SiO2, D)PU-20 wt % SiO2, E)PU-30 wt % SiO2, F)PU-40 wt % SiO2.

As it is well known, the transparency is effect of the polymer chains arrange; amorphous is transparent in contrast the crystalline arrangement is opaque. In this case the composite films do not exhibit a significant change with increasing SiO_2 content. It is possible that the addition of the filler is not enough to make the change evident in the regular structure.

In addition, chemical characterization, thermal and mechanical properties will be analyzed to demonstrate possible interactions between the filler and the PU matrix. As a result, it was possible to select some of them to be evaluated in detail by morphology.

3.4.2.2 Effect of different content of SiO_2 on Chemical Structure

In order to analyze the structure of the nanocomposite films, Fourier transform infrared spectroscopy was performed. Figure 21 shows the FTIR spectra for all the samples, indicating the main functional groups for the polyurethane.

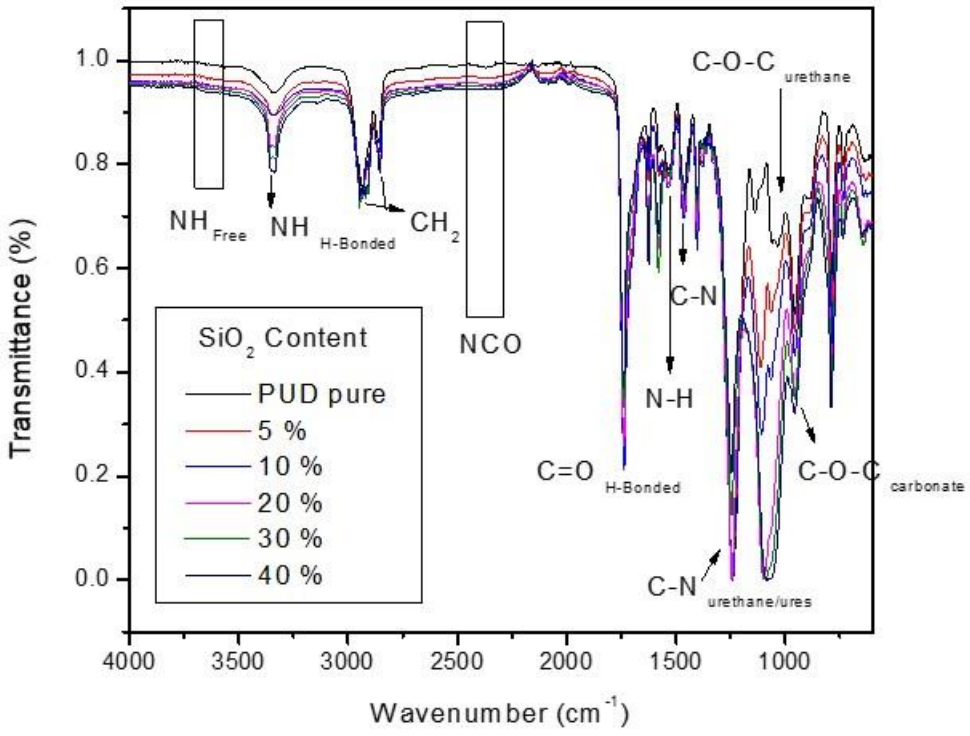

Figure 21. Spectrum FTIR related wavenumber with transmittance of all the PUD with SiO2 content.

As comparison it is important to mention the characteristic peaks for polyurethane. The peaks at 2854 and 2930 cm^{-1} correspond to anti-symmetric and symmetric stretching of CH_2 into soft chain segment, also the peak 1471 cm^{-1} corresponds to symmetrical bending of CH_2. The peak at 1530 cm^{-1} corresponds to couple symmetry bent vibration of N-H bond and stretch vibration of the amidic bond C-N. The strong peak at 1243 cm^{-1} corresponds to anti-symmetrical O-C=O in the soft segment and the peaks at 1050 and 958 cm^{-1} correspond to stretch vibration of C-O-C in urethane group and symmetric stretch C-O-C in carbonate group, respectively.

The absence of unreacted isocyanate peaks (2270 cm^{-1}), demonstrates that it is not present even like residual, due to all isocyanates are reacted during PUD synthesis. Also, the free amidic group peak at 3640 cm^{-1} does not appear because all amidic

groups area engaged in hydrogen bonds, instead to the existence of bonded N-H at 3343 cm^{-1}. The formation of this bonds have an impact the hard-hard segment.

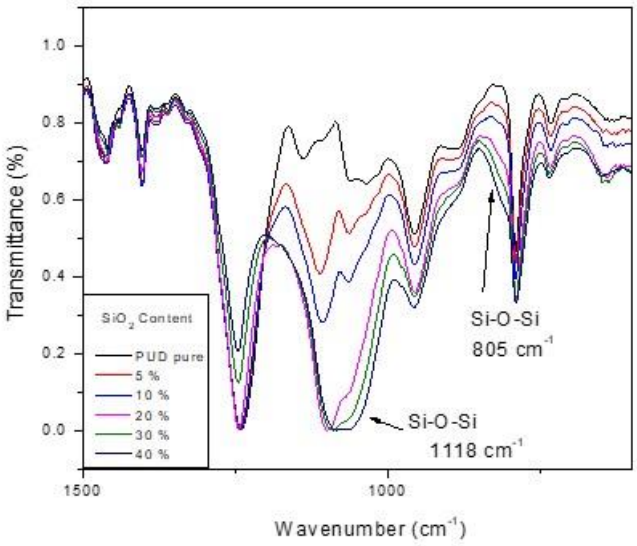

Figure 22. Spectrum FTIR related wavenumber with transmittance in 1500 to 600 cm^{-1} range of all the PUD with SiO_2 content.

On another hand, the characteristic peak of SiO_2 at 3452 cm^{-1} corresponds to OH groups, which is not visible in the spectrum. Nevertheless, in Figure 22 the other peak for Si-O-Si appears at 810 cm^{-1} and 1118 cm^{-1} in the first peak looks like shoulder when increase the percentage and the second appeared as widening in this peak.

Finally, it is important to mention that the possible interactions of PU matrix with SiO_2 particles is with the urethane and urea segment, that correspond to hard segment, due to the physical interaction appeared in peak urea C=O and N-H of urethane.

3.4.2.3 Effect of different content of SiO_2 on mechanical and dynamic properties

The tensile properties (Young's modulus, tensile strength, elongation at break, and energy to break) were determined by universal machine and the effect of SiO_2 content of the nanocomposites is shown in Figure 23.

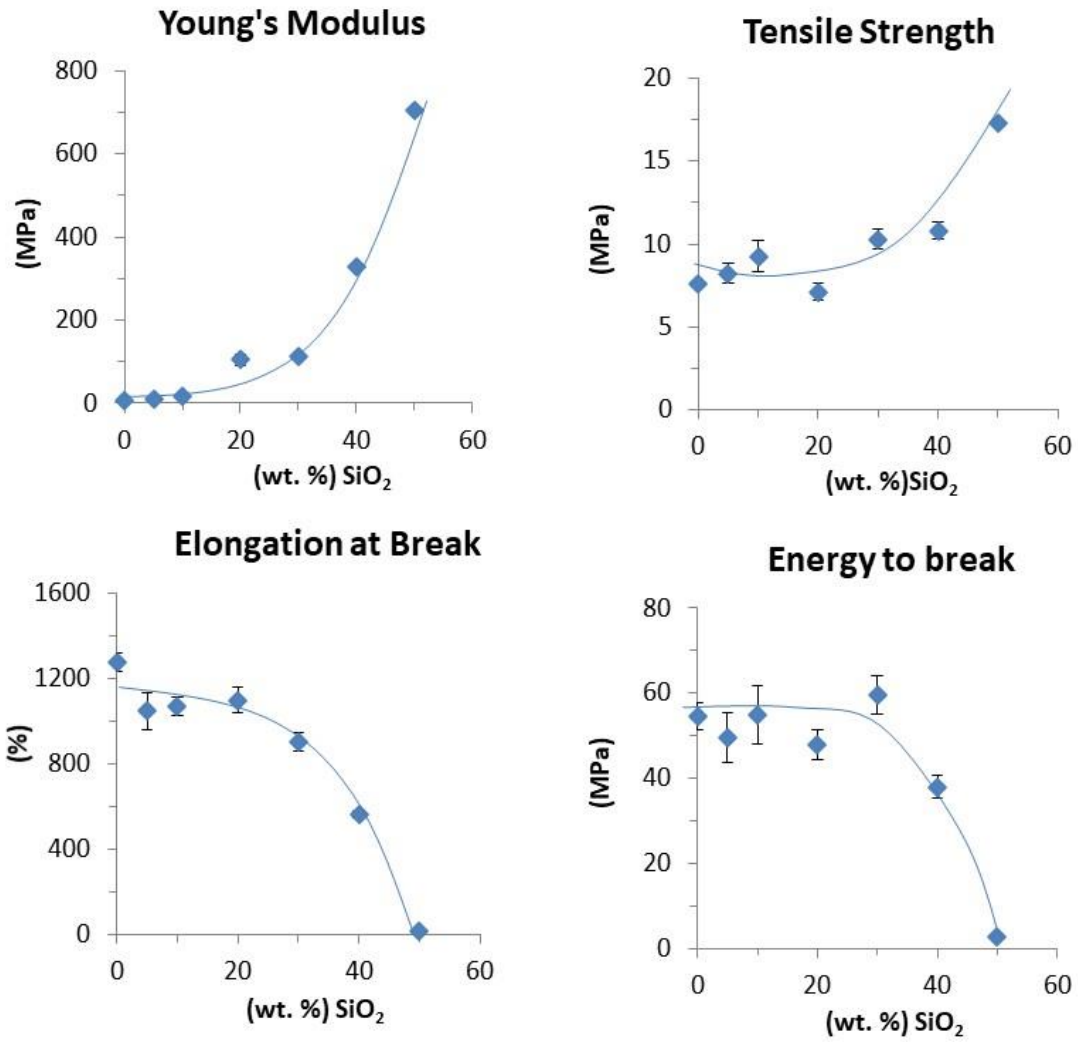

Figure 23. Tensile properties of PU films as a function of SiO2 content.

As it was mention previously, the incorporation of nanoparticles of SiO_2 do not allow the movement between chains, and as result the film shows a more rigid behavior and the aligning of the molecules was slowly giving higher tensile strength, when increase the percentage of the filler.

As consequences of increasing the Young's modulus the elongation at break decreased, because both properties have, usually, an inversed response.

Finally, the plastic deformation and dissipation of absorbed energy without break (toughness) shows that the pure PU film until PU-30 %SiO_2 film have almost the same toughness, it is possible that the dispersion of nanoparticles is enough to allow the absorption of stress without break. But at higher SiO_2 content (40 and 50 % wt) the toughness was reduced since the polyurethane matrix became stiff enough, probably due to agglomeration of filler nanoparticles.

Moreover, as a complement the storage modulus and glass transition temperature were obtained by dynamic mechanical thermal analysis to evaluated viscoelastic properties of PU-SiO_2 films (Figure 24).

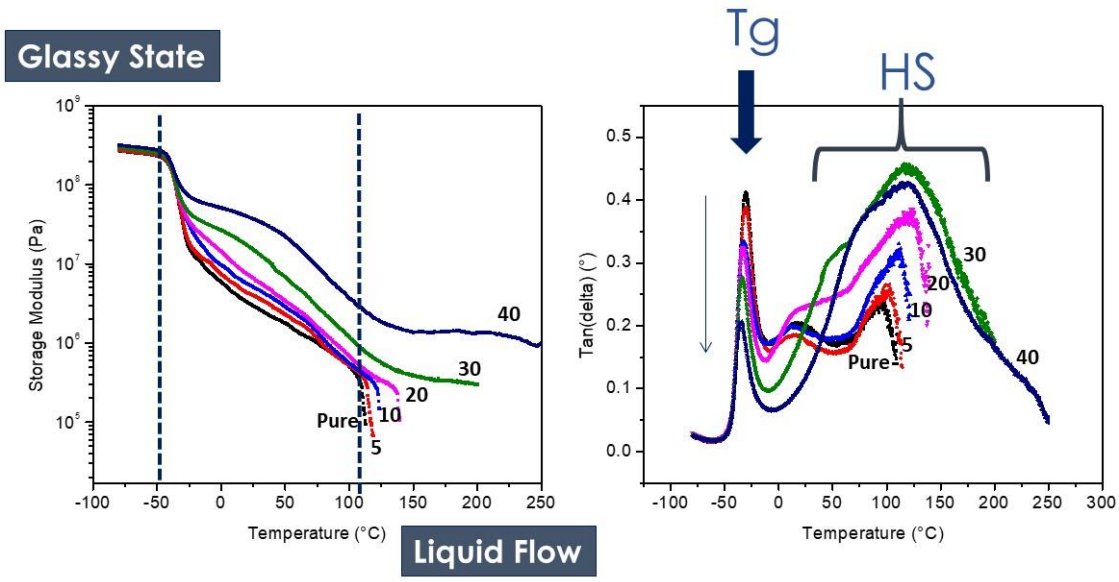

Figure 24. Storage modulus and loss factor tan δ as function of temperature.

The ratio of the loss modulus with storage modulus is represented as tan δ, which related with temperature show the glass transition temperature (Tg).

In this case it is observed that Tg did not suffer changes, since the interaction of SiO_2 is not strong enough with the amorphous portion of PUD. The second delta δ peak, associated with the flow zone, was slightly shifted toward higher temperatures as the SiO_2 content increased, probably due to blocking of PU chains mobility, which would imply more energy for movement due to the silica interacts more with the rigid portion of PU.

Additionally, the storage modulus with temperature show to transition, the first is the movement of the polymer chains of the soft segment and the second it is possible the disruption of hydrogen bonding between urethane groups in the PU sample and with low SiO_2 content, is registered in the temperature region above 110 ºC, showing a good compatibility of hard segment and silica.

Also, it is observed that the absence of a chain extender caused all nanocomposite films to not display a clear plateau region for the elastic modulus, probably due to a short rigid portion into the polyurethane. In addition that region increased as the silica content increased generated an impact that the interaction between nanoparticles and the rigid segment.

3.4.2.4 Effect of different content of SiO_2 on Structure of PU and dispersion of filler

SEM on top and transversal area was performed to analyze the surface characterization of the nanocomposite films. The Figure 25 shows the top of all the samples to compare the effect of the SiO_2 on the morphology.

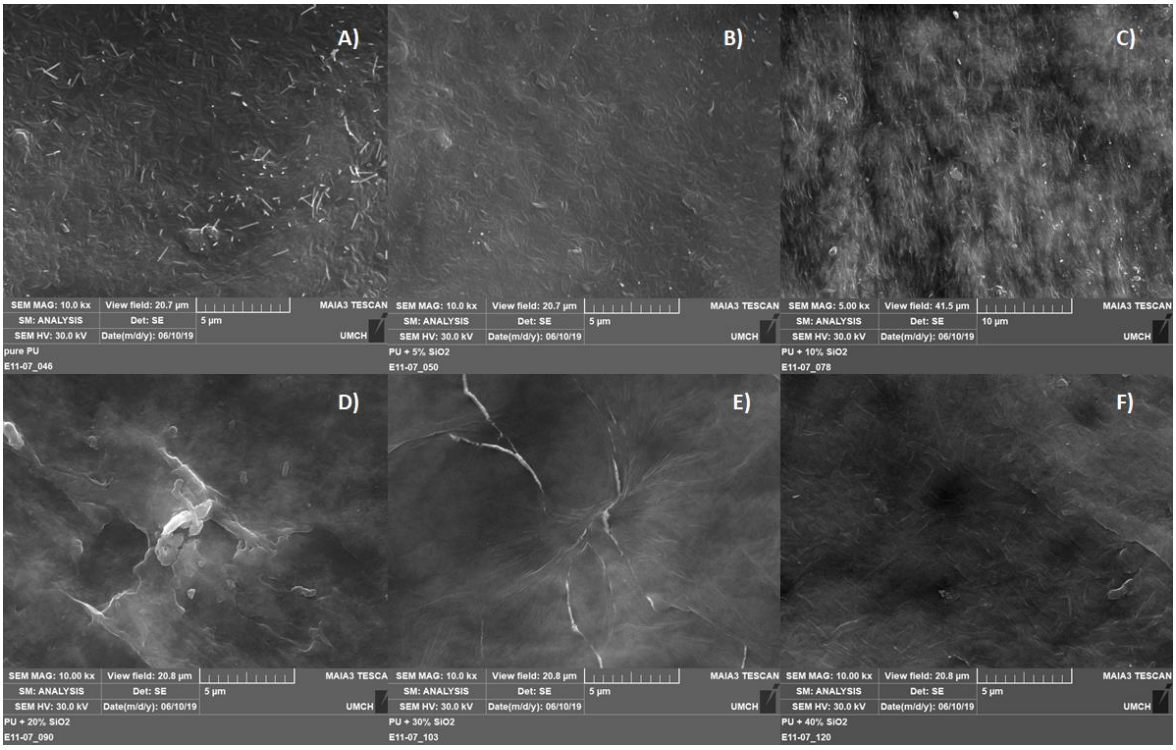

Figure 25. Surface area of the sample A) PU-pure, B) PU-5 wt % SiO_2, C) PU-10 wt % SiO_2, D) PU-20 wt % SiO_2, E) PU-30 wt % SiO_2, F) PU-40 wt % SiO_2.

The slow evaporation of water generated the flat and regular film with fine imperfections. Nevertheless, the films without filler present fibril-like structures, in contrast to films when increase the content of SiO_2 shows the "mountainous" irregular relief, with few scratches and cracks.

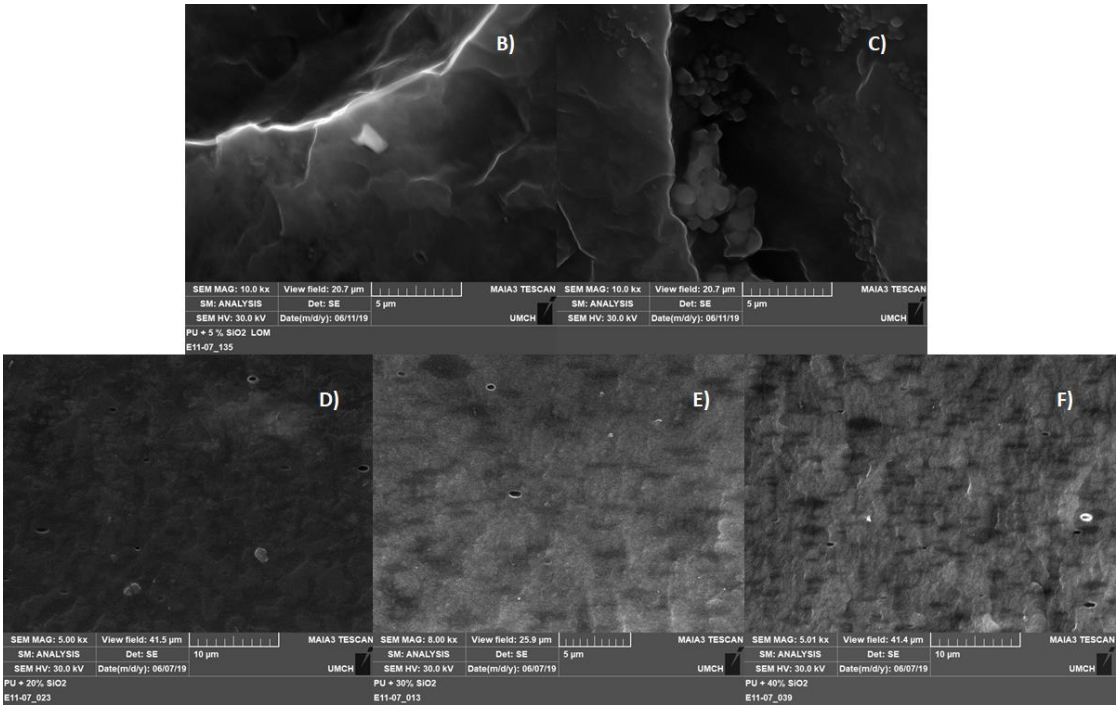

Figure 26. Transversal area of the sample B)PU-5 wt % SiO_2, C)PU-10 wt % SiO_2, D)PU-20 wt % SiO_2, E)PU-30 wt % SiO_2, F)PU-40 wt % SiO_2.

The pure PU sample shows a homogeneous surface of the fractured area, while the sample with 5 wt % SiO_2 shows individual particles with spherical shape, and their size was determined to be about 450nm, for the irregular agglomerates in the composite structure. In the case that silica content increased more than 20 wt % the interface becomes more heterogeneous and rougher than without filler, the effect is probably caused by the limited space to packing of the polymer chains forming PU films.

Additionally, the microstructural analysis for qualitative examination of the dispersion SiO_2 particles in the nanocomposite films was evaluated by TEM (see Figure 27).

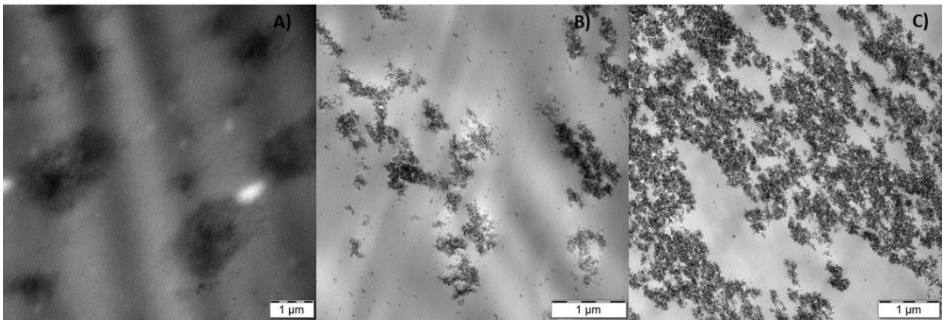

Figure 27. Transversal area of the sample A) PU-pure, B) PU-5 wt % SiO_2, C) PU-20 wt % SiO_2.

In the Figure 27 regular structure crystalline spherules, about 3 µm, were visible in the sample without SiO_2. It means, that during slow water evaporation and drying

the hard segment were self-assembled into organized structures to generate spherulites. In case of the sample with 5% SiO_2 few agglomerations are visible, while in the sample with 20% SiO_2 the agglomerations were more distributed in the nanocomposite film. The spherulites are not visible in the composite films, it is possible that the agglomeration of SiO_2 particles limited the space to polymer chains arrangement in the regular structure.

3.4.2.5 Effect of different content of SiO_2 on Gas transport properties

The influences of SiO_2 nanoparticles content in the films nanocomposites were determined. Thus, the figure 28 shows permeability (barrer), solubility (mol/m^3 Pa) and diffusion coefficients (m^2/s) as function of SiO_2 content (%).

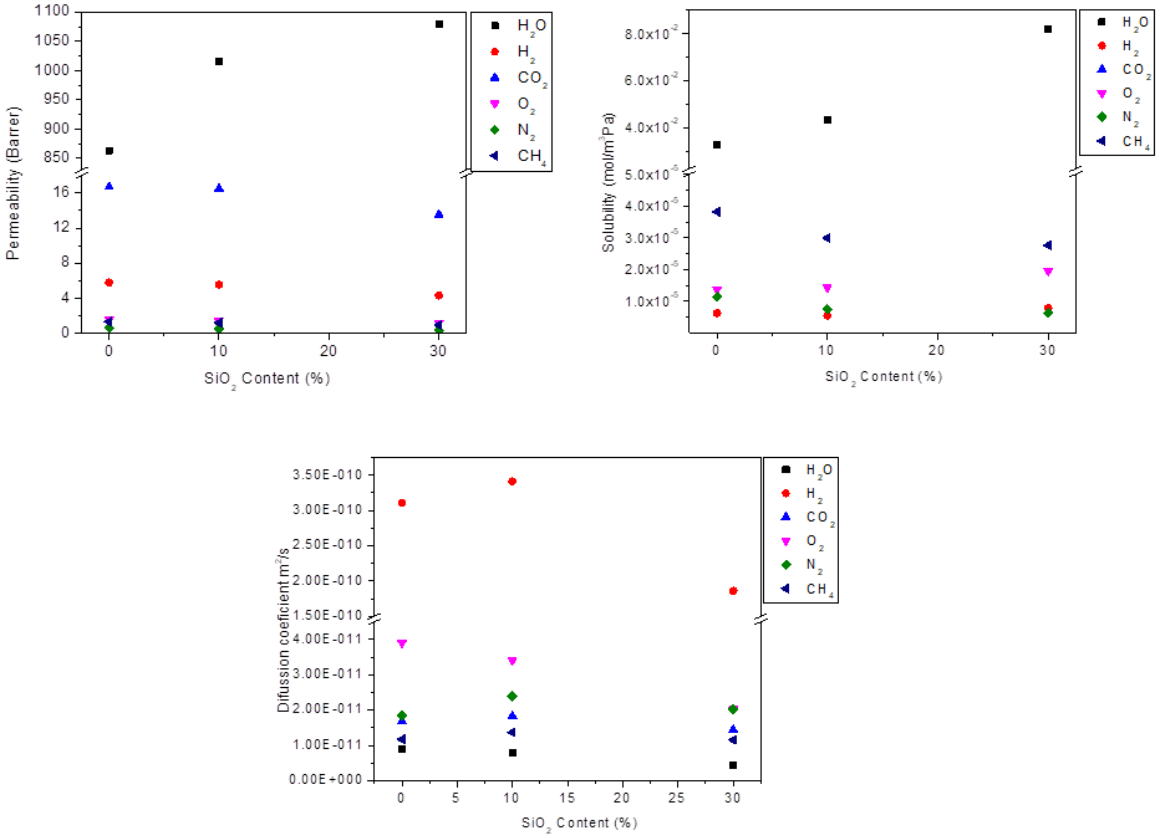

Figure 28. Permeability, solubility and diffusion coefficient with SiO_2 content.

Permeability and solubility of water vapor are higher for more than one magnitude order than those for other gases. The gas transportation properties depend on the constitution of PC chain, in this case the PU base macrodiol T5652 is irregular, but when the SiO_2 nanoparticles were incorporated the structure is more regular and the permeability and selectivity of the other gases are lower that without filler. In contrast, with water vapor the influence of filler incorporation increases in both properties.

Furthermore, it is clear that H_2 has the higher coefficient diffusion and water vapor has the lowest, that means that the molecular size affects the diffusion through the polymer film.

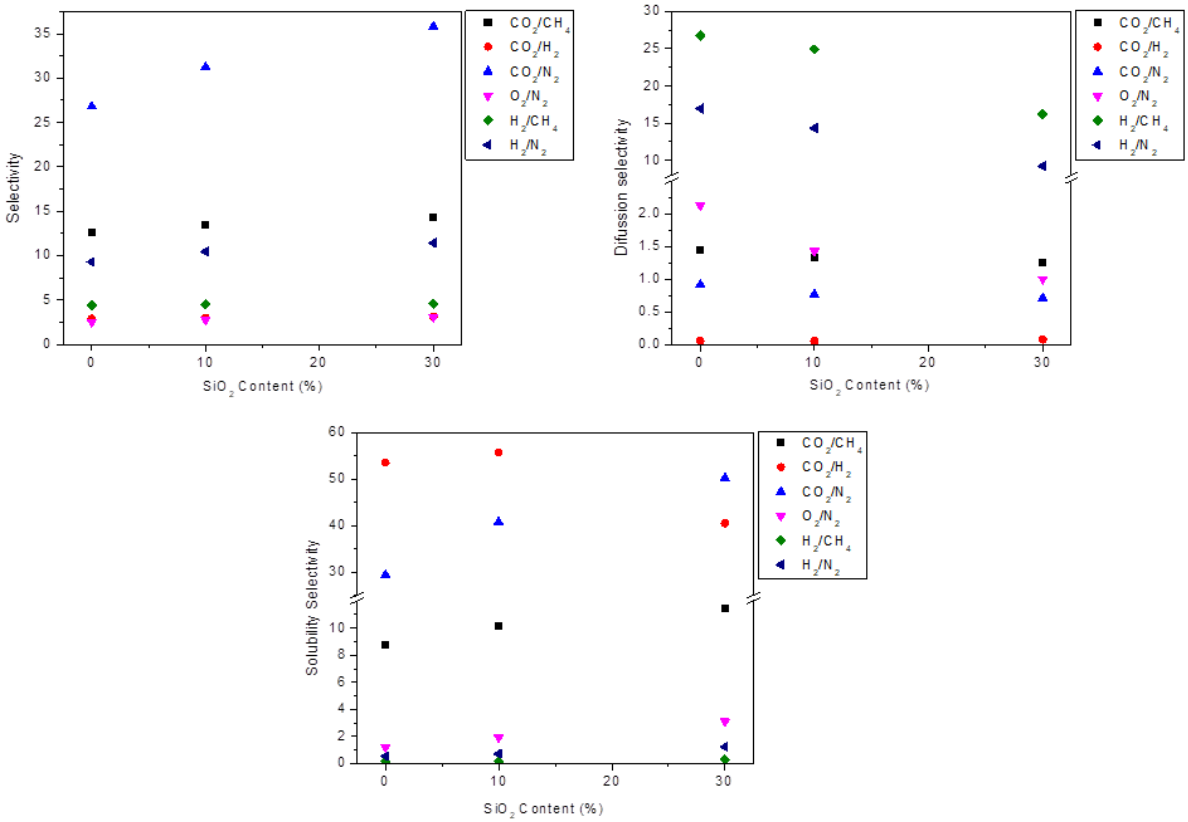

Figure 29. Selectivity, solubility selectivity and diffusion selectivity with SiO2 content.

Finally, the effect of SiO_2 content on the selectivity of the membrane depend of the pairs of gases. In case of CO_2/N_2 the CO_2 is the gas with heights selectivity, in case of the diffusion selectivity the H_2/CH_4 the PU pure film is the heights value. Also, the solubility selectivity CO_2/H_2 the CO_2 has not significant change with 10 % wt SiO_2 but when increases the content of the filler the value of the solubility selectivity decreases.

3.5 Conclusions

FTIR and NMR analysis show that it is not a significant interaction at molecular level between polymer and filler, do to the interaction by hydrogen bonds with hard segment are not enough strong to be detected. However, by DMTA it is evident the effect on the elastic behavior when increase the amount of SiO_2, due to the hard segment interactions with the filler.
Finally, the gas transport properties revealed that water vapor permeability increased in presence of silica because of more open structure and CO_2 is more selectivity.

Chapter 4. Development of membrane based on thermoplastic polyurethane using the stretching process

4.2 Background

4.1.1 Thermoplastic Polyurethane (TPU)

Thermoplastic polyurethane (TPU) is an alternating block copolymer consisting of a soft segment (SS) and a rigid segment (HS) [77]. This material can be process by extrusion, injection, coextrusion, such as commonly used with thermoplastics, however, it in turn exhibits properties of a vulcanized polymer. TPU include high toughness and abrasion resistance, high strength, as well as high elasticity and extensibility. These characteristics are due to strong physical attractions such as Van der Waals forces, hydrogen bridges, and chain entanglement [78,79]. The synthesis method to obtain these materials can be by "one-shot" or "two-shot" process. The one-shot method consists of mixing all the reagents in the established stoichiometric proportions, then pouring them into a mold in which the reticulation reaction is carried out, so that the polymer is shaped like the mold. In the two-step method, first the reaction of the diisocyanate with the oligomer is carried out to obtain the prepolymer and then the prepolymer is reacted with a short organic diol called a chain extender [80].
The properties, morphologies and final structure depend on various physical, chemical and structural factors, listed below:

a) The method, procedure and reaction conditions in the synthesis.
b) The chemical structure, structural symmetry, hydrogen bonding, average chain length, as well as length distribution in the rigid segment.
c) Molecular weight and chemical structure in the soft segments.
d) The extent of hydrogen bonding interactions between the hard segments and interactions between HS and SS.
e) Composition with respect to the fraction of hard and soft segment in the polymer.
f) Thermal history and processing methods of the polymer.
g) The presence of chemical cross-linking.

As it can be seen, there are several factors that condition the final characteristics of a thermoplastic polyurethane. Due to its nature, as it is composed of segments, there is an inherent immiscibility between those segments and they tend to segregate from each other, forming microphases[81] .

4.1.2 Method for obtaining micropores

Conventional techniques for the generation of micropores in dense films is by laser drilling. ArF, KrF and ultrafast lasers have been used as an efficient tool for precise microstructure in polymeric materials. This technique has been used with PLA for

the formation of cell tissue membranes[82]. In addition, it has been used for a 100 mm thin film of TPU in electronic components for textiles [83] .

Other technologies include the use of microneedle array. This method has been considered for skin treatment to generate cellular reconstruction by penetrating and generating small temporary openings and reactivation in the epidermis [84]. However, other areas, like microelectronic, have also used it as a technique for allowing the silicon to be precisely molded into complex microstructures.

This is why this study presents the study of this method to obtain microporous membranes for possible water purification applications.

4.2 Materials and methods

4.2.1 Materials

Polyether-based thermoplastic polyurethane (TPU, Irogran® A80 P5039) was provided by Hutsman, Mexico. Deionized water was obtained after purification using a Milli-Q system (18.2 mΩ cm) (Millipore Co., USA).

4.2.2 Extrusion process

The extrusion process was used to obtain the dense membrane, named like (*Ex)*. Previous to its extrusion, the TPU was dried at 60 °C for 2 h using a PR305140G Standard, Thermo Scientific oven. The temperature profile of the single screw extruder (Beutelspacher model E1930) was set to the desired extrusion temperature profile (3 heating zones) and allowed to stabilize for 15 min (Table 7) and the barrel was purged before feed the TPU pellets. The extrusion was carried out with a constant pitch roller velocity of 70 rpm, using the roller system (Beutelspacher roller system Model CAL 200) (Figure 29).

Table 7. Parameters for extrusion of samples.

Extruder					Chill Roll System	
Feed (°C)	Spindle (°C)	Exit A (°C)	Exit B (°C)	Rev (rpm)	Rev. R (rpm)	Rev. N (rpm)
165	170	171	170	70	55	72

Figure 30. Extrusion equipment for film formation.

3.2.3 Drilling process

The drilling process was used to obtain the porous membranes after extrusion, it was named as *DS*. It was carried out using a roller system DRS50 model with 540 titanium needles (length 0.20 mm, diameter 20µm), which was passed in both directions, transversal and axial, on both sides of the film. Afterward, the film was stretched during 1h into a convection oven at 100 °C, then keep it stretched during 1h at room temperature (Figure 30). As complement, samples at every step, it means stretching at room temperature (*SRT*), stretching at 100 °C (*SHT*), and drilling at room temperature (*DRT*), were obtained and evaluated.

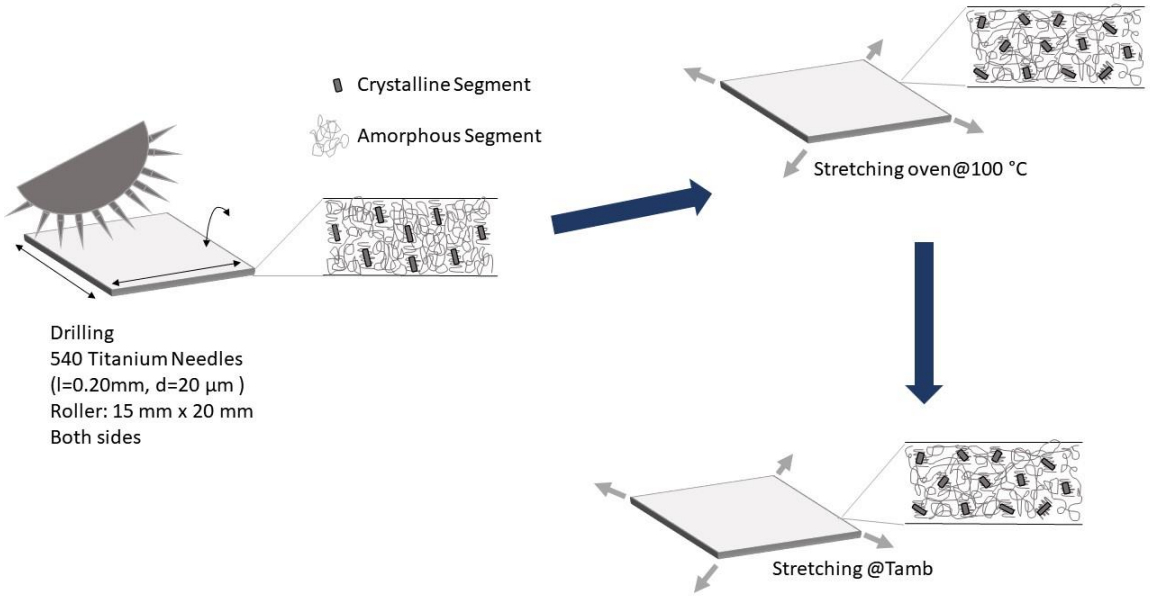

Figure 31. Representation of the drilling and stretching processes.

4.3 Membrane characterization

4.3.1 Tensile Test

Tensile properties of the films were measured using an Instron model 3366 (Instron ®) according to test method ASTM D-412 at room temperature with a cross-head speed of 500 mm/min and a 50 kN load cell. The reported values are the averages of at least five measurements.

4.3.2 Contact Angle

The contact angle of the membrane surface was measured at room temperature by a goniometer (Biolin Scientific, Theta Lite) equipped with the image analysis software One Attention. For this, deionized water drops of about 2.5 µL were placed on the membrane surface using a thin syringe.

4.3.3 Porosity

Porosity was evaluated by thermogravimetric method, the membranes were submerged for 24h in isopropanol (IPA), the excess was removed and registered its weight immediately. The porosity (ε) was calculated using Equation 6 [85] :

$$\in (\%) = \frac{W_2 - W_1}{A * d * \rho_2} * 100 \qquad \textbf{Equation 5}$$

In this equation W_2 and W_1 correspond to wet and dry weight membrane, respectively; A is area, d is thickness and ρ_2 is the IPA density.

4.3.4 Differential Scanning Calorimetry (DSC)

Concerning thermal properties, the DSC analysis was performed using the TA instrument (Q2000) equipment, carrying out two heating-cooling cycles using a ramp of 10 ° C / min from -89 to 200 ° C. The first cycle is to eliminate the thermal history.

4.3.5 Scanning Electronic Microscopy (SEM)

The surface morphology and thickness of the membranes were evaluated by scanning electron microscopy (SEM, QUANTA 200, ESEM FEI Co.). Before evaluation, SEM samples were gold coated for 25 s, at 40 mA under vacuum, and placed on a pin support. Cross-section samples were prepared by immersion in liquid nitrogen for 20 s followed by their immediate fracture.

4.3.6 Atomic Force Microscopy (AFM)

The TPU's topology analysis was carried out by Atomic Force Microscopy (AFM) using a microscope NaioAFM (Nanosurf) equipped with a Silicon tip with a force constant 48 N/m and resonant frequency of 190 kHz. The measurements were performed by dynamic force tapping mode at room temperature.

4.3.7 Water vapor permeability

Water vapor permeability (WVP) of the film was characterized according to the ASTM 96/E96M-16. The PU film was used to seal the open side of a beaker containing distilled water. The diameter of the beaker was 60 mm, and the vertical distance between the water surface and the PU film was fixed to 4 mm with 20 g of water. Then, the film-sealed-beaker was placed inside an oven set at different constant temperatures (50, 60, 70 and 80 °C) until the testing finished. The WVP was calculated using Equation 7 [86].

$$\boldsymbol{WVP(kg \cdot m^{-2} \cdot d^{-1}) = \frac{W_i - W_f}{t \cdot A} \cdot 24} \qquad \textbf{Equation 6}$$

Where W_i and W_f indicate the initial weight and the final weight of the PU film at the end of the analysis, A represents the permeate area of the film, and t indicates the analysis time.

4.4 Results and discussion

4.4.1 Membrane structure on steps of drilling process

Membrane surface area changed depend on the conditions was treated. Figure 32 shows the surface and cross-section for the obtained samples in each treatment step.

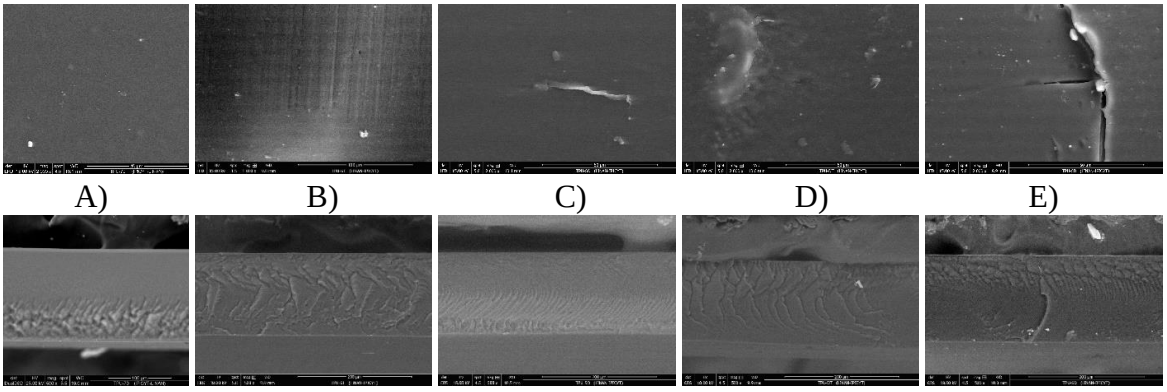

Figure 32. Images of top surface and cross section for dense membrane. a) Ex, b) SRT, c) SHT, d) DRT and e) DS membrane.

The membrane obtained by extrusion shows a smoothy and regular surface, which means that the shock temperature once the polymer get off the extruder suffered an expansion due to a pressure difference, and due to the fast heat interchange the chain polymer contracted and the structure get dense. To determine the effect of drilling and stretching processes, the morphology was evaluated. Thus, for the stretched membrane at room temperature (SRT), the surface area was aligned and when it comeback it looks like roughness surface.

In the case of the stretched sample at 100 °C (SHT) it seems that polymeric chains were re-aligned and a smooth surface is observed (Fig.32-C). On the other hand, when the membrane was drilled at room temperature without stretching, the membrane has some pots, it seems like the strength of the needle when get it inside it cannot create a hole and the polymer has the capacity to dissipate the energy applied to avoid a hole across both sides.

Although, the membrane drilled and stretched at 100 °C showed in the micrography (Fig. 32- e) cross both sides. The crystalline segment, which is the rigid part of polymer chain, could be resistant to the deformation.

On the other hand, Topology is a consequence of the organization of the structural polymer chain [87]. Thus, by AFM it would be possible to elucidate about the polymeric chain arrangement. Figure 33 shows the AFM micrographs for all the membranes.

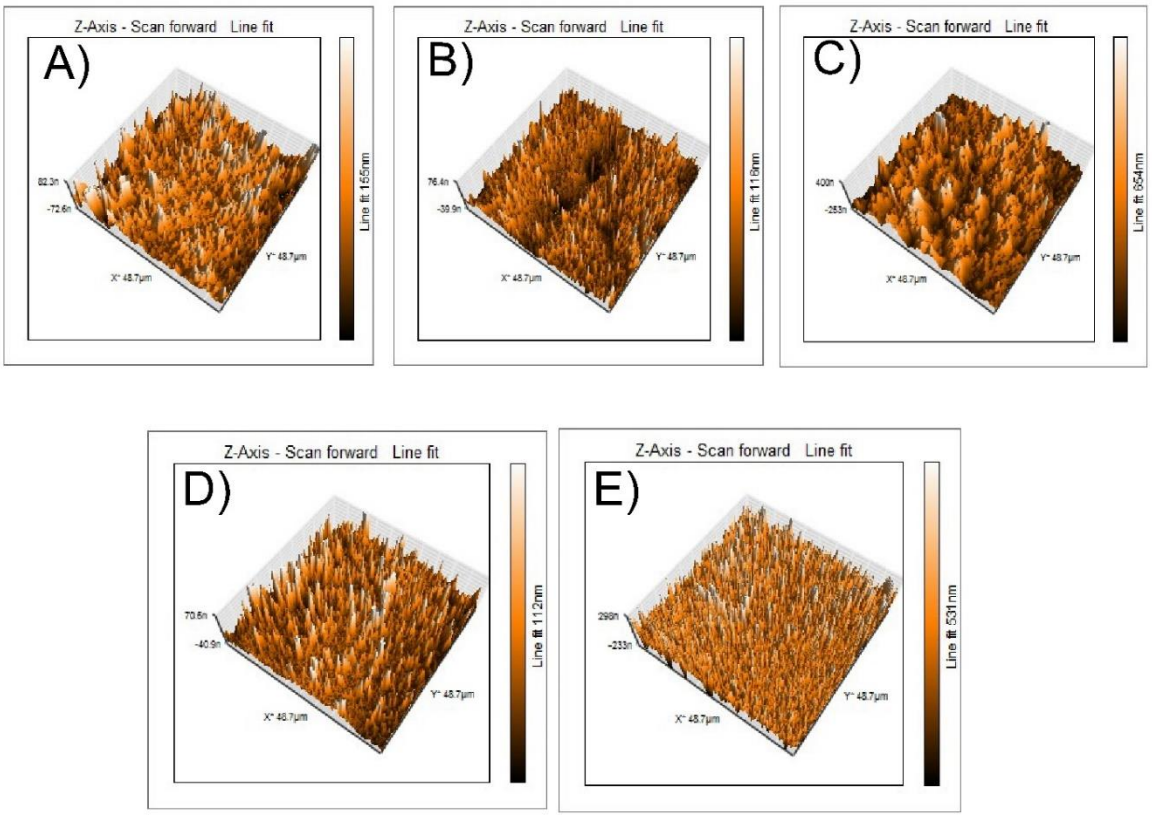

Figure 33. Topology of top 3D Z-Axis-Scan a) Ex, b) SRT, c) SHT, d) DRT and e) DS membrane.

From the AFM images shown in Figure 33, it is clear that the surface topology of the polyurethane obtained by extrusion is rough with peaks and depressions clearly defined and randomly distributed, which changed after drilling giving a more homogenous surface. This can be a consequence of the drilling process where the film is subject to certain pressure on it.

Besides, in Figure 33, when the dense membrane is exposed to external constant stress by stretching, the structure domains also are according whit thermal effect discussed earlier. Different topology is observed between b) SRT and c) SHT membranes, having a macro-structure with less defined porous for the c) SHT due to the higher temperature, which promotes the polymeric chain relaxation imparting higher freedom to move and that is why a rough surface is obtained; meanwhile, the macro-structure of the b) SRT sample show a flatter surface with better defined porous, since at room temperature the recovery depends just on the inherent elastic capacity of the material.

Finally, roughness of e) DS membrane shows similarly than d) DRT, even though the continuity of the sample can be according to fully re-oriented rigid-segment in the polymer matrix.

4.4.2 Thermal and mechanical stability

The thermal transitions, determined by differential scanning calorimetry, are summarized in Table 8, specifically the glass transition temperature (Tg), melting temperature (Tm), melting enthalpy (ΔHm), crystallization temperature (Tc) and crystallization enthalpy (ΔHc).

Table 8. Thermal transitions of all samples, obtained by differential scanning calorimetry.

Sample	Tg (°C)	Tm (°C)	ΔHm (J/g)	Tc (°C)	ΔHc (J/g)
Ex	-42.57	145.24	6.724	60.87	5.648
SRT	-37.79	148.07	7.162	61.28	7.316
DRT	-44.47	128.78	5.304	61.48	8.429
SHT	-39.27	124.98	4.176	61.35	6.349
DS	-40.31	129.43	11.70	61.03	11.08

The typical thermal transitions of the thermoplastic polyurethane are glass transition temperature (Tg) due to the amorphous (soft) segment of the polymer chain; while the second thermal transition corresponds to the melting temperature (Tm) and the third one to the crystallization point (Tc) associate both to the crystalline (rigid) segment. These transitions have changed after drilling process and stretching, as it is observed in Table 8, mainly the Tg and Tm.

In addition, SRT and SHT membranes had a different behavior since they were subjected to different temperature during stretching. For the SHT membrane it is probably that physical entanglements melt out during the stretching process and some polymer chain relaxation effect takes place in combination with the applied stress that reduced the spherulites formation of the rigid domains [88].

Furthermore, the effect of significant crystallization entalphy increment on DS membrane is attributed to formation of spherulites in rigid segment. Due to, the repacked of polymer chain forming larger lamellae.
Tensile tests have been carried out to determine mechanical parameters of each obtained film. Figure 33 shows representative the values of tensile stress vs elongation curves, elongation at break vs Tensile Strength, and Young's Modulus vs Toughness.

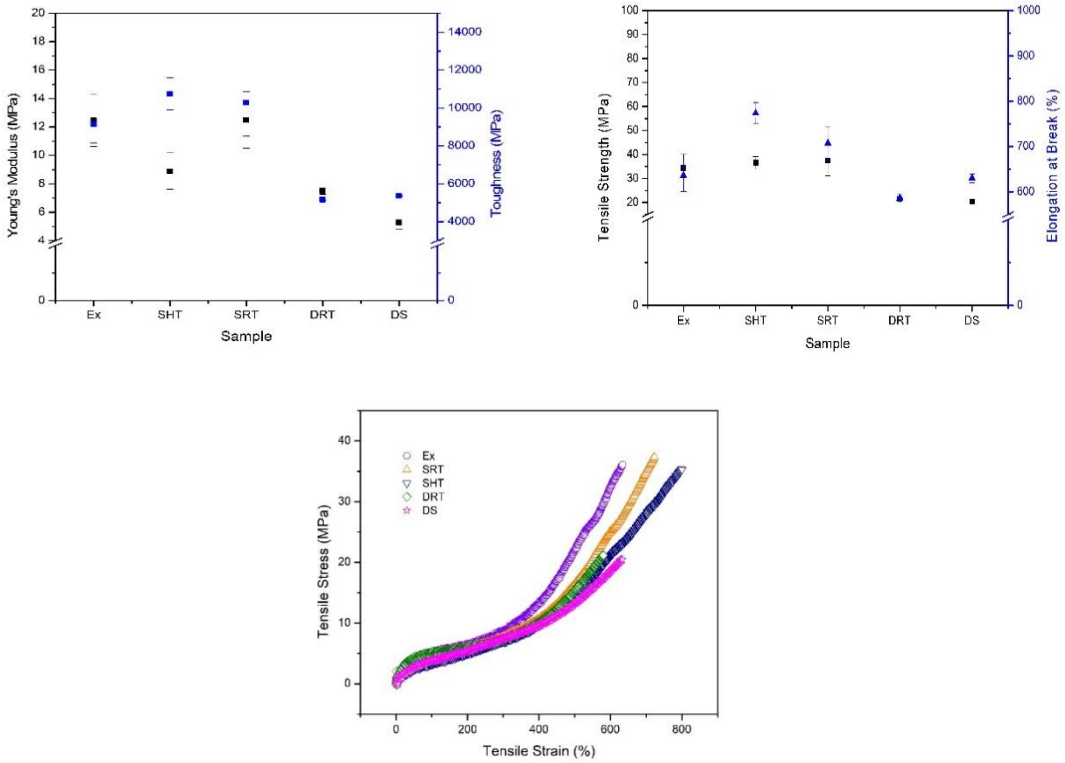

Figure 34. Tensile Test of TPU films using different obtaining process.

In case of the stress-strain curve of the Ex, SHT, SRT sample shows higher tensile strength (34 MPa), unlike the elongation at break, when SHT (800%) present 200% more than Ex, this behavior is attributed to the re-arrangement of the polymeric chains, improving the resistance to be pulled apart when stress was applied. The results are quite similar to those reported in the literature, for example, an extruded film with a thickness of 120 µm had 25 MPa of tensile strength and 800% elongation at break [89].

On the other hand, after the drilling process, the tensile strength value decreased above 50% in comparison to the continuous dense sample, because it had discontinuities generated on the surface area. Such interruptions of the film do not allow the polymer chain rearrangement and even they promote the fracture propagation along the surface.

4.4.3 Hydrophobic, Porosity and Water Vapor Permeability

The contact angle values for each sample are shown in Figure 35.

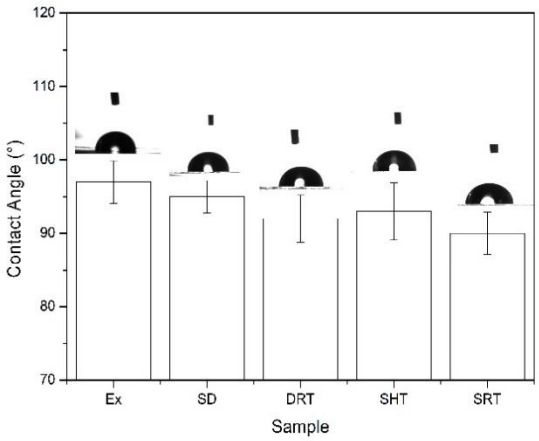

Figure 35. Contact angle of PU films using different obtaining process.

From Figure 35 the sample Ex has a contact angle value quite similar to the other samples that were exposed to physical deformation by stretching. In this case the contact angle was around 90º, which is in the transition zone between a hydrophilic and hydrophobic material. It is worth to mention that a hydrophobic behavior is preferred for the membrane intended for the MD process. Therefore, the impact on this property is not so beneficial for the DCMD process, since what is sought is to reduce the affinity for water in contact with the membrane surface.

Regarding porosity, the DRT sample increased 10% its porosity than dense one, and it is slightly higher than the others membranes. Porosity has a key role in the water vapor permeation; thus, the DRT sample would have the highest amount of water vapor transmission and, at the same time, its transmembrane pressure would be lower compared with Ex sample.

The water vapor transmission (WVT) was evaluated at four different temperatures during same time. In Figure 36, the WVT is shown as a function of temperature for all the films samples.

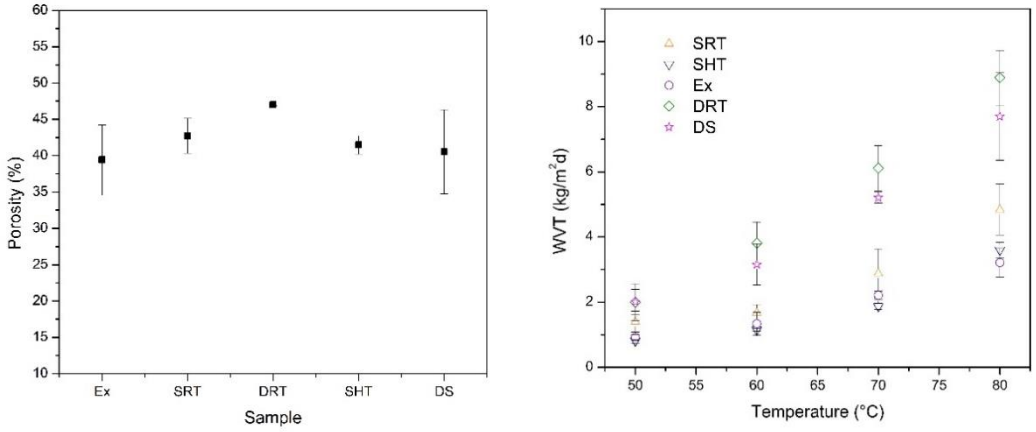

Figure 36. Water vapor permeability curves of PU films using different obtaining process.

In the literature, it is reported a film obtained by extrusion at 25°C and 20 µm thickness to have a WVT of 2.54 kg/m^{2}d [90] , another extrusion film with 25µm thickness evaluated a 25°C had 0.650 kg/m^{2}d [91] and other film with around 25 µm of thickness gave greater than about 5.5 kg/m^{2}d [92].

In this case, the dense membrane after treatment has an effect of re-orientated of soft segment and hard segment on the water vapor properties, because the diffusion trough the free volume of polymer allows an easier mass transfer. The DRT membrane increase 2 times the value of the water vapor transmission respect to the dense membrane, which was related to the re-arrangement of hard-segment.

4.5 Conclusions

The performance of the membrane, especially the water vapor transmission, depends strongly on the re-arrange of polymer chain after drilling process.

Mechanical, surface and thermal properties are related to morphology and topology, i.e., the macro-structure of the membrane.

Then, porosity plays an important role in such properties, increasing the contact angle while reduces the mechanical resistance and promotes the beginning of thermal degradation at a lower temperature.

Chapter 5. Electrospinning membrane based thermoplastic polyurethane

5.1 Background

5.1.2 Self-supporting membrane

Several studies have obtained and reported self-supported membranes by electrospinning technique for distillation membrane application. For instance, M. Essalhi, 2014 used PVDF at an optimum concentration of 25%wt with a cohesive node-free fibrous structure with 99.99% rejection and a flux of $10.8x10^{-3}$ kg/m^2.s of a 30 g/l NaCl solution. Meanwhile, Chunlei Su, 2019, developed PTFE-based hollow fiber membranes, in which he studied the effect of the PTFE/PEO ratio on the sintering process after obtaining the membranes.[93] The result was an increase in mechanical properties, 30.5 MPa maximum tensile, 53 MPa Young's modulus and 315% deformation at break, together with a permeate flux of 27.5 l/hm^2 at a concentration of 35 g/l NaCl. These studies have shown that the electrospinning membranes exhibit acceptable conditions and not requiring a supporting membrane.

5.1.3 Surface modification to improve membrane

One of the main problems with membrane for MD technology is the pore wetting, then surface modification to increase hydrophobicity is being widely studied. Yuan Liao, 2014, reported a superhydrophobic membrane by PVDF-based electrospinning, modified with silica nanoparticles. On the other hand, Madalosso, H. B., 2022 incorporated silica nanoparticles in the PVDF-PDMS solution to obtain the membrane by electrospraying increasing the hydrophobicity 167.13 ± 22.29◦ with a flux of 1.55 kg/m^{2}h. On the other hand, Meng, S., 2014 conducted an investigation of the influence of TiO_2 and 1H,1H,2H,2H-perfluorododecyl-trichlorosilane (FTCS), using the sol-gel method for nanoparticle deposition, using a commercial PVDF membrane as a base, achieving 118° of hydrophobicity[94]. Later in 2013, Liao, Y, increased the hydrophobicity of the PVDF-based membrane surface by electrospinning technique, with the modification of silver nanoparticles and dopamine after obtaining the membrane, achieving a contact angle of 158°±3, with a porosity of 68% and a permeate flux of 31.8l/m^{2}h[95]. Su, C., 2017, on the other hand in PVDF based membrane incorporated silica nanoparticles by spraying with PDMS dissolved in toluene achieving a contact angle of 157 ± 1° and a flux of 25.73 kg/m2h[96]. Performed fluorination using 1H,1H,2H,2H-perfluorodecyltriethoxysilane (FAS) with the incorporation of SiO_2 nanoparticles, considering PVA as the base. Further on Su, C., 2019, in a self-supported PVDF-HFP membrane by electrospinning, Si nanoparticles were spread to then place another layer of the same polymer and join by heat and pressure both layers and remaining between them the Si nanoparticles, after this step was functionalized with flouroalkalinsilane (17-FAS) to obtain the final material[97]. A permeate flow rate of

around 39 L/m^2 h was obtained with a hydrophobicity of 157.19° and a porosity of 80.7 ± 1.2%. These are some of the investigations that have contributed to a surface modification that has been shown to show good results, which gives us cause to explore this alternative to improve the characteristics of the membrane. Thus, this work pretends to contribute with the study of the surface modification correlate with the membrane properties.

5.2 Experimental Methodology

5.2.1 Materials

Thermoplastic Polyurethane-based polyether (TPU-1) Irogran® A80 P5039 was provided by Hutsman, Mexico. N,N,-Dimethylformamide (DMF), Tetrahydrofuran (THF) and (3-Glycidyloxypropyl) trimethoxysilane (GLYMO) were received from Sigma-Aldrich, sulfuric acid 98% (H_2SO_4) provided by Macron, hydrogen peroxide 30% (H_2O_2) by Fermont, Methanol (CH_3OH) provided by Fermont, hydrophobic nanoparticles of silica functionalized with 1,1,1-trimethyl-N- (trimethylsilyl) silanamine, mean size particle 14 nm (Aeroxide LE1®) provided by Degussa, comercial desionized water (Servicios S.A. de C.V., México). All the chemicals were used as received.

5.2.2 Polymer dissolution

The polymer solution was prepared by dissolving TPU-1 (18 % w/w) in a solvent mixture of DMF/THF (70/30 w/w). Then, the TPU was added to the solvent mixture and kept under constant agitation at room temperature for 24 h, until its dissolution.

5.2.3 Membrane preparation

Electrospinning allowed the formation of fibers through an electric potential difference that was applied to the TPU-1 solution. The high voltage is applied to the TPU solution in order to induce polarization. As a result of such polarization, a Taylor cone was formed. When the charge exceeds the surface tension of the solution, a droplet on the tip of the needle (jet) travels towards the region of low potential, in this case the metallic rotary collector. Figure 37, shows the schematic diagram of the electrospinning equipment.

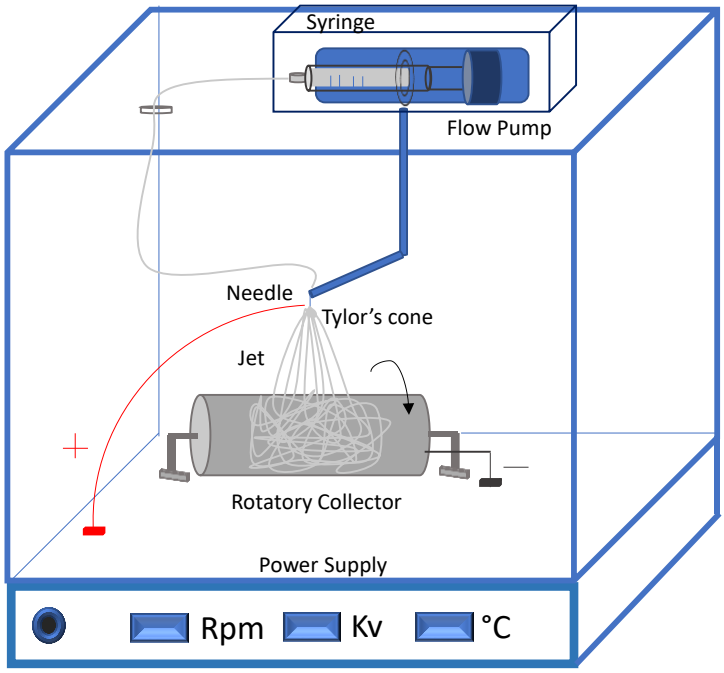

Figure 37. Scheme of electrospinning technique.

It consists of an adjustable DC power supply, which is able to generate a voltage in the range of 0–30 kV. This power supply is connected to a tip of the metallic needle (0.21 mm inner diameter) by two electrodes. The syringe, which contains the polymer solution, is connected to a syringe pump. A positive voltage of 7 kV was applied across a distance of 10 cm between the tip of the needle and the metallic collector (15 × 30 cm). The rotary collector was covered with aluminum foil on which the fibers were deposited. The collector velocity was maintained constant at 300 rpm. Once the membranes were obtained, they were dried for 24 h at room temperature to remove residual solvent.

5.2.4 Surface modification

5.2.4.1 Modification of TPU with oxidant environment via Piranha solution (PS)

Piranha solution is very oxidant toward organic compounds due to the formation of hydroxyl radicals upon mixing acid sulfuric and hydrogen peroxide in 1:3 ratio. Although the inert character of TPU, the hydroxyl radicals interact with urethane group to produce hydroxyl groups. Methanol was used to soaking membranes 15 minutes in 10 ml in ultrasonic bath before immersing with PS.

Different dissolutions of PS were prepared (20%, 30%, 40%, 50%) by carefully mixing of sulfuric acid with 30% hydrogen peroxide and deionized water. Membranes with 30 mm x 30 mm were kept for 30 min in 50 ml of PS at 60 °C. Thereafter, membranes were soaking in DI water for 5 min and washed with water to remove any trace of PS. Finally, membranes were submerged with methanol 5 times and dried at 70°C for 12 h to generate the functionalized TPU membranes[98].

5.2.4.1 Surface modification by sol-gel

The procedure of the reaction was modified from that reported by Fan, H., 2020, as it is mentioned. First, the membrane was immersed in a solution of TEOS, water and ethanol, sonicated for 1 min; then it was stirred for 30 min. Afterwards, the LE1 dissolved in ethanol was added. The pH is then reduced with ammonia added dropwise over a period of 30 min. It is left under continuous stirring for 30 min at 60 °C. Finally, it is left to dry at room temperature. TEOS is an organosilane having ending able methoxysilyl groups, which functions as a coupling agent to bond the polymer to the hydrophobic silica.

5.3 Characterization techniques

5.3.1 Contact angle

The contact angle of the membrane surface was measured at room temperature by a goniometer (Biolin Scientific, Theta Lite) equipped with the image analysis software One Attention. For this, deionized water drops of about 2.5 µL were placed on the membrane surface using a thin syringe.

5.3.2 Scanning Electronic Microscopy (SEM)

The morphology and thickness of the membranes were evaluated by scanning electron microscopy (SEM, QUANTA 200, ESEM FEI Co.). Samples of the membranes were gold coated for 25 s, at 40 mA under vacuum conditions, and placed on a pin support.

5.3.3 Tensile test

Tensile properties of the films were measured using an Instron model 3366 (Instron) according to test method ASTM D-412 at room temperature with a cross-head speed of 508 mm/min and 50 kN cell load. Reported values were the averages of at least five measurements. Presented tensile curves were taken from the measurements closest to each calculated average value.

5.3.4 Porosity

Porosity was performed by thermogravimetric method, the membranes were submerged for 24h in isopropanol (IPA), the excess was removed and weighed immediately. Accorded to Equation 8 were used to calculate the porosity (ϵ) [99].

$$\in (\%) = \frac{W_2 - W_1}{A * d * \rho_2} * 100 \qquad \textbf{Equation 7}$$

In this equation W_2 and W_1 correspond to wet and dry weigth membrane respectively, A is area, d is thickness and ρ_2 is IPA density.

5.3.5 Water vapor permeability

Water vapor permeability (WVP) of the film was characterized according to the ASTM 96/E96M-16. The PU film was used to seal the open side of a beaker containing distilled water. The diameter of the beaker is 60 mm, and the vertical distance between the water surface and the PU film is fixed to 4 mm with 20 g of water. Then the film-sealed-beaker was placed inside an oven set at different constant temperatures (50, 60, 70 and 80 °C) until the testing finished. The WVP was calculated using Equation 9 [86].

$$\boldsymbol{WVP(kg \cdot m^{-2} \cdot d^{-1}) = \frac{W_i - W_f}{t \cdot A} \cdot 24} \qquad \textbf{Equation 8}$$

Where W_i and W_f indicate the initial weight and the final weight of the PU film at the end of the analysis, A represents the permeate area of the film, and t indicates the analysis time.

5.4 Results

5.4.1 Effect of treatment with Piranha solution on the physicochemical properties of the membrane

FTIR-ATR, goniometer and porosity techniques were used to evaluate the influence of the piranha treatment in TPU-based membranes on the physicochemical properties of the membrane. Based on the data obtained, the comparison between the membrane without treatment and the membranes that were treated at different concentrations of piranha solution at the same time is presented. Figure 38 shows the FTIR spectra in transmittance.

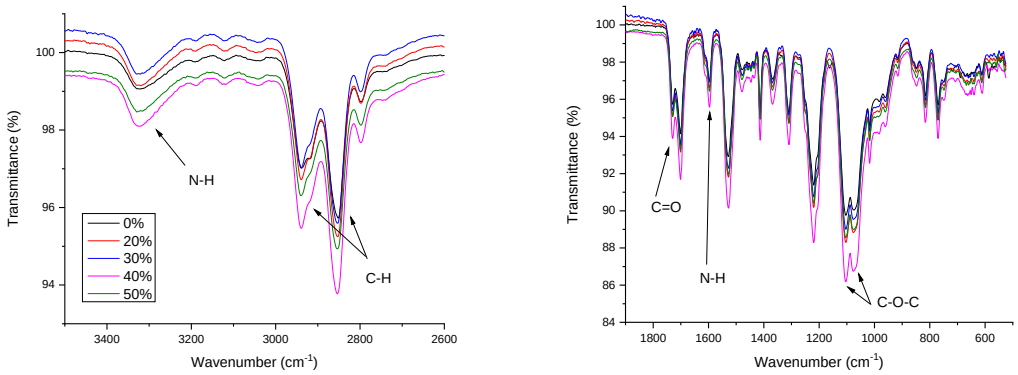

Figure 38. FTIR spectra after the interaction of the different concentrations of piranha solution.

Table 9. Assignment of bands corresponding to FTIR signals.

λ (cm-1)	**Assignment**
3307	N-H Strain (urethane group)
2904, 2860	C-H Antisymmetric stretching
1730	C=O Strain
1531	N-H ending
1104	Antisymmetric C-O stretching of ether C-O-C (nonbonded)
1076	Antisymmetric C-O stretching of ether C-O-C (bonded)

According to the spectra and the signal assignments in Table 9 a change in intensities is observed at 3300 cm-1, which refers to the stretching of the N-H bond, especially for the case of the sample with 50% piranha solution, which would corroborate the breaking of the chains forming hydroxyl groups in the generated chains.

In addition, XRD analysis allow to identify the crystallinity of the material, which exhibits a clear peak at 20 °associated to the rigid segment of the polymer (Figure 39).

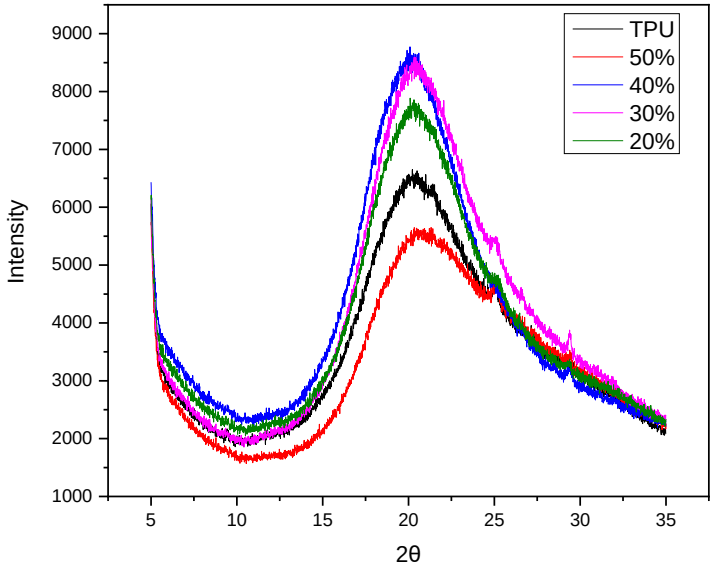

Figure 39. XRD diffractogram after the interaction of the different concentrations of piranha solution.

Figure 39 shows a reduction of the intensity of the peak because the crystallinity has been reduced, and the bonds in the main chain have been broken by the piranha solution.

On the other hand, the porosity and contact angle were evaluated in the different concentrations of the piranha solution, results are shown in Figure 40.

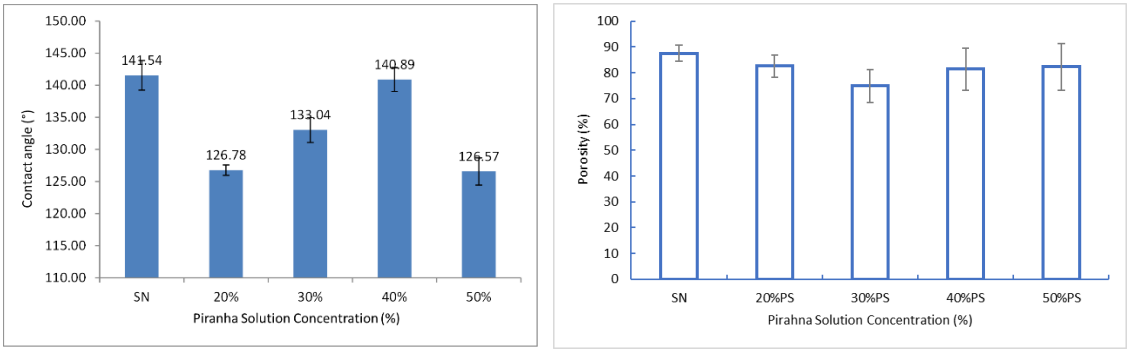

Figure 40. Graphs of a) contact angle and b) porosity with respect to the concentration of the piranha solution.

In this Figure it can be seen that the contact angle decreases when polymer was in contact with the piranha solution. However, as the concentration of the piranha solution increased, the contact angle increased due to the protuberances that are generated when the surface is eroded by the oxidizing medium. The decrease again to 50% may be due to the caking that occurs in the fibers, which would reduce the contact surface. In case of the porosity start to decrease around 20° when the

concentration of piranha solution increase, is due to fiber collapse between each other, as the consequence the free space was reduced.

5.4.2 Effect of treatment with Piranha solution on the morphology and topology of the membrane

The analyzes carried out to analyze the surface morphology and topology of the membranes were performed by SEM and AFM, respectively. The Figure 41 shows the images obtained by both techniques once treated with piranha solution.

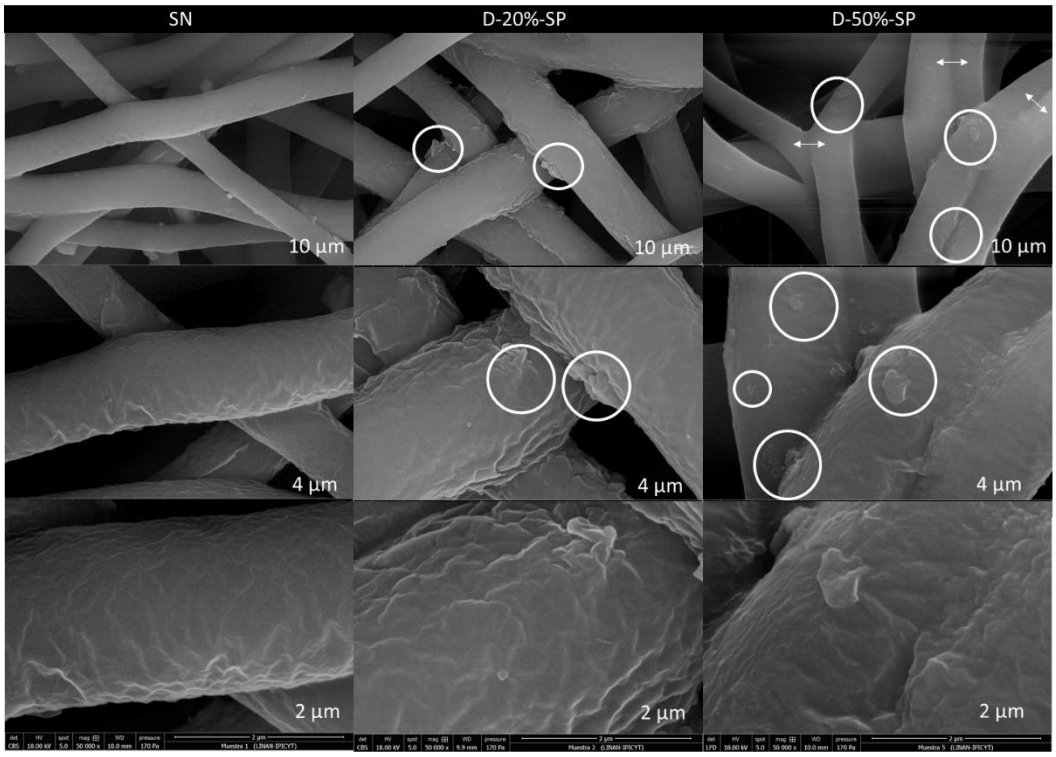

Figure 41. SEM images of TPU base membrane, after immersion in 20% and 50% piranha solution, respectively.

The Figure 41 above shows the fibers after the piranha treatment for the reference membrane, the membrane treated at lowest concentration (20%) and the membrane treated at highest concentration (50%). It is possible to observe that the exposure of an oxidizing medium generates erosions on the membrane surface, which results in protuberances that generate greater surface roughness, as reported in the literature [98,100]. As the concentration of the piranha solution increases, the most prominent protuberances increase and in a larger area of the surface, however, the fusion between the fibers begins to appear, generating a caking, as an indication of the beginning of the dissolution of the polymer, because at 60% it dissolved completely.

In addition to the morphology analysis the membranes were analyzed by Atomic Force Microscopy. The corresponding images are presented in Figure 42.

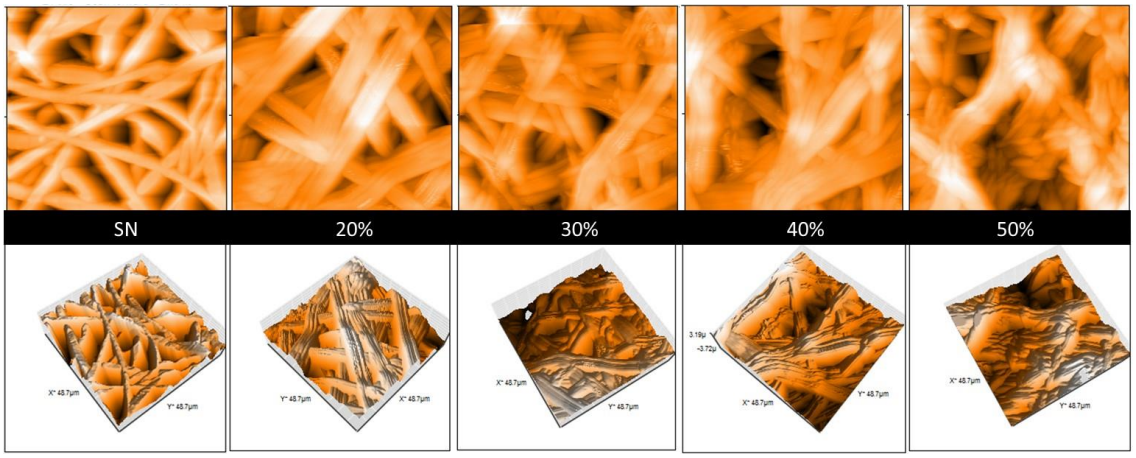

Figure 42. AFM images of the TPU-based membrane, after immersion in 20%, 30%, 40% and 50% piranha solution, respectively.

The AFM images show an evident change in the surface of the membrane at the nanometric level, an increase in the diameter of the fibers can be observed as well as the “fragmentation” as the concentration increased. The chemical resistance of TPU is consequently reduced due to a possible diffusion of the piranha solution inside the polymeric matrix, generating swelling as a result of solvation of the polymeric chains giving a thickening of the fiber.
A possible interaction mechanism between the piranha solution and the TPU is proposed below, as shown in Figure 43.

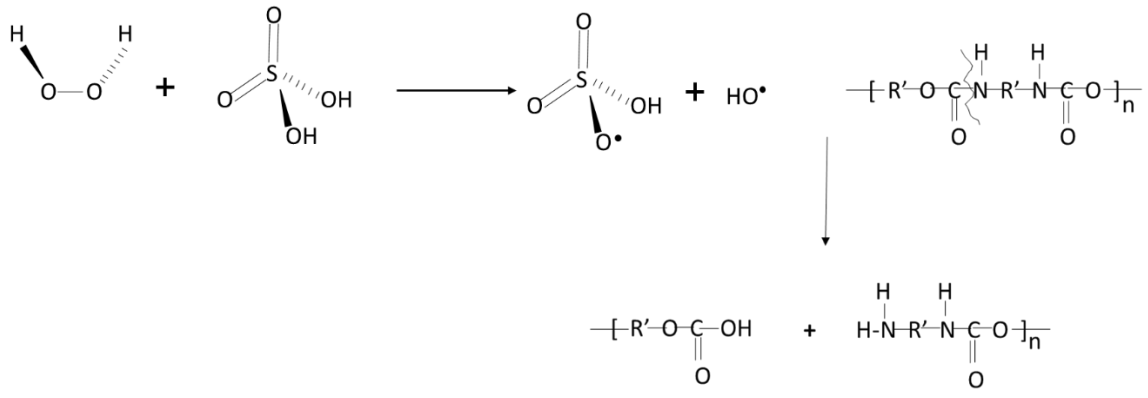

Figure 43. Proposed mechanism of the interaction of the piranha solution and the TPU.

The piranha solution is the combination of sulfuric acid and hydrogen peroxide that, when mixed, generates an exothermic reaction. From this reaction, hydroxyl ions, hydrogen sulfate, are generated, and they can react with the carbonyl group, a group close to the amine of the urethane promoting a chain break. Thus, the chain has a possible carboxyl termination and a hydroxyl end.

On the other hand, the functionalization of the hydrophobic silica was carried out to anchor it to the surface of the membrane, the results of said treatment will be presented below.

5.4.3 Effect of treatment with Sol-gel on the morphology of the membrane

Sol-gel technique show the difference in the structure of the fiber as we can see in the Figure 44.

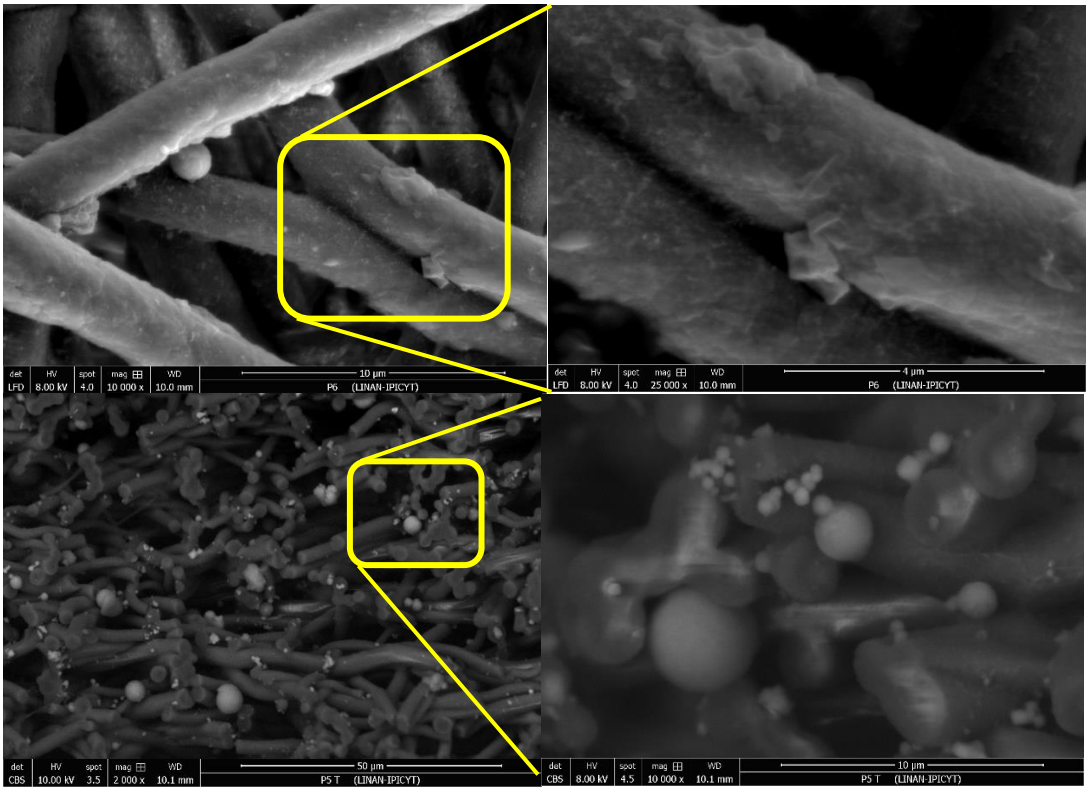

Figure 44. SEM images of TPU base membrane, after immersion in sol-gel with TEOS and SiO2, superficial area and transversal, respectively.

In the micrographs you can see the variation of SiO2 microspheres that were deposited scattered on the surface, its presence is more evident in a cross section. Likewise, there is the presence of a rough texture changing the morphology of the fiber, generating a coating. It is possible that as the surface was modified after the piranha solution, the texture of the fiber facilitated anchoring, in addition to the hydrophilic groups present on the surface with which TEOS will be more attuned. These are the advances that were achieved by modifying the surface to improve the permeability of the membrane, however further characterization is required.

5.5 Conclusions

The electrospinning membranes initially present a porosity of 80% due to the extraction technique and the operating conditions of the system. However, when

subjected to a piranha treatment, which modified the surface of the fibers, the porosity decreased by 20% when subjected to 30% PS, that is, it was significantly reduced. At high concentrations it damaged the material, that is to say 50% PS reduced the crystallinity and hydrophobicity. However, at low concentrations it modified the surface roughness of the fibers and allowed better anchoring of the SiO_2 nanoparticles. As well as, the coating generated by the influence of TEOS when reacting with a sol gel formed a layer of silicone material.

Chapter 6. Performance of the membranes by Direct Contact Membrane Distillation (DCMD)

6.1 DCMD module construction

It is describing the materials and elements used for the construction of Direct contact membrane distillation module (DCMD) and the evaluation of the membrane get in previous methods.

The Figure 45 shows the scheme of the Direct contact membrane distillation module (DCMD) based on previous work on the collaborate group [101].

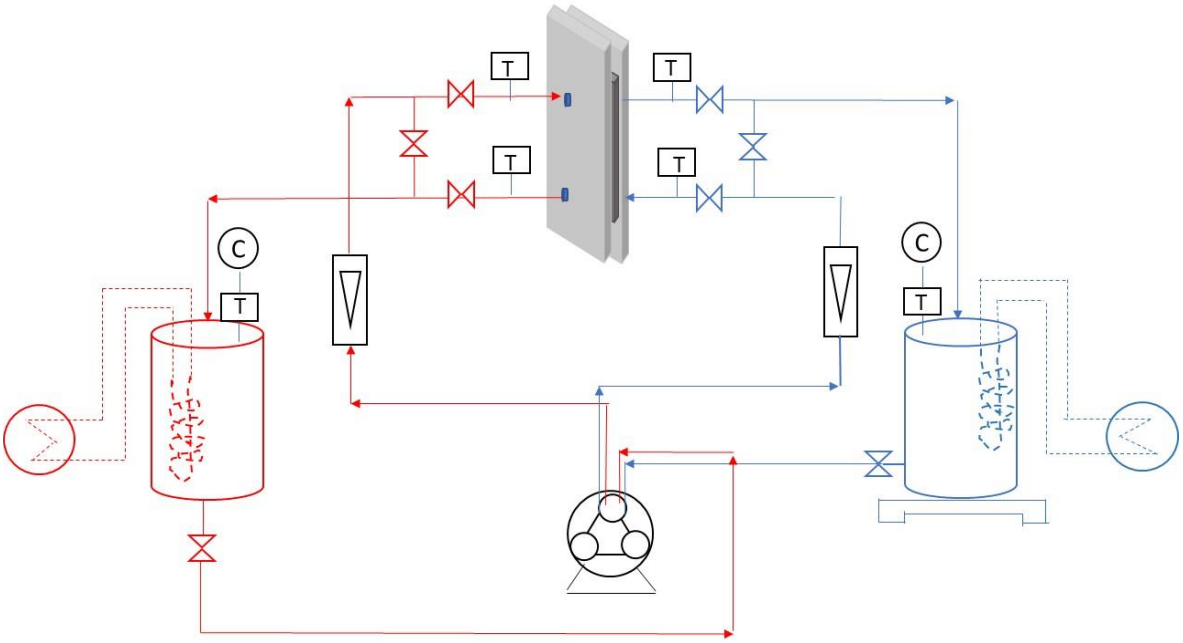

Figure 45. Scheme of DCMD system

The system consists of two flows: the feed flow (red line) and the permeate flow, both converging in the module cell with flat sheet configuration.
The feed stream contains a salt solution that is heated in a tank by a submerged condenser, feed by a closed loop chiller with ΔT-=10 °C relative to the tank. The tank is monitored for conductivity and temperature. The permeate circuit contains distilled water, which is temperature controlled by a condenser, also regulated by a chiller with ΔT=10 °C with respect to the tank. This tank has temperature and conductivity indicators. The weight of the permeate is measured by an analytical balance. Temperature indicators are located at the inlet and outlet of each flow.

6.1.1 Direct Contact Cell

DCMD module was set up by refence of SEPA CF II, Sterlitech®, as commercial filtration cell, even though it was making some modification on active area based on membrane dimension. Also, it is important to mentioned that was referenced by previous group research work [101].

Cell module was constituted by mechanic Nylamid “M”, thermally resistant up to 93 °C, with thermal conductivity 0.29 W/(K.m), 0.3 % weight in 24 h absorption water, 1055 kg/m^2 compression resistance in 10% of deformation at 23°C. (MIDSA® Distributor). This module is conformed for two pieces with 12.72 cm long, 10.15 cm width and 2” thickness dimension (Figure 46).

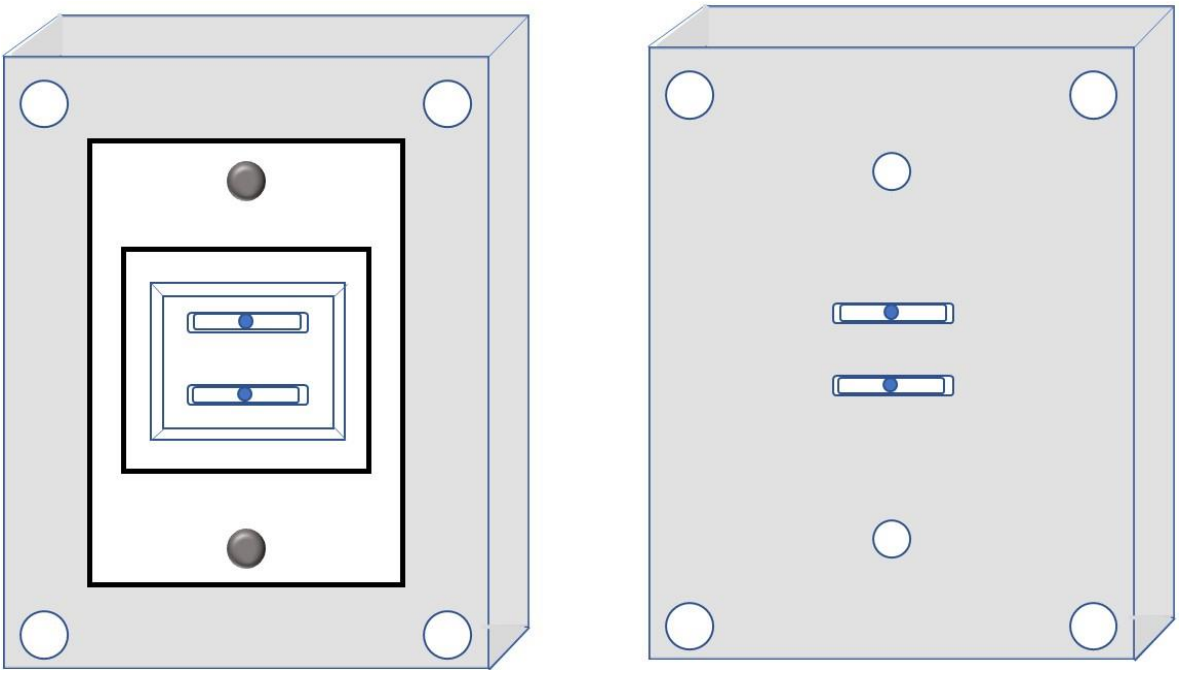

Figure 46. Direct Contact Membrane Distillation (DCMD) module.

The active membrane area was 2.27 cm and 2.44 cm, defined by two neoprene O-rings which keep fixed the membrane, they were made by injection. Furthermore, spacer based on “tulle” with rhomboid geometry were used in the free space between neoprene O-ring and the membrane, in order to generate turbulent flow and help water vapor pass through a membrane. (Figure 47)

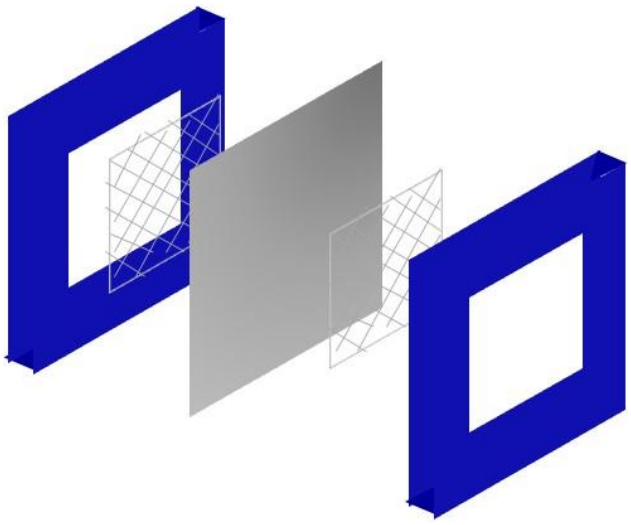

Figure 47. Neoprene O-ring, spacers and membrane on the cell module.

6.1.2 Auxiliar elements

Feed and permeate tanks they were built with a 3 mm thick acrylic tube, with a capacity of 600 ml, the tube was sealed on one side with an acrylic plate, on the other side there is an acrylic cap that is adjusted to the diameter of the tube and with the suitable holes for measuring instruments. Acrylic was chosen for its visible light transmission is 92%, thermal resistance up to 90 °C, resistant to water, alkalis, dilute acids, simple esters, aliphatic hydrocarbons. (MIDSA® Distributor). The feed tank at the bottom has a gate valve with 1/4" quick connections, despite the permeate tank has the valve on the side, for better contact with the analytical balance.

Connections such as the butterfly valves and T-connector used were of a nominal diameter of 1/4" PVC before inlet and outlet of the cell. Although, the stop valves of the feed and permeate tank outlets are made of stainless steel.

The *tubing* used for the whole system was Puri-Flex Tubing Masterflex L / S 16, it supports a maximum temperature of 135 °C and a minimum temperature of -50 °C. The system was thermally insulated with an Armaflex® elastomeric foam with a conductivity 0.25 BTU-in/h-ft^2-°F thermal and 0.05 perm-in water vapor transmission.

The *Peristaltic pump* (Masterflex®) two channel head, HV-07554-90 propelled the cross-flow of permeate and feed.

The *Cooling and Heating Systems* consisted of a 1/4 " polypropylene pipe coil with 4 acrylic plates as a guide, all complete was submerged in each tank. In the case of permeate, the Thermo Scientific Haake ARCTIC SC150 A25 Refrigerated Bath Circulator, Neslab RTE7 & RTE10 Digital One Replacement was connected to the recirculator. In the case of feeding, 45 Liter Advanced Digital Refrigerated Circulator (-25 ° C / 135 ° C) was connected to Polyscience.

The *Analytical Balance* used was Ohaus Adventurer ™ Pro model AV 313, to measure the mass of the permeate.

6.1.3 Instrumentation

The *Portable Conductivity Meter* (Extech EC150) were used to measure conductivity and temperature in the feed and permeate tanks.

The acrylic *flow meters* (LZM-6T) were used to measure the flow rate the connection between the pump and the cell module with range from 100 to 1000 mL / min.

Four *Digital Cable Sensor Temperature* -50 to 110 ° C LCD Control thermometers were used to monitor the temperature at the inlet and outlet of each flow.

6.2 Experimental Methodology

6.2.1 Evaluation conditions

The operating conditions were established due to the limitations of the equipment and measuring instruments. Before operating the equipment, the conductivity meter was calibrated with standard solutions of 84 µS / cm, 1413 µS / cm and 12880 µS / cm. The heating recirculation bath was used at a temperature of 90 ° C, consequently to the heat losses the feed tank reached a maximum temperature of 77 ° C. The cooling recirculation bath was used at a temperature of 15 ° C and the permeate tank reached about 17 ° C.

6.3 Results and Discussions

6.3.1 Evaluation conditions

The operating conditions were established due to the limitations of the measuring equipment and instruments. The NaCl concentration was determined according to the maximum conductivity value that the equipment detects, for which a calibration curve from 0.001 to 0.2 M was performed on both instruments. In addition, at different temperatures was evaluated (Figure 48).

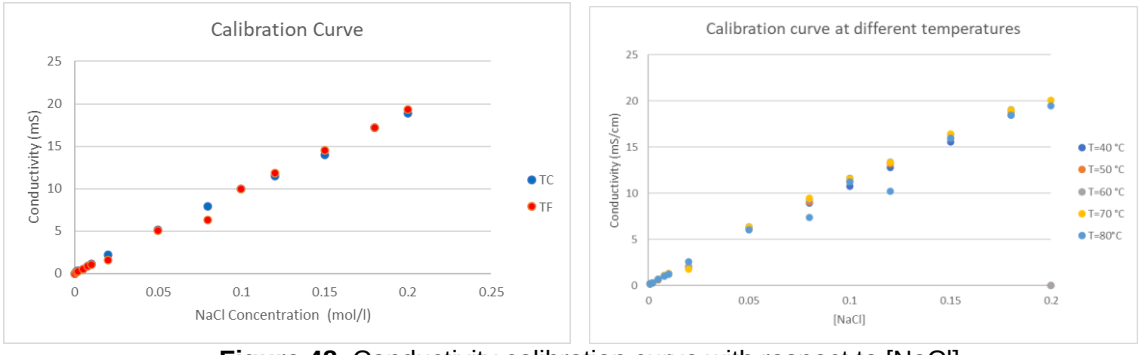

Figure 48. Conductivity calibration curve with respect to [NaCl].

Due to this, it was corroborated that both devices had the same measurement precision, on the other hand, it was considered that the maximum concentration to work with is 0.2 M and as a mid-point it is also possible to work with 0.1 M. Furthermore, it is proposed to calibrate before the tests with standard solutions of 84 µS/cm, 1413 µS/cm and 12880 µS/cm. The maximum stable temperature of the feed tank was defined until the relevant adaptations were found, consisting in the use of a recirculation bath connected to a coil immersed in the tank. The recirculation bath was used with a temperature of 90 °C, due to heat losses through the plastic hoses, consequently the feed tank reaches a maximum temperature and maintain it around 77 °C, demonstrating in preliminary tests that in thermometers placed near the module it is around 60 °C. The minimum stable temperature in the permeate tank was reached at 20°C, using a recirculation bath with a temperature at 15 °C. Preliminary tests showed a value of 20°C at the inlet of the module.

6.3.2 Dye evaluation

The dye test was performed to identify if any permeation was occurring due to poor sealing (Figure 49).

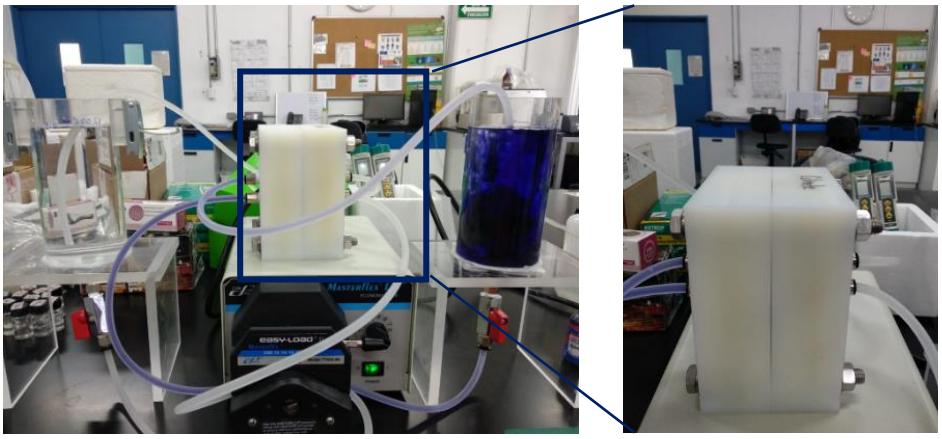

Figure 49. Photograph of the dye test.

The test did not detect any color change in the feed tank. However, a re-structuring of the system was carried out to ensure the tightness of the seals and the membrane. In addition, a tulle net was added to generate more transport through the feed tank.

6.3.3 Water deionized membrane evaluation

The TPU Ex (extrusion), TPU El (electrospinning), PUD (phase inversion) membranes were tested with deionized water in both tanks for a period of 5 hours at 60°C feed temperature and 20°C permeate temperature (Figure 50).

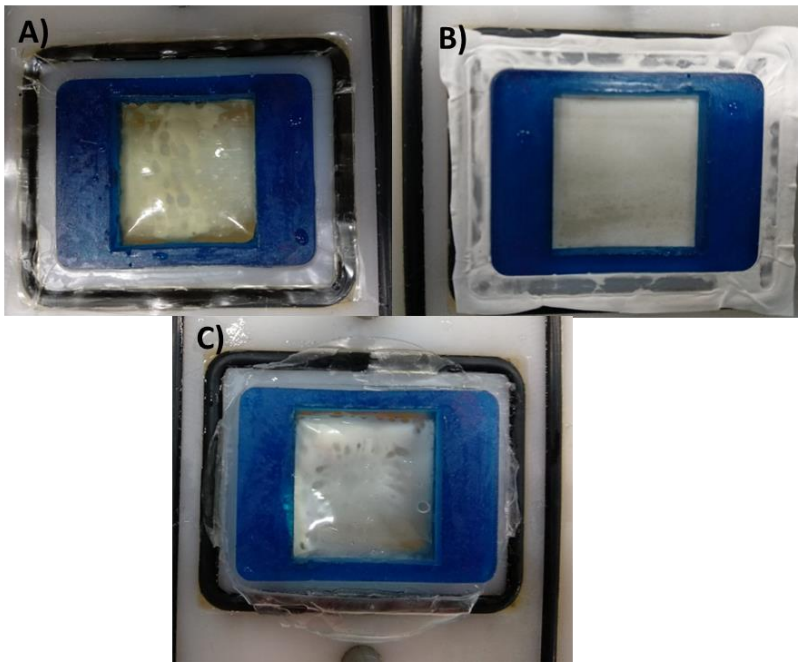

Figure 50. Photography of A) TPU Ex, B) TPU El and C) PUD

In this evaluation, a whitish coloration was identified in the samples obtained by extrusion and evaporation from the PUDs. As a consequence of this behavior, a gravimetric evaluation was performed by heating water to its evaporation point, introducing the sample and then pouring in cold water. The sample showed a change in color, similar to that of the photographs. It was then weighed and dried in the oven at 90°C and weighed again, resulting in 7% water absorption. This shows that these membranes do not have a porosity, so they have a good vapor permeation capacity, however, when exposed to a stream of water with a lower temperature, it is possible that the water vapor molecules condense inside the membrane, and cannot pass completely to the opposite side. The effect of the perforation method in the case of extrusion membranes will be evaluated below. In the case of PUDs, the incorporation of SiO_2 and the effect on water vapor transport will be evaluated.

In the case of the samples obtained by electrospinning, the porosity is so high that the water passes through completely and it can be seen that there is no change in color.

6.3.4 NaCl membrane evaluation

The evaluation of the membranes was carried out with a concentration of 1 g/l in the feed solution. The membranes obtained by extrusion and phase inversion were selected because their behavior in the system was more stable (Figure 51).

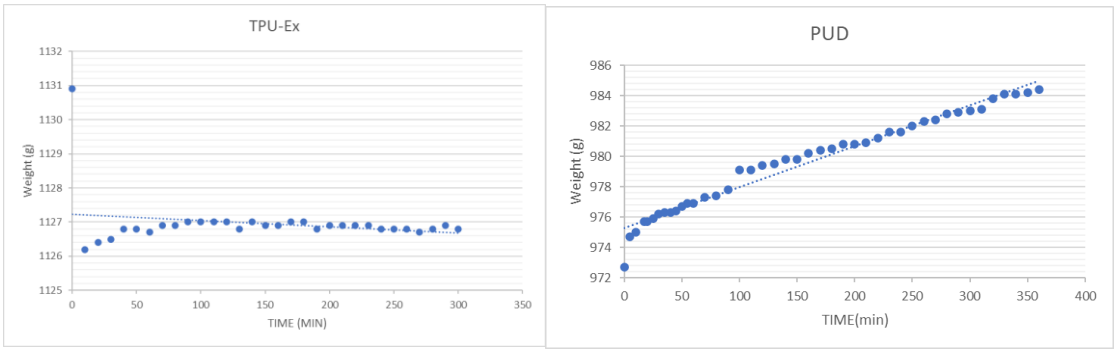

Figure 51. Membrane evaluation by NaCl 1g/l solution.

Figure 51 shows the change in weight with respect to time for each of the membranes. In the membrane that was obtained by extrusion, there is an increase in weight of around 1%, with respect to the initial weight. This is due to the fact that this membrane presents a good efficiency for the passage of steam and there is no transfer of water. On the other hand, in the case of the phase inversion membrane, it turns out to have a more significant tendency with a 10% increase with respect to the initial weight, which may be due to the constitution of the material.

It is worth mentioning that despite being the two polyurethane membranes, they come from a different nature, since the PUD's were generated from polycarbonates and the TPUs are polyether based. This presents a difference in the possible molecular interaction that they present with the water vapor when passing through the membrane.

Chapter 7. General Conclusions

7.1 Final Remarks

In chapter 3, the PUD-based membrane manufactured by evaporation showed various effects when SiO2 was incorporated. In the FTIR analysis there is a significant interaction between the polymer and the filler. DMTA and DSC results show that there is no difference between the pure polymer and the polymer composites (containing the filler) in terms of glass transition temperature because the interaction between the silica and the amorphous part is not strong enough, but by DMTA the interaction between the hard segment and the filler was detected. Gas transport properties revealed that water vapor permeability increased in the presence of silica due to a more open structure and CO2 is more selective.

In chapter 4, the TPU-based membrane obtained by stretching and modified by drilling process, show that the performance of the membrane, especially the water vapor transmission, depends strongly on the re-arrange of polymer chain after drilling process. Mechanical, surface and thermal properties are related to morphology and topology, i.e., the macro-structure of the membrane. Then, porosity plays an important role in such properties, increasing the contact angle while reduces the mechanical resistance and promotes the beginning of thermal degradation at a lower temperature.

In the chapter 5, the TPU- based membrane fabricated by electrospinning initially present a high porosity due to the characteristics of the polymeric solution and the operating conditions of the system. However, when subjected to a piranha treatment, which modified the surface of the fibers, the porosity of the material was also affected, i.e. it was significantly reduced. At high concentrations, it damaged the material and reduced its properties, but at low concentrations it modified the surface roughness of the fibers and allowed a better anchorage of the SiO2 nanoparticles. As well as, the coating generated by the influence of TEOS when reacting with a sol gel formed a layer of siliconized material.

In the chapter 6, the preliminary tests for the evaluation of the membranes present the PUD as a good option, since the nature of the composition of the material presents characteristics that favor the transfer of water vapor. However, it is necessary to work on the balance of matter and energy, work that was not completed and that can expand this evaluation.

7.3 Scientific Products

A) Publications with peer review process

1. Špírková, M., Pavličević, J., Aguilar Costumbre, Y., Hodan, J., Krejčíková, S., & Brožová, L. (2020). Novel waterborne poly (urethane-urea)/silica nanocomposites. Polymer Composites, 41(10), 4031-4042. doi.org/10.1002/pc.25690

2. Špírková, M., Pavličević, J., Aguilar Costumbre, Y., Hodan, J., Urbanová, M., & Krejčíková, S. (2021). Mechanically strong waterborne poly (urethane-urea) films and nanocomposite films. Journal of Applied Polymer Science, 138(11), 50011. doi.org/10.1002/app.50011

3. Gajdošová, V., Špírková, M., Aguilar Costumbre, Y., Krejčíková, S., Strachota, B., Šlouf, M., & Strachota, A. (2023). Morphology, Micromechanical, and Macromechanical Properties of Novel Waterborne Poly (urethane-urea)/Silica Nanocomposites. Materials, 16(5), 1767. doi.org/10.3390/ma16051767

B) Book Chapters

1. Aguilar, Y. Lambert., J. Méndez, M. Escobar, V. “Preparation of Membranes Based on Polysulfone (PSU) and Graphene Oxide (GrO) by Electrospinning” Online ISBN 978-3-319-45315-6.

8. References

[1] E.L. Valor, D. Agua, Informe Mundial de las Naciones Unidas sobre el Desarrollo de los Recursos Hídricos 2021, 2021.

[2] UN-Water Analytical Brief Unconventional Water Resources 0 5 J U N E 2 0 2 0 With support from, n.d.

[3] U.K. Kesieme, N. Milne, H. Aral, C.Y. Cheng, M. Duke, Economic analysis of desalination technologies in the context of carbon pricing, and opportunities for membrane distillation, Desalination. 323 (2013) 66–74. https://doi.org/10.1016/j.desal.2013.03.033.

[4] S. Santoro, A.H. Avci, A. Politano, E. Curcio, The advent of thermoplasmonic membrane distillation, Chem Soc Rev. 51 (2022) 6087–6125. https://doi.org/10.1039/d0cs00097c.

[5] Y. Aguilar-Costumbre, J.A. Lambert, M.A. Meléndez-Lira, V.A. Escobar-Barrios, Preparation of membranes based on polysulfone (PSU) and graphene oxide (GrO) by electrospinning, in: Membranes: Materials, Simulations, and Applications, Springer International Publishing, 2016: pp. 23–30. https://doi.org/10.1007/978-3-319-45315-6_3.

[6] L.E. Maldonado-Lopez, G.A. Fimbres-Weihs, V.A. Escobar-Barrios, Structural modification of polysulfone/NMP membranes: effect of chloroform as co-solvent,

Polymer Bulletin. 79 (2022) 6601–6615. https://doi.org/10.1007/s00289-021-03828-1.
[7] M. Sánchez-Luna, M. Otmar, L. Kobera, J. Žitka, V. Escobar-Barrios, Indirect sulfonation of telechelic poly(styrene-ethylene-butylene-styrene) via chloromethylation for preparation of sulfonated membranes as proton exchange membranes, Express Polym Lett. 16 (2022) 171–183. https://doi.org/10.3144/EXPRESSPOLYMLETT.2022.14.
[8] H.T. El-Dessouk, H.M. Ettouney, Fundamentals of Salt Water Desalination, Elsevier, 2002.
[9] National Academies Press, Frontiers of Engineering: Reports on Leading-Edge Engineering from the 2016 Symposium, 2017.
[10] • Germán, E. Dévora-Isiordia, R. González-Enríquez, S. Ruiz-Cruz, Evaluación de procesos de desalinización y su desarrollo en México, 2013.
[11] M. Takht Ravanchi, T. Kaghazchi, A. Kargari, Application of membrane separation processes in petrochemical industry: a review, Desalination. 235 (2009) 199–244. https://doi.org/10.1016/j.desal.2007.10.042.
[12] R.W. Baker, Membrane technology and applications, third ed., John Wiley & Sons, California, 2012.
[13] M. Mulder, Basic Principles of membrane technology, 1996. https://doi.org/10.1007/978-94-009-1766-8.
[14] P.M. Biesheuvel, J.E. Dykstra, S. Porada, M. Elimelech, New parametrization method for salt permeability of reverse osmosis desalination membranes, Journal of Membrane Science Letters. 2 (2022). https://doi.org/10.1016/j.memlet.2021.100010.
[15] J. Zhao, Q. Chen, J. Wang, Novel ecofriendly cation exchange membranes for low-cost electrodialysis of brackish water: Desalination and antiscaling performance, J Memb Sci. 661 (2022). https://doi.org/10.1016/j.memsci.2022.120908.
[16] R. Pawar, Z. Zhang, R.D. Vidic, Laboratory and pilot-scale studies of membrane distillation for desalination of produced water from Permian Basin, Desalination. 537 (2022). https://doi.org/10.1016/j.desal.2022.115853.
[17] H. Kurokawa, O. Kuroda, S. Takahashi, K. Ebara, Vapor permeate characieristics of membrane distillation, Sep Sci Technol. 25 (1990) 1349–1359. https://doi.org/10.1080/01496399008050396.
[18] T. Khayet, M., Matsuura, Membrane distillation: principles and applications, Elsevier, Oxford, 2011.
[19] H. Du, S. Bandara, L. E. Carson, R. R. Kommalapati, Association of Polyethylene Glycol Solubility with Emerging Membrane Technologies, Wastewater Treatment, and Desalination, in: Water Quality - Science, Assessments and Policy, IntechOpen, 2020. https://doi.org/10.5772/intechopen.89060.
[20] J. Phattaranawik, R. Jiraratananon, A.G. Fane, Heat transport and membrane distillation coefficients in direct contact membrane distillation, J Memb Sci. 212 (2003) 177–193. https://doi.org/10.1016/S0376-7388(02)00498-2.
[21] E. Gontarek-Castro, R. Castro-Muñoz, M. Lieder, New insights of nanomaterials usage toward superhydrophobic membranes for water desalination via membrane distillation: A review, Crit Rev Environ Sci Technol. 52 (2022) 2104–2149. https://doi.org/10.1080/10643389.2021.1877032.

[22] Z. Ding, R. Ma"', A.G. Runyu, DESALINATION ELSEVIER Desalination 15 l(2002) 2 17-227 A new model for mass transfer in direct contact membrane distillation, n.d. www.elsevier.comAocate/desal.
[23] J.G. Lee, E.J. Lee, S. Jeong, J. Guo, A.K. An, H. Guo, J. Kim, T.O. Leiknes, N. Ghaffour, Theoretical modeling and experimental validation of transport and separation properties of carbon nanotube electrospun membrane distillation, J Memb Sci. 526 (2017) 395–408. https://doi.org/10.1016/j.memsci.2016.12.045.
[24] S. Srisurichan, R. Jiraratananon, A.G. Fane, Mass transfer mechanisms and transport resistances in direct contact membrane distillation process, J Memb Sci. 277 (2006) 186–194. https://doi.org/10.1016/j.memsci.2005.10.028.
[25] L. Zou, P. Gusnawan, G. Zhang, J. Yu, Novel Janus composite hollow fiber membrane-based direct contact membrane distillation (DCMD) process for produced water desalination, J Memb Sci. 597 (2020). https://doi.org/10.1016/j.memsci.2019.117756.
[26] L. Martõ Ânez-Dõ Âez, M.I. Va Âzquez-Gonza Âlez, Temperature and concentration polarization in membrane distillation of aqueous salt solutions, n.d.
[27] R.W. Schofield, A.G. Fane, C.J.D. Fell, HEAT AND MASS TRANSFER IN MEMBRANE DISTILLATION*, 1987.
[28] M. Gryta, M. Tomaszewska, Heat transport in the membrane distillation process, n.d.
[29] J.C. Chen, Q. Li, M. Elimelech, In situ monitoring techniques for concentration polarization and fouling phenomena in membrane filtration, Adv Colloid Interface Sci. 107 (2004) 83–108. https://doi.org/10.1016/j.cis.2003.10.018.
[30] K.W. Lawson, R.L. Douglas, Membrane Distillation, J Memb Sci. 124 (1997) 1–25. https://doi.org/https://doi.org/10.1016/S0376-7388(96)00236-0.
[31] L. Francis, F.E. Ahmed, N. Hilal, Electrospun membranes for membrane distillation: The state of play and recent advances, Desalination. 526 (2022). https://doi.org/10.1016/j.desal.2021.115511.
[32] M. Pagliero, A. Bottino, A. Comite, C. Costa, Novel hydrophobic PVDF membranes prepared by nonsolvent induced phase separation for membrane distillation, J Memb Sci. 596 (2020). https://doi.org/10.1016/j.memsci.2019.117575.
[33] N. Alberto, M.A. Fonseca, V. Neto, R. Nogueira, M. Oliveira, R. Moreira, Membrane properties in membrane distillation, in: Emerging Technologies for Sustainable Desalination Handbook, Elsevier, 2018: pp. 107–156. https://doi.org/10.1016/B978-0-12-815818-0.00004-7.
[34] S. Zare, A. Kargari, Membrane properties in membrane distillation, in: Emerging Technologies for Sustainable Desalination Handbook, Elsevier, 2018: pp. 107–156. https://doi.org/10.1016/B978-0-12-815818-0.00004-7.
[35] A. Alkhudhiri, N. Darwish, N. Hilal, Membrane distillation: A comprehensive review, Desalination. 287 (2012) 2–18. https://doi.org/10.1016/j.desal.2011.08.027.
[36] A. Franken, J.A.M. Nolten, M.H. v Mulder, D. Bargeman, C.A. Smolders, WETTING CRITERIA FOR THE APPLICABILITY OF MEMBRANE DISTILLATION*, Elsevier Science Publishers B.V, n.d.
[37] L. Eykens, I. Hitsov, K. de Sitter, C. Dotremont, L. Pinoy, I. Nopens, B. van der Bruggen, Influence of membrane thickness and process conditions on direct contact membrane distillation at different salinities, J Memb Sci. 498 (2016) 353–364. https://doi.org/10.1016/j.memsci.2015.07.037.

[38] M.S. El-Bourawi, Z. Ding, R. Ma, M. Khayet, A framework for better understanding membrane distillation separation process, J Memb Sci. 285 (2006) 4–29. https://doi.org/10.1016/J.MEMSCI.2006.08.002.
[39] P. Castejón, K. Habibi, A. Saffar, A. Ajji, A.B. Martínez, D. Arencón, Polypropylene-based porous membranes: Influence of polymer composition, extrusion draw ratio and uniaxial strain, Polymers (Basel). 10 (2018). https://doi.org/10.3390/polym10010033.
[40] A.A.I.A.S. Komaladewi, P.T.P. Aryanti, G. Lugito, I. Wayan Surata, I. Gede Wenten, Recent progress in microfiltration polypropylene membrane fabrication by stretching method, in: E3S Web of Conferences, EDP Sciences, 2018. https://doi.org/10.1051/e3sconf/20186703018.
[41] H. Chae Park, Y. Po Kim, H. Yong Kim, Y. Soo Kang, Membrane formation by water vapor induced phase inversion, J Memb Sci. 156 (1999) 169–178. https://doi.org/10.1016/S0376-7388(98)00359-7.
[42] D.R. Lloyd, K.E. Kinzer, H.S. Tseng, MICROPOROUS MEMBRANE FORMATION VIA THERMALLY INDUCED PHASE SEPARATION. I. SOLID-LIQUID PHASE SEPARATION*, 1990.
[43] A.K. Hołda, B. Aernouts, W. Saeys, I.F.J. Vankelecom, Study of polymer concentration and evaporation time as phase inversion parameters for polysulfone-based SRNF membranes, J Memb Sci. 442 (2013) 196–205. https://doi.org/10.1016/j.memsci.2013.04.017.
[44] H. Caquineau, P. Menut, A. Deratani, C. Dupuy, Influence of the Relative Humidity on Film Formation by Vapor Induced Phase Separation, Polym Eng Sci. 43 (2003) 798–808. https://doi.org/10.1002/pen.10066.
[45] M. Dasdemir, M. Topalbekiroglu, A. Demir, Electrospinning of thermoplastic polyurethane microfibers and nanofibers from polymer solution and melt, J Appl Polym Sci. 127 (2013) 1901–1908. https://doi.org/10.1002/app.37503.
[46] H. Emad Abdoluosefi, G. Honarasa, Fabrication of polyurethane and thermoplastic polyurethane nanofiber by controlling the electrospinning parameters, Mater Res Express. 4 (2017). https://doi.org/10.1088/2053-1591/aa9191.
[47] L. Han, T. Xiao, Y.Z. Tan, A.G. Fane, J.W. Chew, Contaminant rejection in the presence of humic acid by membrane distillation for surface water treatment, J Memb Sci. 541 (2017) 291–299. https://doi.org/10.1016/j.memsci.2017.07.013.
[48] M. Sivakumar, M. Ramezanianpour, G. O'Halloran, Mine Water Treatment Using a Vacuum Membrane Distillation System, APCBEE Procedia. 5 (2013) 157–162. https://doi.org/10.1016/j.apcbee.2013.05.028.
[49] N.M. Mokhtar, W.J. Lau, A.F. Ismail, D. Veerasamy, Membrane distillation technology for treatment of wastewater from rubber industry in Malaysia, in: Procedia CIRP, Elsevier B.V., 2015: pp. 792–796. https://doi.org/10.1016/j.procir.2014.07.161.
[50] D. Qu, J. Wang, B. Fan, Z. Luan, D. Hou, Study on concentrating primary reverse osmosis retentate by direct contact membrane distillation, Desalination. 247 (2009) 540–550. https://doi.org/10.1016/j.desal.2008.08.004.
[51] D. González, J. Amigo, F. Suárez, Membrane distillation: Perspectives for sustainable and improved desalination, Renewable and Sustainable Energy Reviews. 80 (2017) 238–259. https://doi.org/10.1016/J.RSER.2017.05.078.
[52] K.-L. Noble, Waterborne polyurethanes, 1997.

[53] F. Zafar, A. Ghosal, E. Sharmin, R. Chaturvedi, N. Nishat, A review on cleaner production of polymeric and nanocomposite coatings based on waterborne polyurethane dispersions from seed oils, Prog Org Coat. 131 (2019) 259–275. https://doi.org/10.1016/j.porgcoat.2019.02.014.
[54] Polyurethanes: Science, Technology, Markets, and Trends - Mark F. Sonnenschein - Google Libros, (n.d.). https://books.google.com.mx/books?id=K2wOEAAAQBAJ&printsec=frontcover&dq=Polyurethanes:+Science,+Technology,+Markets,+and+Trends&hl=es-419&sa=X&redir_esc=y#v=onepage&q=Polyurethanes%3A Science%2C Technology%2C Markets%2C and Trends&f=false (accessed November 25, 2022).
[55] J.O. Akindoyo, M.D.H. Beg, S. Ghazali, M.R. Islam, N. Jeyaratnam, A.R. Yuvaraj, Polyurethane types, synthesis and applications-a review, RSC Adv. 6 (2016) 114453–114482. https://doi.org/10.1039/c6ra14525f.
[56] A.L. Silva, J.C. Bordado, Recent developments in polyurethane catalysis: Catalytic mechanisms review, Catal Rev Sci Eng. 46 (2004) 31–51. https://doi.org/10.1081/CR-120027049.
[57] C. Hepburn, Polyurethane elastomers, 2 edition, Elsevier Applied Science, 2012.
[58] H. Honarkar, Waterborne polyurethanes: A review, J Dispers Sci Technol. 39 (2018) 507–516. https://doi.org/10.1080/01932691.2017.1327818.
[59] M. Serkis-Rodzeń, M. Špírková, P. Matějíček, M. Štěpánek, Formation of linear and crosslinked polyurethane nanoparticles that self-assemble differently in acetone and in water, Prog Org Coat. 106 (2017) 119–127. https://doi.org/10.1016/j.porgcoat.2017.03.003.
[60] B. Ranjbarfar, S. Taghvaei Ganjali, M.M. Alavi Nikje, S. Moradi, Synthesis, Characterization and Physicomechanical Properties of Novel Water-based Biodegradable Polyurethane Dispersion, Russian Journal of Applied Chemistry. 91 (2018) 1198–1208. https://doi.org/10.1134/S1070427218070200.
[61] A.P. More, S.T. Mhaske, Synthesis of polyurethane dispersion from polyesteramide polyol, Pigment & Resin Technology. 47 (2018) 154–163. https://doi.org/10.1108/prt-07-2016-0071.
[62] A. Santamaria-Echart, I. Fernandes, F. Barreiro, M.A. Corcuera, A. Eceiza, Advances in waterborne polyurethane and polyurethane-urea dispersions and their eco-friendly derivatives: A review, Polymers (Basel). 13 (2021) 1–32. https://doi.org/10.3390/polym13030409.
[63] B.X. Cheng, W.C. Gao, X.M. Ren, X.Y. Ouyang, Y. Zhao, H. Zhao, W. Wu, C.X. Huang, Y. Liu, X.Y. Liu, H.N. Li, R.K.Y. Li, A review of microphase separation of polyurethane: Characterization and applications, Polym Test. 107 (2022). https://doi.org/10.1016/j.polymertesting.2022.107489.
[64] Technical Information - Properties of polyurethane using each polyol, (n.d.). http://www.asahi-kasei.co.jp/pcdlhp/en/technical/ (accessed November 25, 2022).
[65] V. Garca-Pacios, V. Costa, M. Colera, J. Miguel Martn-Martnez, Affect of polydispersity on the properties of waterborne polyurethane dispersions based on polycarbonate polyol, Int J Adhes Adhes. 30 (2010) 456–465. https://doi.org/10.1016/j.ijadhadh.2010.03.006.
[66] D.K. Lee, H.B. Tsai, R.S. Tsai, P.H. Chen, Preparation and properties of transparent thermoplastic segmented polyurethanes derived from different polyols, Polym Eng Sci. 47 (2007) 695–701. https://doi.org/10.1002/pen.20742.

[67] E. Foy, J.B. Farrell, C.L. Higginbotham, Synthesis of linear aliphatic polycarbonate macroglycols using dimethylcarbonate, J Appl Polym Sci. 111 (2009) 217–227. https://doi.org/10.1002/app.28887.
[68] D.K. Lee, H.B. Tsai, H.H. Wang, R.S. Tsai, Aqueous polyurethane dispersions derived from polycarbonatediols, J Appl Polym Sci. 94 (2004) 1723–1729. https://doi.org/10.1002/app.21090.
[69] A. Pattanayak, S.C. Jana, Synthesis of thermoplastic polyurethane nanocomposites of reactive nanoclay by bulk polymerization methods, Polymer (Guildf). 46 (2005) 3275–3288. https://doi.org/10.1016/J.POLYMER.2005.02.081.
[70] I. V. Khudyakov, D.R. Zopf, N.J. Turro, Polyurethane nanocomposites, Des Monomers Polym. 12 (2009) 279–290. https://doi.org/10.1163/156855509X448253.
[71] L. Bistričić, G. Baranović, M. Leskovac, E.G. Bajsić, Hydrogen bonding and mechanical properties of thin films of polyether-based polyurethane-silica nanocomposites, Eur Polym J. 46 (2010) 1975–1987. https://doi.org/10.1016/j.eurpolymj.2010.08.001.
[72] Y. Wattanodorn, R. Jenkan, P. Atorngitjawat, S. Wirasate, Antibacterial anionic waterborne polyurethanes/Ag nanocomposites with enhanced mechanical properties, Polym Test. 40 (2014) 163–169. https://doi.org/10.1016/j.polymertesting.2014.09.004.
[73] J. Pavličević, S. Sinadinović-Fišer, M. Špírková, J. Budinski-Simendić, O. Borota, M. Janković, Ž. Knez, The phase structure of novel polycarbonate-based polyurethaneorganoclay nanocomposites, Adv Mat Res. 560–561 (2012) 771–775. https://doi.org/10.4028/www.scientific.net/AMR.560-561.771.
[74] J. Pavličević, M. Špírková, M. Jovičić, O. Bera, R. Poreęba, J. Budinski-Simendić, The structure and thermal properties of novel polyurethane/organoclay nanocomposites obtained by pre-polymerization, Compos B Eng. 45 (2013) 232–238. https://doi.org/10.1016/j.compositesb.2012.09.018.
[75] M. Serkis, M. Špírková, J. Hodan, J. Kredatusová, Nanocomposites made from thermoplastic waterborne polyurethane and colloidal silica. The influence of nanosilica type and amount on the functional properties, Prog Org Coat. 101 (2016) 342–349. https://doi.org/10.1016/j.porgcoat.2016.07.021.
[76] E. Tocha, H. Janik, M. Dębowski, G.J. Vancso, Morphology of polyurethanes revisited by complementary AFM and TEM, J Macromol Sci Phys. 41 B (2002) 1291–1304. https://doi.org/10.1081/MB-120013098.
[77] H. Koerner, J.J. Kelley, R.A. Vaia, Transient microstructure of low hard segment thermoplastic polyurethane under uniaxial deformation, Macromolecules. 41 (2008) 4709–4716. https://doi.org/10.1021/ma800306z.
[78] H.J. Qi, M.C. Boyce, Stress-strain behavior of thermoplastic polyurethanes, Mechanics of Materials. 37 (2005) 817–839. https://doi.org/10.1016/j.mechmat.2004.08.001.
[79] C.S. Schollenberger, F.D. Stewart, Thermoplastic Polyurethane Hydrolysis Stability, Journal of Elastomers and Plastics. 3 (1971) 28–56. https://doi.org/10.1177/009524437100300103.
[80] J. Datta, P. Kasprzyk, Thermoplastic polyurethanes derived from petrochemical or renewable resources: A comprehensive review, Polym Eng Sci. 58 (2018) E14–E35. https://doi.org/10.1002/pen.24633.

[81] I. Yilgör, E. Yilgör, G.L. Wilkes, Critical parameters in designing segmented polyurethanes and their effect on morphology and properties: A comprehensive review, Polymer (Guildf). 58 (2015) A1–A36. https://doi.org/10.1016/j.polymer.2014.12.014.
[82] K.S. Tiaw, M.H. Hong, S.H. Teoh, Precision laser micro-processing of polymers, J Alloys Compd. 449 (2008) 228–231. https://doi.org/10.1016/j.jallcom.2006.01.145.
[83] S. Takamatsu, S. Sato, T. Itoh, Stress concentration-relocating interposer in electronic textile packaging using thermoplastic elastic polyurethane film with via holes for bearing textile stretch, Sci Rep. 12 (2022). https://doi.org/10.1038/s41598-022-13493-7.
[84] H. Juster, B. van der Aar, H. de Brouwer, A review on microfabrication of thermoplastic polymer-based microneedle arrays, Polym Eng Sci. 59 (2019) 877–890. https://doi.org/10.1002/pen.25078.
[85] Z.-T. Qu, S.-Y. Duan, B.-B. Li, D. Sun, Y.-L. Gu, PDMS/PVDF microporous membrane with semi-interpenetrating polymer networks for vacuum membrane distillation, J Appl Polym Sci. 135 (2018). https://doi.org/10.1002/app.45792.
[86] S. Iizuka, K. Murata, M. Sekine, C. Sato, A novel cup with a pressure-adjusting mechanism for high-temperature water vapor transmission rate measurements, Polym Test. 50 (2016) 73–78. https://doi.org/10.1016/j.polymertesting.2015.11.018.
[87] H. Sato, D. Aoki, H. Marubayashi, S. Uchida, H. Sogawa, S. Nojima, X. Liang, K. Nakajima, T. Hayakawa, T. Takata, Topology-transformable block copolymers based on a rotaxane structure: change in bulk properties with same composition, Nat Commun. 12 (2021). https://doi.org/10.1038/s41467-021-26249-0.
[88] A. Eceiza, M. Larrañaga, K. de la Caba, G. Kortaberria, C. Marieta, M.A. Corcuera, I. Mondragon, Structure-Property relationships of thermoplastic polyurethane elastomers based on polycarbonate diols, J Appl Polym Sci. 108 (2008) 3092–3103. https://doi.org/10.1002/app.
[89] P. Russo, D. Acierno, G. Marletta, G.L. Destri, Tensile properties, thermal and morphological analysis of thermoplastic polyurethane films reinforced with multiwalled carbon nanotubes, Eur Polym J. 49 (2013) 3155–3164. https://doi.org/10.1016/j.eurpolymj.2013.07.021.
[90] J.C.W. Spijkers, A. Hendricus J.M. Van De Ven, W. Mezger Thomas, E. Dirk Bontinck, U. Luc De Koninck, Water vapor permeable thermoplastic polyurethane film, US 6,790,926 B1. (2004).
[91] U.G. Makal, Breathable and crosslinkable thermoplastic polyurethane, US 2017 / 0215756A1. (2017).
[92] X. Wang, X. Luo, X. Wang, Study on blends of thermoplastic polyurethane and aliphatic polyester: Morphology, rheology, and properties as moisture vapor permeable films, Polym Test. 24 (2005) 18–24. https://doi.org/10.1016/j.polymertesting.2004.08.003.
[93] C. Su, Y. Li, H. Cao, C. Lu, Y. Li, J. Chang, F. Duan, Novel PTFE hollow fiber membrane fabricated by emulsion electrospinning and sintering for membrane distillation, J Memb Sci. 583 (2019) 200–208. https://doi.org/10.1016/j.memsci.2019.04.037.
[94] S. Meng, J. Mansouri, Y. Ye, V. Chen, Effect of templating agents on the properties and membrane distillation performance of TiO2-coated PVDF membranes, J Memb Sci. 450 (2014) 48–59. https://doi.org/10.1016/j.memsci.2013.08.036.

[95] Y. Liao, R. Wang, A.G. Fane, Engineering superhydrophobic surface on poly(vinylidene fluoride) nanofiber membranes for direct contact membrane distillation, J Memb Sci. 440 (2013) 77–87. https://doi.org/10.1016/j.memsci.2013.04.006.
[96] C. Su, J. Chang, K. Tang, F. Gao, Y. Li, H. Cao, Novel three-dimensional superhydrophobic and strength-enhanced electrospun membranes for long-term membrane distillation, Sep Purif Technol. 178 (2017) 279–287. https://doi.org/10.1016/J.SEPPUR.2017.01.050.
[97] C. Su, T. Horseman, H. Cao, K.S.S. Christie, Y. Li, S. Lin, Robust Superhydrophobic Membrane for Membrane Distillation with Excellent Scaling Resistance, Environ Sci Technol. (2019). https://doi.org/10.1021/acs.est.9b04362.
[98] S. Al-Gharabli, W. Kujawski, H.A. Arafat, J. Kujawa, Tunable separation via chemical functionalization of polyvinylidenefluoride membranes using piranha reagent, J Memb Sci. 541 (2017) 567–579. https://doi.org/10.1016/j.memsci.2017.07.047.
[99] Z.T. Qu, S.Y. Duan, B.B. Li, D. Sun, Y.L. Gu, PDMS/PVDF microporous membrane with semi-interpenetrating polymer networks for vacuum membrane distillation, J Appl Polym Sci. 135 (2018) 1–10. https://doi.org/10.1002/app.45792.
[100] S. Al-Gharabli, B. Al-Omari, W. Kujawski, J. Kujawa, Biomimetic hybrid membranes with covalently anchored chitosan – Material design, transport and separation, Desalination. 491 (2020) 114550. https://doi.org/10.1016/j.desal.2020.114550.
[101] S.A. Castillo Berrones, Diseño, construcción y caracterización de un destilador por membrana, Universidad de Guanajuato, División de Ciencias Naturales y Exactas., 2015.